NUMERICAL AND EXPERIMENTAL INVESTIGATIONS OF THE FREEZING OF CNT-WATER NANOFLUIDS IN A RECTANGULAR CAVITY

BY

Alshehri, Ali M.

A Thesis Presented to the

DEANSHIP OF GRADUATE STUDIES

KING FAHD UNIVERSITY OF PETROLEUM & MINERALS

DHAHRAN, SAUDI ARABIA

In Partial Fulfillment of the

Requirements for the Degree of

MASTER OF SCIENCE

In

MECHANICAL ENGINEERING

January 2017

KING FAHD UNIVERSITY OF PETROLEUM & MINERALS

DHAHRAN- 31261, SAUDI ARABIA

DEANSHIP OF GRADUATE STUDIES

This thesis, written by ALSHEHRI, ALI MOHAMMAD under the direction of his thesis advisor and approved by his thesis committee, has been presented and accepted by the Dean of Graduate Studies, in partial fulfillment of the requirements for the degree of MASTER OF SCIENCE IN MECHANICAL ENGINEERING.

Dr. Rached Ben-Mansour
(Advisor)

Dr. Mohammad Antar
(Co-Advisor)

Dr. Saidur R. Abdul Hakim
(Member)

Dr. Zuhair Gasem
Department Chairman

Dr. Salam A. Zummo
Dean of Graduate Studies

13/4/17

Date

NUMERICAL AND EXPERIMENTAL INVESTIGATIONS OF THE FREEZING OF CNT-WATER NANOFLUIDS IN A RECTANGULAR CAVITY

BY

ALSHEHRI, ALI MOHAMMAD

A THESIS PRESENTED TO THE

DEANSHIP OF GRADUATE STUDIES

KING FAHD UNIVERSITY OF PETROLEUM AND MINERALS

DHAHRAN, SAUDI ARABIA

IN PARTIAL FULFILLMENT OF THE

REQUIREMENTS FOR THE DEGREE OF

MASTER OF SCIENCE

IN

MECHANICAL ENGINEERING

January 2017

KING FAHD UNIVERSITY OF PETROLEUM & MINERALS

DHAHRAN- 31261, SAUDI ARABIA

DEANSHIP OF GRADUATE STUDIES

This thesis, written by ALSHEHRI, ALI MOHAMMAD under the direction of his thesis advisor and approved by his thesis committee, has been presented and accepted by the Dean of Graduate Studies, in partial fulfillment of the requirements for the degree of MASTER OF SCIENCE IN MECHANICAL ENGINEERING.

_____

Dr. Rached Ben-Mansour
(Advisor)

_____

Dr. Mohammad Antar
(Co-Advisor)

_____

Dr. Saidur R. Abdul Hakim
(Member)

_____

Dr. Zuhair Gasem
Department Chairman

_____

Dr. Salam A. Zummo
Dean of Graduate Studies

_____

Date

To my family especially Sara without whom this work would have been done earlier

ACKNOWLEDGMENTS

My highest gratitude goes to Almighty Allah for giving me life, love, and strength to accomplish this work.

My gratitude goes to KFUPM authorities for giving me the opportunity to do my master's degree. I extend my gratitude to KACST for selecting my thesis in the Graduate Students Grant Program and for providing me with funds in the cause of my research work. I am very grateful to my advisor Dr. Rached for his support and guidance throughout my stay at KFUPM. I appreciate how helpful he was with me during my studies as well as my visit to MIT. I would like to extend my gratitude to Dr. Saidur Rahman for guiding me at the beginning of my thesis work and giving me the honor of discussing my thesis. I would like to extend my gratefulness to Dr. Antar for being part of my thesis committee. I would like as well to thank Dr. Jihad Al-Sadah for trying to help me with the experimental setup and discussing his wonderful views and ideas to further enhance this work. I would not forget to thank and appreciate the assistance of Eng. Bahaa, Eng. Kamal, Eng. Al-Yousef, and Eng. Saeed, wonderful people.

I would also like to thank with all my heart my family. This work could not have been completed without their support, sacrifice, devotion, and love. I thank every single one of my family; my father, mother, sisters and brothers. I extend heartfelt thanks to my wife, Asma, for her support, love, patience and encouragement. My thanks goes to my daughter, Sara, who was born during my first year of studies. When she came, love, joy and happiness were my motives to finish this work. Finally, I would like to thank my friends and colleagues for their support, guidance, and assistance throughout my stay at KFUPM.

TABLE OF CONTENTS

LIST OF TABLES

LIST OF FIGURES

LIST OF ABBREVIATIONS

CFD	:	Computational Fluid Dynamic
CNT	:	Carbon Nanotubes
DAQ	:	Data Acquisition
DE	:	Decene
DW	:	Deionized Water
EG	:	Ethylene Glycol
EO	:	Engine Oil
GA	:	Gum Arabic
LCM	:	Lumped Capacitance Method
MWCNT	:	Multi-walled Carbon Nanotubes
NePCM	:	Nano-enhanced Phase Change Material
PCM	:	Phase Change Material
PDE	:	Partial Differential Equation
PO	:	Pump Oil
PRESTO	:	Pressure Staggering Option
PVP	:	PolyVinylPyrrolidone
QUICK	:	Quadratic Upstream Interpolation for Convective Kinematics
SCN	:	Surface-controlled Nucleation
SIMPLE	:	Semi-Implicit Method for Pressure Linked Equations
SWCNT	:	Single wall Carbon Nanotubes
TC	:	Thermocouple
TCNT	:	Tangled Carbon Nanotubes
VCN	:	Volumetric-controlled Nucleation
VI	:	Virtual Instrument

THESIS ABSTRACT (ENGLISH)

Full Name : Alshehri, Ali Mohammad

Thesis Title : Numerical and experimental investigations of the freezing of CNT-water Nanofluids in a rectangular cavity

Major Field : Mechanical Engineering

Date of Degree : March 2017

Nanofluids are defined as conventional liquids seeded with small nano-sized metallic particles. The fact that metals possess higher thermal conductivities than liquids gives Nanofluids an advantage of having high thermal conductivities as well as liquid-like behavior. Recently, Nanofluids have been developed and introduced into different engineering applications, such as cooling industrial processes, electronic cooling, and thermal energy storage, to name a few.

In this work, numerical and experimental investigations were performed in order to obtain a good insight on the freezing process of CNT-water Nanofluids and their potential use in cold energy storage. An experimental setup was designed and built to test the total freezing time of different Nanofluids. Different stable CNT-water Nanofluids were prepared prior to making the experiment corresponding to CNT weight concentrations of 0.3% and 1%. Thermal behavior and total freezing times were tested for the aforementioned Nanofluids and compared to that of water, as it is the base liquid. It was found that Nanofluids were able to reduce the total freezing time only in the absence of natural convection. A reduction in total freezing time of 11% and 14.4% was noticed upon adding 0.3% and 1% of CNT particles to water, respectively. This result benefits many industries making use of cold energy storage in reducing the charging/discharging times of ice batteries. The existence

of natural convection in water was found to reduce the total freezing time tremendously; however, upon adding CNT particles viscosity increases as well suppressing natural circulations.

To understand the experimental results, thermal conductivities of the studied Nanofluids were measured and enhancement of 4.2% was found upon adding 1% of CNT particles. In addition, the reason of the failure of CNT to reduce freezing time in cases where natural convection existed was found to be due to a probable failure of Gum Arabic to withstand low temperatures.

Temperature readings from the experiment showed interesting behavior of the tested liquids. Therefore, a two-dimensional CFD model was developed to study the flow and thermal fields. Results showed that the flow field is characterized by two circulation zones caused by the fact that water has a density-inversion point at a temperature of 4 ^{o}C. This zone was first noticed in the experiment and then a new code was written and implemented into FLUENT software to simulate the flow field. In the numerical work, it was found that adding CNT particles to water reduces total freezing time for all studied cases. Numerical results matched the case of diffusion-dominant freezing experiments (Stratified); however, cases with natural convection (Non-stratified) failed to match due to the lack of agglomeration information in the CFD model. The CFD model was extended to simulate higher CNT concentration. A reduction of 27.2% in total freezing time was observer upon adding 2% of CNT particles in non-stratified simulations.

THESIS ABSTRACT (ARABIC)

ملخص الرسالة

الاسم الكامل: علي محمد الشهري

عنوان الرسالة: دراسة عملية و رياضية لتجمد سائل الماء المضاف إليه جسيمات نانوية (CNT) في صندوق

التخصص: الهندسة الميكانيكية

تاريخ الدرجة العلمية: مارس 2017 ميلادي

نستطيع تعريف السوائل النانوية بأنها سوائل متعارف عليها مدعمة بجسيمات معدنية متناهية الصغر قطرها يحسب بالنانومتر. كما هو معلوم فإن المعادن تمتلك موصلية عالية للحرارة بينما السوائل تعتبر موصليتها ضعيفة جدًا مقارنة بالمعادن، لذلك فإن السوائل النانوية تمتلك خواص موصلية المعادن وسيلان الموائع في آن واحد. هذه الخواص جعلت من هذا النوع من السوائل محل دراسة كثير من الباحثين في الوقت الراهن. تتعد استخدامات السوائل النانوية في الصناعة ومن الأمثلة عليها صناعة المبردات وتبريد الأجهزة الالكترونية وكذلك في تخزين الطاقة الحرارية.

لقد تمت دراسة عملية ورياضية في هذا العمل لنوع واحد من السوائل النانوية ألا وهو ماء مدعم بأنابيب الكربون النانوية (CNT). الهدف من هذه الدراسة هو معرفة تأثير هذا السائل على عملية التجمد الحاصلة في الماء ما له أهمية كبيرة في تخزين الطاقة الباردة. لقد صُممت تجربة لدراسة الوقت المستغرق في عملية التجمد في عينات من هذا السائل تختلف في تركيز الجسيمات النانوية. هذه العينات تم تكوينها في المعمل قبل البدء بالتجربة وكانت عبارة عن عينتين إحداهما بتركيز 0.3% والأخرى بتركيز 1%. قورنت هذه العينات مع بعضها ومع الماء الذي يعتبر هو السائل المستضيف في هذه الحالة. أبدت النتائج انخفاضًا ملحوظًا في الوقت المستغرق للتجمد في حالة واحدة من حالات التجربة ألا وهي حالة انعدام الحمل الحراري الطبيعي. عندما قورن الوقت المستغرق لهذه العينات للتجمد مقارنة بالماء وجدنا انخفاضًا بنسبة 11% عند إضافة 0.3% وبنسبة 14.4% عند إضافة 1%. لهذه النتيجة أهمية كبيرة للمهتمين بصناعة بطاريات الثلج حيث أن انخفاض الوقت المستغرق للتجمد يقلل الوقت المستغرق لشحن أو تفريغ البطارية حسب الحاجة. وفي محاولة لتفسير الانخفاض في الوقت المستغرق للتجمد قيست الموصلية الحرارية لهذه السوائل ما أظهر ارتفاعًا في قيمها اطرادًا مع تركيز الجسيمات النانوية. الحالة الأخرى من التجارب هي بوجود الحمل الحراري الطبيعي. لقد أبدت التجارب المقامة على الماء بأن الوقت انخفض بشكل ملحوظ عن الحالة الأولى. مع ذلك فإن الانخفاض لم يكن ظاهرًا على السوائل الأخرى بل العكس تمامًا هو ما حصل.

إن دراسة الموضوع تجريبيا أبدى بعض الظواهر المشوقة لدراسة أعمق حيث أن قراءات درجة الحرارة انخفضت بشكل مفاجئ في وقت معين من التجربة بشكل متكرر. لأجل دراسة أعمق لقد قمنا بتطوير أنموذج رياضي يحاكي عملية التجمد المستخدمة في التجربة المعملية. النتائج أظهرت أن حركة السوائل داخل الصندوق تمتاز بتواجد دوامتين تعملان على الحمل الحراري الطبيعي متعاكستين في الاتجاه. السبب في وجود هاتين الدوامتين هو أن الماء يمتاز بخاصية و هي أن كثافته تصل لقمتها عند درجة حرارة 4 °C. تم كتابة برنامج خاص لتفعيل هذه الخاصية للماء في البرنامج الرياضي المستخدم وهو برنامج عالمي موثوق اسمه FLUENT. وبالقيام بالمحاكاة الرياضية تبين أن إضافة الجسيمات النانوية إلى الماء تؤدي إلى انخفاض الوقت المستغرق لعملية التجمد بغض النظر عن حالة العملية أي ما إذا كانت بوجود أو انعدام الحمل الحراري الطبيعي. بل على العكس من التجربة المعملية حيث أبدت النتائج الرياضية أن وجود الحمل الحراري الطبيعي يخفض وقت التجمد بشكل أكبر من انعدامه. بمقارنة النتائج الرياضية والتجريبية يتبين التوافق بينهما في حالة انعدام الحمل الحراري الطبيعي أما في حالة وجوده فهما لا يتفقان البتة. تم العمل على بناء تجربة أخرى لمعرفة السبب وراء هذا التناقض وفهم ما يحصل للسوائل النانوية عند تجميدها وقد أظهرت الدراسة أن السوائل تبدأ بالترسب والتجمع مع بعضها عند درجات حرارة منخفضة. والسبب في ذلك هو المادة المعلِقة المستخدمة هنا وهي اللبان العربي. في الدراسة الرياضية تم اختبار تركيز أعلى من الجسيمات النانوية وأظهرت النتائج أن إضافة جسيمات نانوية بتركيز 2% يخفض الوقت المستغرق للتجمد بنسبة 27.2% مقارنة بالماء.

CHAPTER 1

INTRODUCTION AND LITERATURE REVIEW

1.1 Introduction

Phase-change process in materials is considered a key player in many industrial and natural applications. Studying heat transfer combined with phase change has undergone a lot of research work, such as the studies done on the processes of boiling, evaporation, condensation, melting, and freezing, to name a few. The reason of the intensive focus on such problems stems from their importance in many industrial applications, such as casting of metals, latent heat in energy storage systems, water desalination and purification, plastic manufacturing, and many others. Many scientists have used certain substances to study the problem of phase change, which are called phase change materials (PCM). The choice of those materials in a certain application depends on many factors and most importantly two: phase-change temperature and enthalpy of phase-change, sometimes called Latent heat of phase-change. The latent heats of melting/freezing of some typical PCM along with their melting/freezing temperatures are presented in Figure 1-1. The required PCM is to be chosen based on the application requirements of latent heat of melting, melting temperature, and other important parameters, such as cost, and chemical stability. Water is considered a very good PCM because of its abundance and its availability in natural processes.

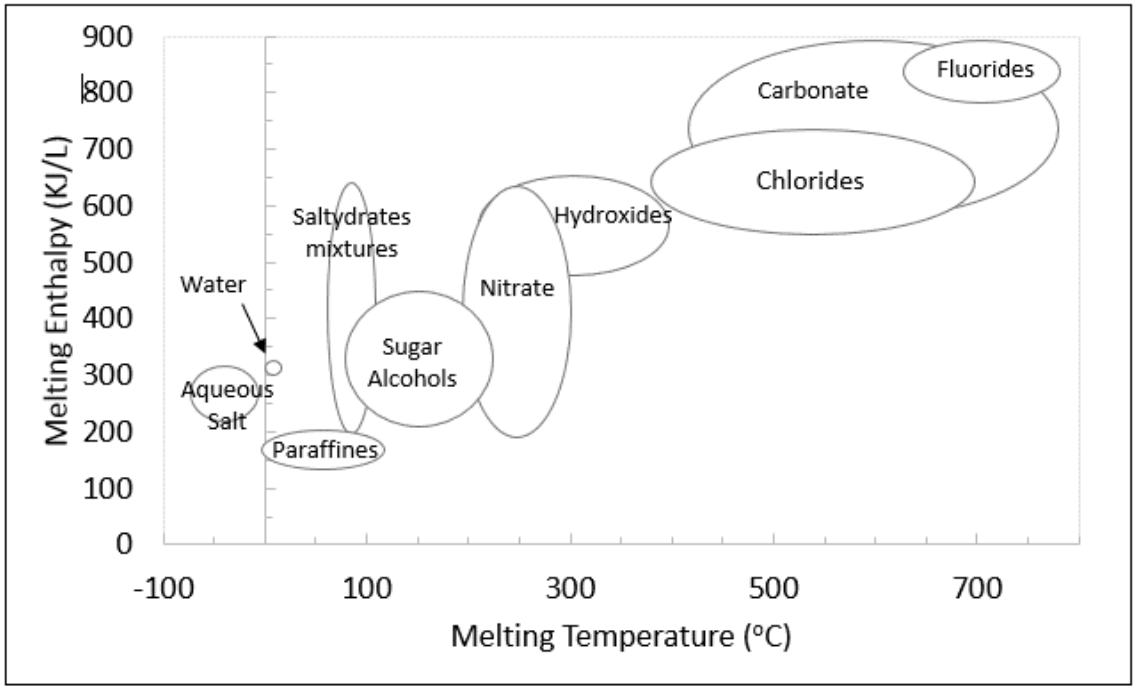

Figure 1-1: Different groups of materials used as PCMs along with their melting enthalpy versus melting temperature (Reconstructed from [2])

The application of PCM in thermal energy storage systems have been the course of many research work. However, undesirable properties of conventional PCM emerged as the research has developed on this topic. One of those problems is the poor thermal conductivity of this class of materials, which suppresses the energy transfer rate significantly which will consequently decrease the duration of phase change process. As a direct solution to the problem, providing PCM along with thermal conductivity enhancers can be a promising way of solving the problem. In a recent review by Fan and Khodadadi [1], thermal conductivity promoters for PCM were discussed in a well-organized review paper. Those promoters range from changing the geometry of heating/cooling surfaces to seeding PCM with ultra-fine Nano-sized particles. The latter material is called Nano-enhanced phase change materials (NePCM).

Nanoparticles are metallic particles that are ultra-fine in size, about less than 100 nm in diameter. Their small size enables scientists to insert them in other material in order to come up with a different property-enhanced material, which is physically mixed and stable. Since nanoparticle are made up of metals usually, they possess good thermophysical properties compared with non-metallic materials. This fact opened many areas of research in which scientist use nanoparticles for enhancing thermal conductivities of conventional PCM, thus promoting more heat to transfer and in turn increasing their efficiencies in many heat transfer applications.

Utilization of nanoparticles (diameters less than 100 nm) opens the door to number of opportunities leading to new innovations and technologies in many areas, such as biotechnology, design of microfluidic devices, emission control, electronic devices cooling and energy efficiency [3]. Masuda et al. [4] reported an enhancement of thermal conductivity by dispersing nano-sized particles in liquids. Soon after that, Choi [5] was the first to mention the term "Nanofluid" for this new class of fluids with enhanced thermophysical properties. After this breakthrough, many studies have been conducted to better use this class of fluids to maximize the efficiencies and minimize the cost and size of heat transfer applications. Figure 1-2 shows the growth of papers published in this new area of research over the year between 1994 and 2016, based on a report obtained from (www.sciencedirect.com). The search was made such that any paper titled with the word (Nanofluid) or (Nanofluids) are counted.

In the following sections, a literature review will be presented that will look through the preparation methods of Nanofluids, Nanofluids thermophysical properties, applications of Nanofluids, and using Nanofluids in phase-change problems.

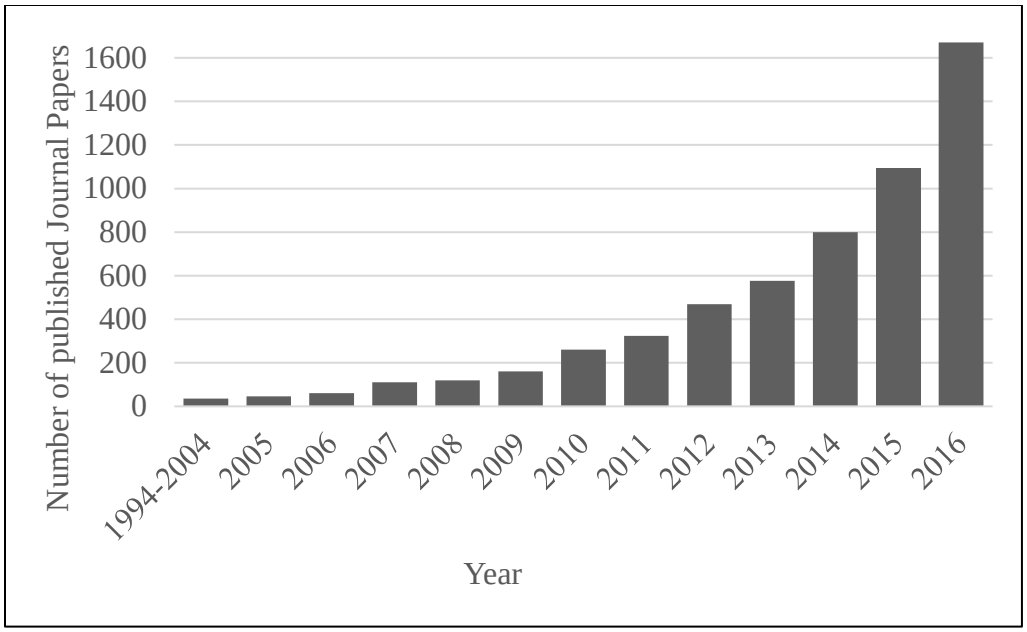

Figure 1-2: Published journal papers related to Nanofluids over the span of more than 20 years (Taken from Science Direct website as of November 4, 2016 [6])

1.2 Nanofluid Preparation and Stability Review

Nanofluid preparation is the most important process for better dispersion of nanoparticles into the base fluid. In 1993, Masuda et al. [4] found that Nanofluids are instable since the particles tend to precipitate after a short time. For that reason Grimm [7] conducted his experiments quickly for agglomeration of particles not to occur. Nowadays, Nanofluids are well-prepared thanks to the state-of-the-are technologies available. Those technologies enabled scientists to produce Nanofluids with high stability and chemical compatibility with the base fluid. There are two main methods by which Nanofluids are prepared; Single-step method, and two-step method. In the following sections both methods are going to be discussed followed by a discussion of the stability of Nanofluids.

1.2.1 Single-step method

In this method, Nanofluids are prepared by producing and dispersing nanoparticles in the base fluid in a single cycle. Eastman et al. [8] was among the first efforts in developing this technique using a physical vapor condensation method to produce Copper ethylene glycol Nanofluids. One of the advantages of this method is that many processes are sidestepped such as drying, storage, transportation, and dispersion of nanoparticles, hence minimizing the nanoparticles agglomeration and thus the stability of fluids is obtained to a good extent [9]. This method cannot be used to synthesize large quantities of Nanofluids. Adding to this disadvantage the high cost of the process itself which limits this method to laboratory and research use [10].

1.2.2 Two-step method

This method is widely used for preparing Nanofluids. Nanofluids are produced by first preparing dry powders such as nanoparticles, nanotubes, and nanofibers using chemical or physical methods. Then, this powder is dispersed into the base fluid with the help of ultrasonic agitation, magnetic force agitation, high shear mixing, or ball milling [10]. The enhancement of Nanofluid stability is the most important step in the process of preparing Nanofluids, however the two-step method does not help in the stability of Nanofluids. As a proposed remedy, adding surfactants to the Nanofluid proofed to be effective in enhancing stability and dispersity into the host fluid, as going to be discussed in the next section. Figure 1-3 shows an example of a Nanofluid with and without surfactants that was left for enough time to show the precipitation of nanoparticles. It can be noticed that the surfactant plays a role in stabilizing the Nanofluids over time.

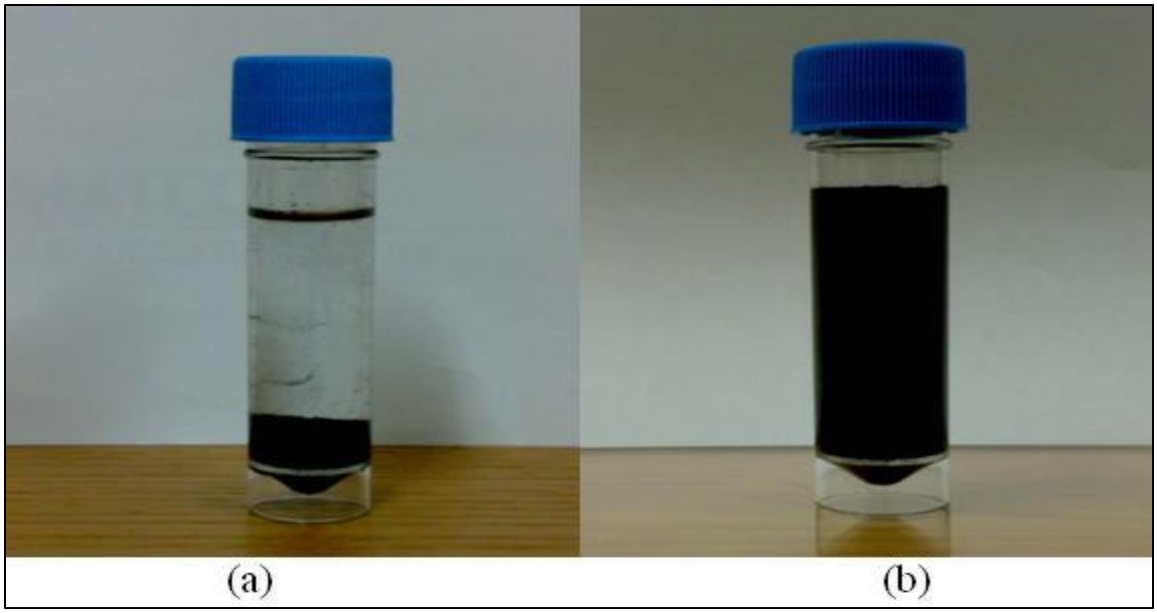

Figure 1-3: Photos of Carbon nanotubes and distilled water Nanofluid (a) with surfactant and (b) without surfactant)

1.2.3 Nanofluids stability

Preparing a Nanofluid that is not stable does not result only in the settlement of nanoparticles, which might block the flow in a pipe for instance, but also results in altering the desirable properties of the Nanofluid. The main reason Nanofluids are used is their enhanced properties without which there is no point of using them. Hence, many attempts were made to stabilize Nanofluids.

In order to check the stability of Nanofluid, many methods have been proposed by scientists. One of the simplest methods is the sedimentation method [11]. In this method, the stability of Nanofluids can be observed visually by the sediments settling on the walls of the container. Alternatively and more accurately, the sediment weight of nanoparticles in a Nanofluid when exposing the Nanofluid to an external force is a sign of its stability. The Nanofluid is considered stable if the weight of the nanoparticles keeps constant over the needed period of time. A disadvantage of the sedimentation method is that it requires a long period for testing. Centrifugation method was proposed as a solution to that problem. Singh et al. [12] used this method to test the stability of silver Nanofluids. It was observed that the Nanofluid has a good stability of one month in the stationary state and more than ten hours under the centrifugation state of 3,000 rpm. There are other methods to test the stability of Nanofluids, such as Zeta potential analysis, and Spectral absorbency analysis [10].

The silver Nanofluids prepared by Singh et al. [12] were considered excellent stable Nanofluids because of the use of PolyVinylPyrrolidone (PVP) as a surfactant. This brings about the point of stability enhancers. The widely used technique is the use of surfactants,

which are called in this case as dispersants. Most of the Nanofluids are hydrophobic in nature so the purpose of adding a dispersants to them is to increase their wettability.

In general, a dispersant contains a hydrophobic tail portion and a hydrophilic polar head group [10]. Usually, dispersants are placed at the interface between two materials, i.e. nanoparticles and base liquid, where they give sort of a continuity link between the two materials. In an effort to extend the stability time of Nanofluids, surface modifications of the nanoparticles was proposed, where it is known as the process of functionalizing nanoparticles. Yang and Liu synthesized a functionalized silica nanoparticles by grafting Silanes directly into the nanoparticles' surface [13]. Wepasnick et al [14] reviewed the surface modification or functionalizing of carbon nanotubes.

1.3 Nanofluid Properties

Different methods have been proposed to enhance the heat transfer of fluids. One of those methods is achieved by enhancing thermal conductivity of the fluid. In the past, scientists tried to increase the thermal conductivity of base fluids by suspending micro-particles of metals or carbons in fluids since their thermal conductivities are typically much higher than that of liquids, as apparent in Figure 1-4. However, due to the size of those particles, there appeared the sedimentation problem where those particles settle out of the base fluid after some time. This is the main problem with suspending micro-particles along with other problems, such as increasing the viscosity of the base fluid, which increases pumping power needed to move the fluid. Modern nanotechnology provides new opportunities to process and produce materials with average sizes below 50 nm. The much larger surface area of nanoparticles, compared to the old micro-particles, will not only improve heat transfer capabilities, but also will increase the stability of the suspensions in base fluids [15]. In this section, three main properties are to be discussed namely, thermal conductivity, heat capacity, and viscosity, due to their importance in heat transfer problems.

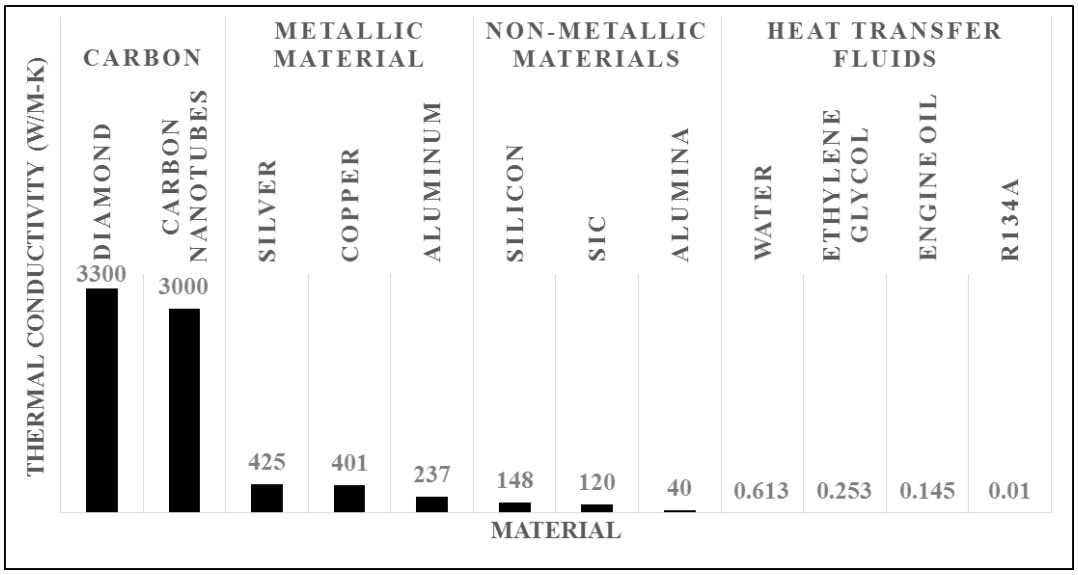

Figure 1-4: Thermal conductivity comparison between different materials used in heat transfer applications.

1.3.1 Thermal conductivity

Thermal conductivity is the most important parameter responsible for enhancing heat transfer. As a result, many experiments have been reported on this property to show how thermal conductivity of fluids are enhanced by dispersion nanoparticles in them. In Table 1-1, which is reconstructed from a review of Wang and Mujumdar [15], a summary of the experimental investigations researchers have done is presented. It is important to note that the highest values of effective thermal conductivity was gained by using carbon nanotubes as reported by Choi et al. [16]. Their work was performed using multi-walled carbon nanotubes (MWCNT) dispersed in oil with a volume fraction of 1 percent. They concluded that the thermal conductivity increased by more than 250 percent which is an enormous amount of increase. It was also discussed in the aforementioned review [15] that there are many factors affecting the thermal conductivity in Nanofluids. An example of the reviewed work regarding this matter is the work of Xie et al. [17], where they studied the effect of different parameters, such as the pH level of the base fluid, the specific surface area of the dispersed nanoparticles, and the thermal conductivity of the base fluid on that of the Nanofluid. It was discussed that the most important factor affecting thermal conductivity of Nanofluids is the concentration of the nanoparticles in the base fluid. As apparent in Table 1-1, many researchers investigated the effect of increasing the percentage of nanoparticles on thermal conductivity of the Nanofluid. All results showed a definite increase in the value of thermal conductivity by increasing the number of dispersed nanoparticles.

Table 1-1: Summary of experimental work on the analysis of thermal conductivity of Nanofluids (Reconstructed from the review of Wang and Mujumdar [15])

Papers of	Nanoparticles	Base Fluid	Maximum thermal conductivity improvement or/and other observations
Eastman et al. [18]	Al_2O_3/CuO/Cu	Water/HE-200 oil	60% for 5 vol% CuO/water
Lee et al. [19]	Al_2O_3/CuO	Water/EG	20% for 4 vol% CuO/EG
Wang et al. [20]	Al_2O_3/CuO	Water/EG/PO/EO	12% for 3 vol% Al_2O_3/water
Das et al. [21]	Al_2O_3/CuO	Water	2-4 fold increase over the range 21°C-52°C
Xie et al. [17]	Al_2O_3	Water/EG/PO	Studied the effect of pH value, Surface area, crystalline phase
Li and Peterson [22]	Al_2O_3/CuO	Water	Studied the effect of volume fraction, and temperature
Xuan and Li [23]	Cu	Water/Oil	Successful suspension of large metallic nanoparticles (Diameter of 100nm)
Eastman et al. [8]	Cu	EG	40% for 0.3 vol% Cu/EG

Hong and Yang [24]	Fe	EG	18% for 0.55 vol% Fe/EG
Patel et al. [25]	Au/Ag	Water/Toluene	Effect of size, temperature, chemical characteristics
Murshed et al. [26]	TiO_2	DW	33% for 5 vol% of TiO_2/Water. Also, studied the effect of nanoparticle size.
Xie et al. [17], [27]	SiC	Water/EG	22.9% for 4 vol% SiC/Water. Also, studied the effect of nanoparticle size.
Choi et al. [16]	MWCNT	Oil	Exceeds 250% for 1 vol% MWCNT/Oil
Biercuk et al. [28]	SWCNT	Epoxy	125% for 1 wt% of SWCNT/Epoxy
Xie et al. [29]	TCNT	DW/EG/DE	19.6% for 1 vol% TCNT/DE
Choi et al. [30]	SWCNT	Epoxy	300% for 3 wt% SWCNT/Epoxy
Wen and Ding [31]	CNT	Water	31% for 0.84 vol% CNT/Water. Also, studied the temperature effect.
Assael et al. [32]–[34]	MWCNT/DWCNT	Water	38% for 0.6 vol% MWCNT/Water. Also, studied the effect of two dispersants on the stability.
Liu et al. [35]	CNT	EG/EO	30% for 2 vol% CNT/EO

1.3.2 Heat capacity

Developing fluids with higher heat capacities than those currently used would have an enormous effect in increasing the efficiency and decreasing the amount of coolant required for many industrial heat transfer processes. Furthermore, the heat capacities of heat storage fluids need to be increased to bring down the cost of many renewable energy technologies, such as waste heat recovery and solar energy.

Although adding metallic nanoparticles to a host fluid increases its thermal conductivity, it sometimes decreases its heat capacity [36]–[38]. Vajjha and Das [36] observed a 20% decrease in specific heat of ethylene glycol/water mixture after adding Zinc-Oxide nanoparticles at a volume concentration of 7%. Zhou and Ni [37] reported a decrease of 40% in specific heat by adding Alumina nanoparticles to water at 22% volume concentration. Namburu et al. [38] added 10% volume fraction of SiO_2 nanoparticles to water and obtained a 12% decrease in specific heat. The fact that nanoparticles decrease the fluid specific heat hinders the possibility of using Nanofluids as efficient coolants in refrigeration systems or otherwise.

On the other hand, several other researchers reported an enhancement in the specific heat by adding nanoparticles [36], [39]–[41]. Ho and Pan [39] observed a maximum enhancement in specific heat of 19.9% when adding a weight concentration of 0.063% of Alumina nanoparticles into HITEC molten salt. Nelson et al. [40] reported an enhancement of 50% after adding 0.6% weight concentration of graphite nanoparticle fibers into PolyAlphaOlefin. Jo and Banerjee [42] reported an increased specific heat of 15% by adding 5 wt% of MWCNT in a carbonate salt eutectic.

To understand the differences between the reported results. The effective specific heat can be estimated by Equation 1-1 which is derived from classical and statistical mechanics [37]. The effective specific heat ($C_{p,nf}$) as apparent in the equation is obtained by averaging the specific heats of both the base fluid ($C_{p,f}$) and the nanoparticle ($C_{p,s}$) according to the nanoparticles volumetric concentrations (φ).

$$\left(\rho C_p\right)_{nf} = (1-\varphi)\left(\rho C_p\right)_f + \varphi\left(\rho C_p\right)_s \quad (1\text{-}1)$$

Where ρ_f and ρ_s are the base fluid and nanoparticle densities, respectively and the Nanofluid density ρ_{nf} is given by

$$\rho_{nf} = (1-\varphi)\,\rho_f + \varphi\,\rho_s \quad (1\text{-}2)$$

Angayarkanni and Philip [43] reported a decreasing trend of specific heat as the concentration of Fe_3O_4 nanoparticles increases into pure Kerosene. According to Equation 1-1, the effective specific heat of the Nanofluid should be less than the specific heat of pure Kerosene (2.01 J/g K) because of the lower specific heat of Fe_3O_4 nanoparticles (0.79 J/g K). Equation 1-1 showed an excellent agreement with the experimental investigations done by Angayarkanni and Philip [43]. Because the specific heat of nanoparticles is less than that of the host fluid, the addition of nanoparticles will decrease the specific heat. However there are other factors affecting the specific heat of Nanofluids which can be further read in the literature, such as aggregation of nanoparticles[44], size, and shape of nanoparticles[45].

1.3.3 Viscosity

Compared with the studies done on thermal conductivity of Nanofluids, there are limited studies on this property of Nanofluids. However, it is of much importance when comes to finding pressure drops in any application where fluid flow is to be utilized.

The most important factor affecting the viscosity of Nanofluids is the nanoparticle concentration. Wang et al. [20] measured the viscosity of Al_2O_3–water Nanofluids at different nanoparticle concentrations. Results showed that the increase of viscosity is proportional to the increase of nanoparticle concentration in the Nanofluids. This is, in fact, a problem, because enhancing the thermal conductivity of Nanofluids is directly proportional to the concentration of the nanoparticles. Hence, a tradeoff is needed between enhancing heat transfer and increasing pressure drops.

A solution for that was proposed by Ding et al. [46] where they found out that using carbon nanotubes as nanoparticles forms a shear thinning behavior in the Nanofluid. That means the Nanofluids can decrease the amount of pressure drop of the flow due to the high shear rate at the wall of the pipe, which results in lower viscosity there.

The influence of nanoparticles concentration and temperature on the viscosity of CNT-water Nanofluids were investigated by Halelfadl et al. [47]. The work reported viscosity data of CNT-water Nanofluids within 3.5% error. They range studied was such that concentrations of 0.0055 vol% to 0.55 vol%, a temperature range of $0 - 40\ ^oC$, and shear rates between 10 to 1000 s^{-1}. The observation of increased viscosity with concentration was confirmed here as well. In addition, the shear thinning behavior was observed above a concentration of 0.055 vol% at high shear rates.

1.4 Nanofluid Applications

Having recognized the importance of Nanofluids as they have enhanced thermal characteristics. It is important to shed some light on their use in applications that may benefit humanity. In this section several applications are to be discussed namely, energy storage, solar absorption, and electronic devices cooling.

1.4.1 Thermal energy storage

The time-based differences of energy availability and energy needs made important the development of energy storage systems. The storage of thermal energy in the form of latent heat has been the course of many energy management research works. The reason of the emphasis on thermal energy is due to the fact that many industrial power plants and solar energy plants or in buildings reject heat as a waste that is never used again [48]. Wu et al. [49] investigated the potential of using Alumina-water Nanofluids as a new phase change material (PCM) for thermal energy storage. The Nanofluid showed promising results namely, a decrease in the supercooling degree of water, and a reduced total freezing time. Because of the high thermal conductivity those nano-enhanced PCMs possess, the cold storage and supply capacity will be greater than the normal PCMs. Copper nanoparticles turned out to be also an efficient additives to normal PCMs to improve their heating and cooling rates [50].

1.4.2 Solar absorption

Solar energy is one of the best sources of renewable energy with less environmental impact. Solar thermal collectors are a well-established technology and it has many applications, such as water heating. However, the efficiency of the existing solar collectors are influenced by many variables. The degree of absorption coefficient of the working fluid plays an important role in absorbing much of the solar irradiation. Recently, the solar collector technology was combined with the Nanofluid technology with the hope to get better efficient solar collectors. Otanicars et al. [51] studied different types of Nanofluids as the working fluids on solar collectors. The highest efficiency improvement obtained was around 5%. Both experimental and numerical results showed a strong increase in the efficiency of solar collectors as volume concentration of nanoparticle increases. This increase in efficiency levels of after adding more particles, which shows a saturation-like behavior. Otanicar and Golden [52] evaluated the overall environmental and economic impacts of using those two technologies together. They concluded that using Nanofluids has a marginally longer payback period but eventually it will have the same economic savings as conventional solar collectors. However, more investigations needs to be done regarding this issue.

1.4.3 Electronic devices cooling

Due to increased density of electronic chips and the trend of designing electronic components as compact as possible, it becomes difficult to solve the problem of heat dissipation from those components. The problems emerging from this trend is that high level of heat is generated while less available spaces for heat removal. In fact, there are two approaches to solve this problem. One is to optimize the space of both the electronic component and the cooling device, such as a simple fan with a heat sink. The other solution is to increase the heat capacity of coolants that can bypass the electronic components, take that heat, and dissipate it elsewhere. Nanofluids offer a solution due to their enhanced thermal conductivity, which means they will provide a coolant with higher heat transfer coefficient. Jang and Choi [53] investigated the design of a new cooler which consists of Nanofluids flowing in microchannel heat sink. Compared to the heat sink containing pure water, Nanofluids showed a better efficient cooling behavior. It was also noticed that the pumping power required to move the Nanofluid is the same as that to move pure water, which suggests that no extra pressure drop is accompanied with adding nanoparticles in such small scale.

1.5 Freezing Phenomenon and Nanofluids

Freezing of water occurs in many engineering and natural processes. One example of the engineering applications of freezing is the artificial ground freezing which is a famous process in civil engineering. It is a process of freezing the soil to prevent leakages of contaminants through the soil to groundwater. This process was used in Fukushima Daiichi nuclear power plant cleanup (refer to the news article at http://www.dailymail.co.uk/news/article-2686462/Fukushima-build-mile-long-wall-ice-crippled-plant-stop-radioactive-water-leaking-Pacific.html).

In addition, freezing occurs naturally in many areas, such as in the poles of the earth. An important unnoticeable natural area where freezing occurs is desert. This might be a surprising fact but it was observed that low humidity areas like deserts can be exposed to large temperature drops: ". . . temperature differences as large as 40^{o}C have been measured for thermally insulated approximate black bodies in the Atacama desert in Chile" [54]. This phenomenon is known as radiative cooling which can occur in deserts at night when the sky is clear.

Using Nanofluids instead of conventional fluids to be frozen in many heat transfer applications can be beneficial due to its enhanced thermal properties. Nanofluids are considered good PCM candidates when comes to the freezing process. The reason is that they overcome many problems with conventional PCM, such as the high degrees of supercooling and the long time of total freezing [49].

In the following sections, three main topics are going to be discussed; supercooling phenomenon, freezing experimental work, and finally freezing numerical work.

1.5.1 Supercooling phenomenon

The freezing phenomenon starts by first what is called as the nucleation process. Nucleation is the process of forming a nucleus; it is the initial step to full crystallization/freezing of the fluid. There are two types of nucleation: heterogeneous nucleation and homogeneous nucleation. The heterogeneous nucleation occurs when there are suspended particles, i.e. nanoparticles in this case, or minute bubbles that provide nucleation sites. On the other hand, homogeneous nucleation occurs without the existence of preferential nucleation sites and is a random event. For example, if there are particles in the fluid or cracks on the wall of the container, heterogeneous nucleation may occur at the freezing point of water (0^oC). However, if we have a pure water, nucleation will be delayed to a lower temperature. Water temperature of less than -30^oC was reported at which homogenous nucleation started [55]. Water existing in its liquid state below the heterogeneous freezing temperature is called super-cooled water.

The supercooling phenomenon drew some attention in food industry. An example is the work done be Coca Cola company where it marketed for a vending machine in UK and Singapore that sells soda products that are super-cooled. As the costumers open those cans of soda they get frozen in seconds making a slush [56].

Jacoby et al. [57] have discovered a liquid crystal that can be engineered such that it can crystallize after controlled time. Researchers are thinking of using this idea in drug delivery in human or animal bodies. The drug is delivered in the liquid crystal to the sick site where a slight controlled change in the environment changes the liquid crystal rapidly to a solidified crystal releasing the drug.

Jinze, Zhenliang, and Hanyan [58] studied the process of nucleation of Alumina-water Nanofluids. Results showed that the degree of supercooling of the Nanofluids decreased with the increase of concentration of nanoparticles. The main rational explanation is that more nucleation sites were present. Mare et al. [59] found out the same result for the same Nanofluid. They also stated that the agglomeration of nanoparticles does not affect the temperature of the freezing point. However, it prolongs the freezing process. Wu et al. [49] found that adding more Alumina nanoparticles did not only decrease the supercooling degree of the Nanofluid but also decreased the freezing time as well.

Hong et al. [60] reported for the first time that adding carbon nanotubes (CNT) to a liquid made up by 50%of water and 50% of ethylene glycol (EG). The nucleation starting temperature was found to be $4-5^{o}C$ lower than that of pure liquid when adding only 0.05 wt.% of CNT.

Mo et al. [61] investigated the supercooling of water when adding TiO_2 nanoparticles. It was confirmed in their work that the degree of supercooling decreases by adding nanoparticles. They also studied another factor affecting the supercooling degree of the Nanofluid namely, the cooling rate by which the Nanofluid is frozen. They noticed that lower cooling rates are accompanied with faster initiation of the nucleus as well as shorter time of total freezing. Mo et al. concluded that there are two mechanisms by which freezing is initiated; volumetric-controlled nucleation (VCN) and surface-controlled nucleation (SCN). The former mechanism is the only mechanism by which homogeneous nucleation takes place while heterogeneous nucleation can occur by the two mechanisms. Both mechanisms of nucleation can co-exist in the case of heterogeneous nucleation but one is dominant over the other. In the aforementioned work of Mo et al., it was concluded that

for high cooling rate and low particle concentration, VCN is dominant and it becomes difficult to heterogeneously nucleate. On the other hand, low cooling rate and high particle concentration increases the diffusion characteristics of the flow, which in turn promotes heterogeneous nucleation, meaning less supercooling of the Nanofluid.

1.5.2 Freezing experimental work

Experimental work is an essential tool to provide reasonable explanations for existing phenomena under controlled environments. Freezing is a phenomenon that has undergone several research work over the years. In a try to study the freezing process and ice formation, Josef Stefan in 1891 published a work titled " The theory of ice formation" [62]. Even though Stefan is well known for his work on radiation heat transfer, where he discovered that the radiated heat is proportional to the forth power of the absolute temperature, his work on ice formation caught a lot of attention as well. The work of Stefan was made to solve the problem of ice formation in the polar seas. The physical definition of his problem was that the sea water was cooled down to its freezing temperature, then at some time the temperature of air above the water goes below the freezing temperature and it keeps steady. Stefan noticed from an experimental observation of the sea that the ice forms from the contacting surface of the water and air. He proposed a one-dimensional differential equation describing this situation. The solution of this basic problem showed that the depth of the ice is proportional to the square root of the elapsed time. The exploration of more complex problems was initiated since then, and this problem was called "Stefan Problem".

After Stefan, many scientists has tried to investigate the freezing phenomenon by fabricating well-controlled environments, as opposed to Stefan where he could control neither the sea nor the air. Among those is the work of Borger and Westwater [63] in which they built a rectangular cavity, filled with water, consisting of adiabatic vertical walls and cooled/heated horizontal walls. It was noticed that the ice forms on the colder side and it advances towards the other sides. The purpose of their experimental work was to measure the solid-liquid interface velocity and temperature during the freezing of water and the melting of ice. Diaz and Viskanta [64] visualized the solid-liquid interface while freezing n-octadecane from the bottom surface of a rectangular cavity. The effect of initial supercooling was found only to delay the nucleation initiation. Hale and Viskanta [65] investigated the solid-liquid interface motion during the freezing and melting from above and below of several different substances in a rectangular cavity suitable for photographing purposes. Cao and Poulikakos [66] studied the effect of the position of the cooling side by changing the inclination angle of the rectangular cavity they made. They found out that when the cooling plate was placed in the bottom, the nucleation initiation was faster, however, total freezing time was the longest. In addition, it was noticed that at an inclination angle of 60^o, the nucleation initiation time was at its maximum compared to other inclinations. The possible explanation they gave is that when the cavity position is placed at the bottom, convection circulations caused by buoyancy forces are negligible and conduction is the main mode of heat transfer. This proves that the freezing time is affected by natural convection in such situations, such that the existence of natural convection delays the freezing initiation and shortens its completion time. Many other experiments on phase change process have been conducted not only in rectangular cavities, but also in a

cylindrical cavity [67], a spherical cavity [68], a wavy cavity [69], and in porous media [70].

Tan et al. [71] studied experimentally the freezing of n-octadecane paraffin wax in a spherical capsule as it gets frozen inside a temperature-controlled freezer. The freezing process was visualized as well as the flow behavior of the wax. It was noticed that at start-up, the freezing was taking place rapidly, however after some time the freezing was slower. The reason is that at the beginning of the freezing process, conduction was the main heat transfer mode, then, after sometime convection became dominant because of the existence of a solid-liquid interface that started from the center of the sphere.

Wu et al. [49] investigated the freezing process of $Al_2O_3 - H_2O$ Nanofluid to evaluate the potential of using this type of fluids in thermal energy storage. After preparing stable samples of different concentrations of Nanofluids, they filled tubes and placed them in a constant temperature bath. The conclusion of their work is that the addition of nanoparticles decreased the supercooling degree remarkably and reduces the total freezing time as well. Adding 0.2wt% of Alumina nanoparticles reduced the total freezing time by 20.5%.

Fan and Khodadadi [72] investigated the potential of using copper oxide nanoparticles in Cyclohexane-based Nanofluids as PCM in freezing. They placed the Nanofluids in a tube that is cooled from the bottom and has a unidirectional freezing characteristic. They observed that the time of freezing was reduced by 5.2% upon adding 2wt% of nanoparticles to the base fluid. They compared their work with a one-dimensional Stephan numerical model and they found a good agreement between results, even though numerical predictions showed slightly underestimations of the results.

1.5.3 Freezing numerical work

Nanofluids have been undergoing experiments for two decades now, while numerical studies are scarce. The contradictory experimental results force scientists to step forward to improve current numerical techniques to be able to solve Nanofluid problems [73]. Generally, the algorithm would be similar to the conventional fluids; however the presence of nanoparticles forces changes in the numerical process when solving the transport equations, for instance, whether to consider Nanofluids as single-phase or two-phase fluids [73]. Furthermore, research groups of Khodadadi and Fan have shown that the contradictory results are caused by the lack of information about the thermophysical properties of Nanofluids [72].

The freezing process is considered difficult to solve numerically due to many reasons. It is considered a three dimensional problem, in most cases, and transient in nature with highly nonlinear boundary conditions. Freezing is also considered as a difficult problem because it belongs to the class of boundary value problems with moving boundaries [74]. Voller and Prakash [75] suggested to use finite difference method with fixed grid approach to solve phase change problems. Additionally, they suggested using suitable source terms in Navier-Stokes equations in order to account for the solid-liquid interface. The fixed grid method or sometimes-called enthalpy-porosity method approach in phase change problems is simply done by introducing a volumetric source term in the transport equations, which will affect the enthalpy solution along with the other variables. This method simplifies the complexity of the phenomenon by eliminating the need to track the interface numerically, which used to be tackled by introducing dynamic meshing. The strategy of the method is based on the fact that the enthalpies of both liquid and solid phases of a material are already

known. Hence, the solution obtained for each grid using the enthalpy equation can lead to knowing the amount of solid and liquid contents in that grid. Knowing that would make determining the solid-liquid interface easy but with approximation errors. Zubkov et al. [76] studied numerically the freezing of water in a round pipe. They used the Semi-Implicit Method for Pressure Linked Equations Revised algorithm (SIMPLER) for solving the continuity, Navier-Sroke's equations, and the energy equation. The fixed grid method was adopted in their work. The convection terms were approximated using the power scheme law.

Khodadady et al. [3] studied numerically the solidification of different particle loadings of Nanofluid in a rectangular cavity with cooled vertical walls. They compared their work to the numerical work of khanafer et al. [77]. Results showed that Nanofluids have great potential for improving thermal energy storage. The method used by Khodadady et al. is the fixed grid method. Sebti et al. [78] investigated the melting of paraffin with copper nanoparticles infused in it in a square cavity heated from one wall. The parameters studied in this work are; nanoparticles volume fraction, size of the cavity, and the temperature difference between the hot wall temperature and the initial temperature of the Nanofluid. Results showed that the molten fraction increases linearly with time at the beginning of the melting process, however, the rate of this increase is decreased with time. In addition, it was noticed that increasing the volume fraction of nanoparticles decreased the melting time. The effect of the volume fraction was observed to be more pronounced at larger cavity sizes and at higher temperature differences. Kashani et al [79] studied the solidification of Copper and n-hexadecane Nanofluid in rectangular cavity. Results showed that using this type of Nanofluids has a great potential in the energy storage. Sebti et al. [80] looked at the

solidification of Nanofluids in a horizontal concentric annuli cooled from the sides. They observed that increasing the volume fraction of nanoparticles enhanced the heat transfer and thus reduced the solidification time. Kashani et al. [69] investigated the solidification of Nanofluids in a wavy cavity. Two parameters were discussed in that paper namely, the cavity waviness and the nanoparticle volume fraction. Jourabianand and Farhadi [81] studied the melting of water and cupper Nanofluids in a semicircular cavity.

1.6 Research Motivations

Our recent literature survey [3], [69], [73], [77]–[82] has shown that there are few published papers dealing with freezing of Nanofluids. In particular, a small number of studies are published on numerical simulations and experimental observations of the process of freezing of Nanofluid. To the author's knowledge there are no papers published that examines the effect the CNT particle loading, and the cavity aspect ratio on the solidification time and the flow process during freezing. In addition, CNT-water Nanofluids thermal conductivity has not been studied for the current prepared samples. In this work, thermal conductivities of two stable samples are measured at different temperatures, including temperatures below the freezing point of the Nanofluids. Finally, Stability of CNT-water Nanofluids is studied for the first time as the prepared samples are frozen to different temperatures.

1.7 Research Objective

In a contribution to a better understanding and to evaluate the potential of using CNT-water Nanofluid as efficient NePCM, The overall objective of the thesis is to investigate experimentally and numerically the freezing process of CNT-water Nanofluid. The specific tasks to accomplish the objective are:

1) To design and construct a suitable experimental setup for studying the freezing process of CNT-water Nanofluid.
2) To carry out an experimental parametric study on the freezing of CNT-water Nanofluid by varying the CNT concentration.
3) To develop a computational fluid dynamic model that is capable of studying the freezing process of CNT-water Nanofluid. This model will be validated against the experimental results obtained during this study.

1.8 Research Methodology

The methodologies that are employed in this thesis in order to achieve the mentioned objectives include both experimental and numerical tools. These are:

1) A freezing experimental setup containing evenly spaced thermocouples mounted along the freezing front direction to record continuously the transient temperature variations during the freezing process of CNT-water Nanofluid, which in turn allows determination of the progress of the freezing front.

2) Multi-walled Carbon Nanotubes (MWCNT), purchased from Chengdu Organic Chemicals Co. Ltd. (TimesNano), China.

3) Gum Arabic (GA), purchased from SIGMA ALDRICH, USA.

4) Ultrasonic processor with a model number VC 505, purchased from SONICS & MATERIALS, INC.

5) Steady-state thermal conductivity measuring device with a model number FOX50 110^{o}C, purchased from LaserComp-TA Instruments, Massachusetts, United States.

6) A refrigeration unit, purchased from Julabo, a Temperature Control Company with a model number FP51-SL. The refrigeration unit is used to circulate ethylene glycol at low temperatures.

7) Data acquisition unit (DAQ) with a model number NI 9162, purchased from National Instruments, USA.

8) ANSYS FLUENT V14.5, a numerical commercialized software, made especially for computational fluid dynamic purposes, to mimic numerically the freezing experiment and to do further numerical parametric studies.

CHAPTER 2

NANOFLUIDS PREPARATION AND THERMOPHYSICAL PROPERTIES EVALUATION

The main objectives of this thesis is to investigate experimentally and numerically the freezing process of Nanofluids. Therefore, in this chapter, discussions and details of the preparation of Nanofluids, and evaluation of their thermophysical properties are presented. Thermal conductivities of the tested Nanofluids were measured experimentally, while all other properties were obtained from predictive models. The importance of obtaining thermophysical properties is to be able to simulate the freezing process numerically, see Chapter 5.

2.1 CNT-Water Nanofluid Preparation

Raw Multi-Walled Carbon Nanotubes (MWCNT) were used in this work. The specifications of the purchased MWCNT state that the nanotubes have an outer diameter of 10 to 20 nm, a length of 10 to 30 μm, a specific surface area of 200 m^2/g, and 95% MWCNT purity percentage. A sample of the MWCNT is shown in Figure 2-1.

Figure 2-1: Sample of the used MWCNT of purity of 95%, only one gram is shown in the figure.

As discussed in the literature review, and as can be clearly noticed that in this work, the two-step preparation method was used. The second step is dispersing the nanoparticles in tap water, as it is the base fluid in this work. In order to do so, two quantities were prepared corresponding to two different percentage loadings of MWCNT. Weight percentages of 0.3 wt%, and 1 wt% of MWCNT were added to tap water. A similar amount of Gum Arabic (GA) was mixed with the needed amount of MWCNT. The combination of GA, MWCNT, and sweet tap water was sonicated for about an hour using a probe sonicator, displayed in Figure 2-2. The sonication frequency was set to 20 kHz at 750 W in order to have a better sustainable mixture. The reason of adding GA to the mixture is to enhance the stability of the Nanofluid, as it is considered a good surfactant, as discussed in the literature review chapter. In addition, this surfactant has a minimal effect on the properties of the prepared Nanofluid as discussed in the work of Manasrah [1].

To assess the stability of the prepared Nanofluid quantities, three bottles were filled and left on a table for more than six months. Checking the sedimentation by the eye showed that they are still stable, i.e. MWCNT neither stuck on the bottle walls nor agglomerated on the bottom of the container. Since the experimental work to be done does not involve high-speed movement of the Nanofluid, centrifugation method, discussed previously, is not necessary.

Figure 2-2: Probe sonicator device used in preparing the Nanofluids.

2.2 Thermophysical Properties Evaluation

In this section, thermophysical properties of the used Nanofluids are evaluated. First, a detailed presentation of one measured thermophysical properties is given namely, thermal conductivity. Then, some of the predictive models used in estimating thermophysical properties of Nanofluids are discussed and compared to the measured values. Finally, a summary of the thermophysical properties is given for further utilization in the numerical model to be discusses in the next chapter.

2.2.1 Measurements of thermal conductivity

In the following paragraphs, thermal conductivity was measured for the two prepared samples and tap water sample as a base fluid. The measurements were taken at different temperatures, in order to observe differences, if any.

There are many methods by which sample's thermal conductivity can be measured depending on the state, and type of the material. Those methods can be categorized to two broad classes; transient and steady state methods. The transient techniques provide a rapid way of measuring thermal conductivities within a short time. However, the steady-state techniques requires a long waiting time to establish a thermal gradient over a specimen placed between two constant-temperature plates. In this work, a commercialized steady-state device was used to measure thermal conductivities of the prepared Nanofluids at different temperatures. The device, which can be seen in Figure 2-3, is model FOX50 110^{o}C, purchased from LaserComp-TA Instruments, Massachusetts, United States. The accuracy in measuring thermal conductivity by this device is said to be 3.5%. The range of measured temperature is from room temperature 25^{o}C to -5^{o}C. Figure 2-4 presents the

obtained results from the device in a normalized form, relative to the base fluid's thermal conductivity. It can be noticed that upon adding more MWCNT, thermal conductivity is enhanced. A maximum enhancement of 4.2% was observed with a weight percentage of 1 wt% at a temperature of 25^{o}C. The Nanofluid showed a jump in thermal conductivity upon freezing. Measured values of thermal conductivities of the base liquid as well as the Nanofluids are presented in the summary of this section.

Figure 2-3: Device of FOX50 110^{o}C, used for measuring thermal conductivity of working liquids.

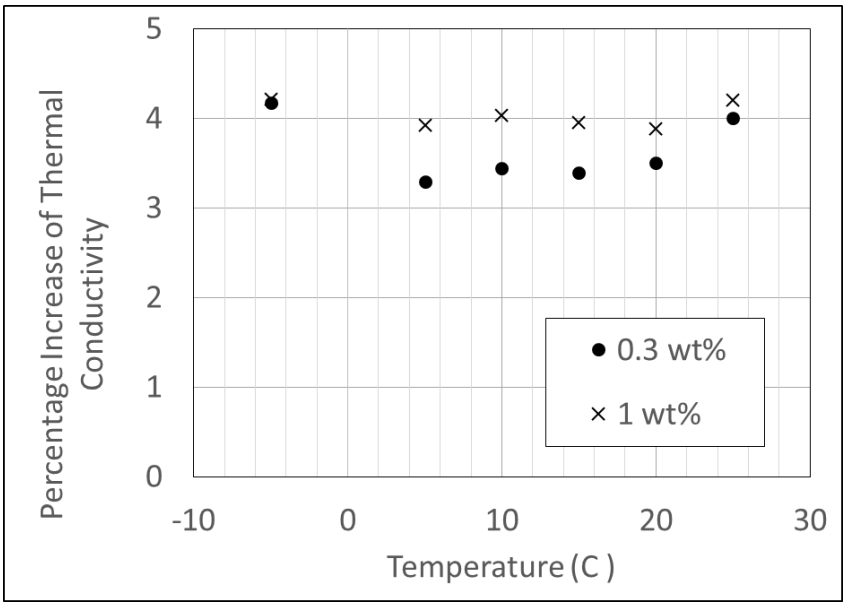

Figure 2-4: Percentage increase of thermal conductivity of different CNT weight loadings compared to thermal conductivity of water.

2.2.2 Effective thermophysical predictive models

Despite the fact that Nanofluids are considered as two-phase fluids, it has been discussed by many researchers that they can be treated as homogeneous fluids with effective thermophysical properties accounting for the presence of the nanoparticles. Even though thermal conductivity was measured experimentally, this properties is also evaluated using different predictive models available in the literature. The reason behind that is to determine the best model that fits the experimentally obtained properties. Other thermophysical properties, such as specific heat, density, viscosity, latent heat of fusion, and thermal expansion coefficient are obtained by the available models. Summary of numerical values of thermophysical properties can be found in the summary of this section. It is important to note that properties are obtained on a temperature range that is above the freezing point of water, because it is the range important for simulating natural convection in Chapter 5.

(a) Density:

Many researchers have measured the density of different Nanofluids, including MWCNT-water Nanofluids [47], [83]. It was found that the correlation developed based on the mixing theory by Pak and Cho is a valid one in determining the effective Nanofluid density [84]. The effective density is given by

$$\rho_{nf} = (1 - \varphi_{CNT} - \varphi_{GA})\,\rho_w + \varphi_{CNT}\,\rho_{CNT} + \varphi_{GA}\,\rho_{GA} \quad (2\text{-}1)$$

Where φ is the volume concentration of CNT particles in the Nanofluid, ρ is density of material. Subscripts CNT, GA and w stand for Carbon nanotubes, Gum Arabic, and water, respectively. The density of CNT particles is taken as 2000 kg/m^3 (http://www.doiserbia.nb.rs/img/doi/0354-9836/2015%20OnLine-First/0354-

98361500028G.pdf) , and ρ_{sur} is density of Gum Arabic is taken as 1400 kg/m^3 (http://www.merckmillipore.com/INTL/en/product/Gum-arabic,MDA_CHEM-104228?ReferrerURL=https%3A%2F%2Fwww.google.com.sa%2F).

Because this thesis work intends to study the freezing process with the existence of natural convection, it is customary to express the Nanofluid's density as a function of Temperature. It is assumed that only density of water to change with temperature, while CNT and GA densities are constant, which is a valid approximation for low temperature changes. Density of water is well established in literature; hence, curve fitting of water density was performed to obtain the best-fitted polynomial given as

$$\rho_w = -9965.954931 + 165.8045156T - 1.009240881T^2 + 3.0959333 \times 10^{-3}T^3 - 4.7846647 \times 10^{-6}T^4 + 2.9705375 \times 10^{-9}T^5 \quad (2\text{-}2)$$

Where T is temperature in Kelvin. Notice that the equation is lengthy and the reason is that it is the best fit of the density variation of water, taking into account the density inversion of water at 4℃, discussed in the previous chapter. Density of water as well as the tested Nanofluids are illustrated in Figure 2-5.

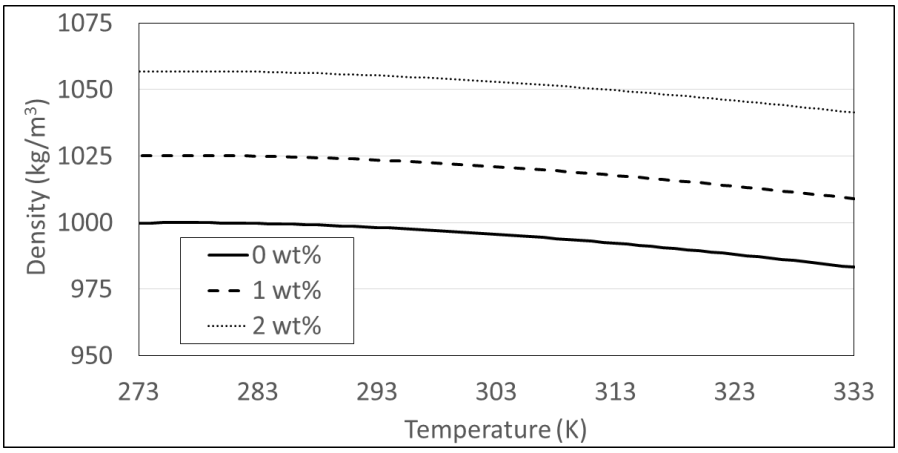

Figure 2-5: Density of different CNT weight loadings at different temperature values.

(b) Viscosity:

Viscosity of Nanofluids have been studied a lot since it is important in determining pumping power in heat exchangers and pipelines. Number of models have been tried to estimate the viscosity, however, a few were successful in doing so. Ganesh et al. [83] presented experimental measurements of viscosity of CNT-water-ethylene-glycol and compared different models to those values. It was found that all compared models were successful in estimating the viscosity of Nanofluids at low CNT concentrations. In addition, in that work, it was noticed that CNT Nanofluids are Newtonian at lower concentrations and low shear rates. Thus, the model of Brinkman is used, which expresses Nanofluid's viscosity as

$$\mu_{nf} = \mu_w/(1 - \varphi_{CNT} - \varphi_{GA})^{2.5} \quad (2\text{-}3)$$

Where μ_w is the viscosity of water, which can be expressed as a function of temperature. Figure 2-6 shows the viscosity values of water as well as Nanofluids at different temperatures.

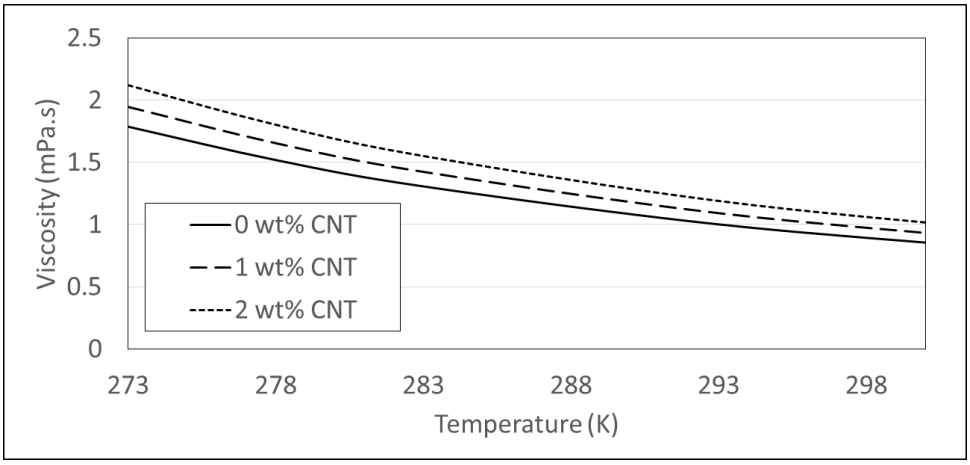

Figure 2-6: Viscosity of different CNT weight loadings at different temperature values.

(c) Latent heat of fusion:

Latent heat of solidification is a property of water only because water is the only material that solidifies in this phase change problem. However, due to the change of the structure of water molecules upon adding CNTs and GA, many researchers have used the traditional effective medium theory, which states that latent heat decreases linearly by adding nano-structured material [85], [86] . The following relation is used to calculate latent heat of fusion within 10% unaccounted-for error

$$L_{nf} = (1 - \theta_{CNT} - \theta_{GA})L_w \quad (2\text{-}4)$$

Where θ is a weight/mass concentration. The weight concentrations of CNT and GA are similar in value.

(d) Thermal expansion Coeffecient:

Since thermal expansion coefficient of Nanofluid is an extensive property, i.e. changes with mass of the sample, a mass-averaging is suggested to be used as follows [86]

$$\beta_{nf} = (1 - \theta_{CNT} - \theta_{GA})\beta_w + \theta_{CNT}\beta_{CNT} + \theta_{GA}\beta_{CNT} \quad (2\text{-}5)$$

Where β is thermal expansion. Thermal expansion of CNT have not be confirmed but it falls within the range of $2.7 \times 10^{-6} - 4.4 \times 10^{-6}\ 1/K$, and average value was considered in this study (http://imechanica.org/node/9962). Even though thermal expansion coefficient of GA is important to account for, its value was not found in literature; hence, it is going to be omitted. Thermal expansion of water was obtained by

$$\beta_w = -\frac{1}{\rho}\frac{d\rho}{dT} \quad (2\text{-}6)$$

(e) Specific Heat:

Specific heat of CNT Nanofluids have not been studied thoroughly; however, in this paragraph a trial to estimate specific heat of the used Nanofluids is presented. O'Hanley et al. [87] suggested a model that uses a mass-averaging technique to assure thermodynamic equilibrium in the Nanofluid, given as

$$C_{p_{nf}} = \frac{\varphi_{CNT}\left(\rho_{CNT}C_{p_{CNT}}\right) + (1-\varphi_{CNT}-\varphi_{GA})\left(\rho_w C_{p_w}\right)}{\varphi_{CNT}\rho_{CNT} + (1-\varphi_{CNT}-\varphi_{GA})\rho_w} \qquad (2\text{-}7)$$

Where C_p is specific heat capacity. It can be noticed that GA's specific heat is neglected, since its effect on the total specific heat is negligible [88]. Specific heat of MWCNT is similar to that of Graphite according to the work of [89], hence a value of 0.71 KJ/kg-K ins used and assumed to be constant over the range of the experimental and numerical work (http://www.engineeringtoolbox.com/specific-heat-solids-d_154.html). Specific heat of water is assumed constant with respect to temperature, since the variations do not exceed 0.5% if an average value of 4.1975 KJ/kg-K is used over a range of temperature between 60 ℃ and 0 ℃.

(f) Thermal Conductivity:

Xue [90] discussed two different models of evaluating thermal conductivity in CNT-based composites namely CNT-oil and CNT-decene. The models of the respective order are given as

$$k_{nf} = k_w \frac{1 - \varphi_{CNT} + \left(\frac{4\varphi_{CNT}}{\pi}\right)\sqrt{\frac{k_{CNT}}{k_w}}\, tan^{-1}\left(\frac{\pi}{4}\sqrt{\frac{k_{CNT}}{k_w}}\right)}{1 - \varphi_{CNT} + \left(\frac{4\varphi_{CNT}}{\pi}\right)\sqrt{\frac{k_w}{k_{CNT}}}\, tan^{-1}\left(\frac{\pi}{4}\sqrt{\frac{k_{CNT}}{k_w}}\right)} \tag{2-8}$$

$$k_{nf} = k_w \frac{1 - \varphi_{CNT} + 2\varphi_{CNT}\frac{k_{CNT}}{k_{CNT} - k_w} ln\frac{k_{CNT} + k_w}{2k_w}}{1 - \varphi_{CNT} + 2\varphi_{CNT}\frac{k_w}{k_{CNT} - k_w} ln\frac{k_{CNT} + k_w}{2k_w}} \tag{2-9}$$

Where Xue suggested that the thermal conductivity of CNT is in the range of 600-3000 W/m-K. Xue proved that the first equation works for CNT-oil based Nanofluids and the latter suits the CNT-decene Nanofluids. However, in the current work both models were tried and compared to the obtained values using the two models as in Table 2-2. It was found that a combination of thermal conductivity of 600 W/m-K and the CNT-oil model yield the lowest error value in estimating CNT-water thermal conductivity of 4.18%.

2.2.3 Summary of thermophysical evaluation of Nanofluids

Table 2-1 presents the numerical values of the average specific heat obtained by Equation 2-7. A main conclusion drawn from the specific heat capacity results is that specific heat capacity is influenced by seeding the base fluid with MWCNT particles. The model given by equation 2-7 shows a decreasing trend by adding more CNT particles.

Table 2-1: Summary of numerical values of the average specific heats of different Nanofluids.

CNT weight concentration (wt%)	Effective solid specific heat capacity (KJ/kg-K)	Effective liquid specific heat capacity (KJ/kg-K)
0	2000	4.1975
1	1949.4	4.0607
2	1900.77	3.9292

Table 2-2 shows the values of thermal conductivity of water as well as the tested Nanofluids. It is shown that adding more CNT particles enhances thermal conductivity of the base fluid by as much as 25% by adding 1 wt% of CNT. Furthermore, Equation 2-8 can be used to estimate thermal conductivity of the tested CNT-water Nanofluids within a minimal error.

Table 2-2: Summary of numerical values of thermal conductivities of different Nanofluids.

Temperature (K)	Thermal Conductivity (W/m^2-K)						
	Water	0.3 wt% CNT-water			1 wt% CNT-water		
	Measured	Measured	Eq.2-8	Eq.2-9	Measured	Eq.2-8	Eq.2-9
298	0.5633	0.5859	0.6058	0.7786	0.581	0.7056	1.2832
293	0.5593	0.5789	0.6015	0.7738	0.581	0.7007	1.2767
288	0.5522	0.5709	0.5940	0.7653	0.574	0.6921	1.2651
283	0.5440	0.5628	0.5853	0.7557	0.566	0.6822	1.2519
278	0.5369	0.5546	0.5778	0.7472	0.558	0.6736	1.2403
273	0.7643	0.6183	0.8192	1.0139	0.601	0.9480	1.5989
268	2.1620	2.2523	2.2902	2.5721	2.253	2.5911	3.5328

Table 2-3 presents the numerical values of the obtained density and viscosity of water and the two tested Nanofluids. Density and viscosity are increased upon increasing CNT particles; however, the trend of property behavior with respect to temperature is similar in all cases.

Table 2-3: Summary of numerical values of density and viscosity of different Nanofluids.

Temperature (K)	Viscosity (mPa.s)		
	Water	0.3 wt% CNT	1 wt% CNT
298	0.8784	0.9011	0.9813
293	0.9888	1.0144	1.1047
288	1.1340	1.1633	1.2669
283	1.3140	1.3480	1.4680
278	1.5289	1.5684	1.7080
277	1.5760	1.6167	1.7606
276	1.6245	1.6665	1.8149
275	1.6745	1.7178	1.8706
274	1.7258	1.7704	1.9280
273	1.77849	1.8245	1.9869

Finally, latent heat of fusion is presented in Table 2-4. It is observed that latent heat of fusion decreases upon adding more CNT particles, which hinders the use of Nanofluids as a phase change material for energy storage, assuming Equation 2-4 is accurately estimating those values. Experimental measurements are needed to evaluate this property correctly.

Table 2-4: Summary of numerical values of latent heat of fusion of different Nanofluids.

CNT weight concentration (wt%)	Latent heat of fusion (J/kg)
0	335000
1	328300
2	319670

2.3 Stability of Nanofluids

It is important to test the stability of the used Nanofluid under low temperature environments. Therefore, another experimental procedure was followed for this matter. Glass cylindrical containers were filled with 100 grams of tested Nanofluids. A thermocouple was inserted in the container to monitor the temperature of the sample under the test upon cooling. The container was sealed so that vapor will not be allowed to escape from the top of the container. Two Nanofluids were prepared and put under the test, namely with CNT concentrations of 0.3 wt% and 1 wt%. The containers were placed inside a constant temperature bath, described in the previous chapter. Placing the two samples together and monitoring their temperatures assures that they are exposed to a similar environment and initial conditions.

Figure 2-7 shows an interesting sample of temperature readings of two samples upon cooling to a temperature of -10 ^{o}C. The samples were water only and another one with a 0.3 wt% of CNT-water Nanofluid. One may notice that both samples experienced a similar cooling rate behavior before freezing. Assuming they were exposed to a similar cooling power, this result means both samples possess approximately the same specific heat capacity. However, as discussed in the predictive models adding more CNT particles decreases the specific heat. Thus, it is really needed to measure the actual specific heats of CNT-water Nanofluids before using the predictive models. Another as-important note from Figure 2-7, is the fact that upon adding CNT particles the supercooling degree is was reduced by 2 ^{o}C saving about two minutes on total freezing time.

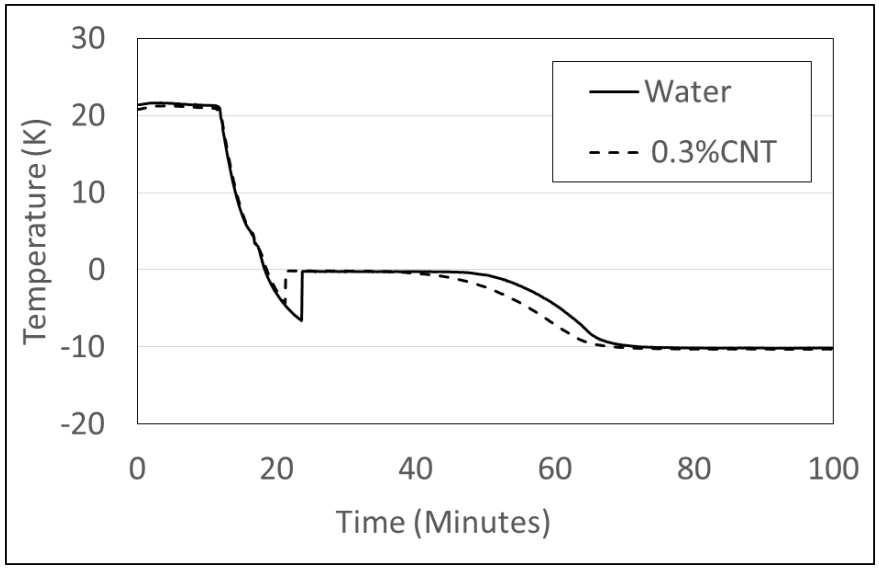

Figure 2-7: Sample of temperature readings of two tested samples showing the reduction of supercooling degree by adding CNT to water.

Figure 2-8 shows a sample of photos taken of the containers before the freezing process of samples with CNT concentrations of 0.3 wt%, and 1 wt%. The Nanofluid samples in this photo was frozen in a container to a temperature of about -10 ^{o}C. Figure 2-9 shows photos of one sample with 0.3wt% CNT concentration after one day from the freezing process. In this figure, the sample was taken out and placed in a tilted holder to visualize how Nanofluids disintegrate completely from water upon freezing. Two hypotheses were proposed as explanations of the destabilization of Nanofluids. First, it was thought that during the freezing process, the solid-liquid front acts to swap out all particles suspended in water. Another hypothesis is that the GA surfactant fails to withstand low temperatures.

Figure 2-8: Photos of the containers containing the tested Nanofluids before freezing process.

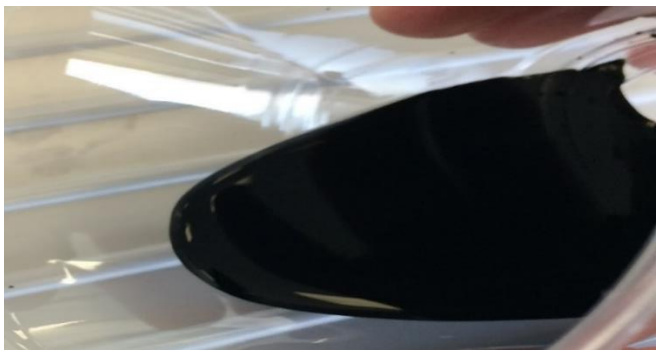

(a)

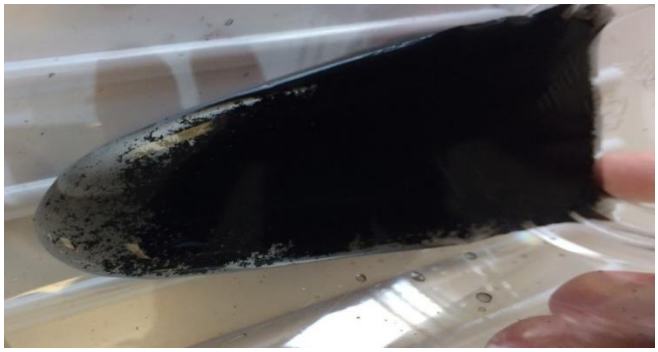

(b)

Figure 2-9: Photos of Nanofluid with 0.3 wt% CNT concentration placed in a tilted holder one day after freezing to a temperature of -10 ^{o}C.

Figure 2-10 shows a photo of a 0.3 wt% CNT-water Nanofluid frozen to a temperature of -10 ^{o}C removed from the container while frozen. The photo shows that CNT particles are still homogenously distributed and were not swapped out of water, thus the first hypothesis fails to explain the instability problem. The efficiency of the used surfactant remains the only explanation. In order to understand the mechanisms of full disintegration due to surfactant efficiency, samples of Nanofluids were tested under different temperatures namely 0 ^{o}C, -5 ^{o}C, and -10 ^{o}C.

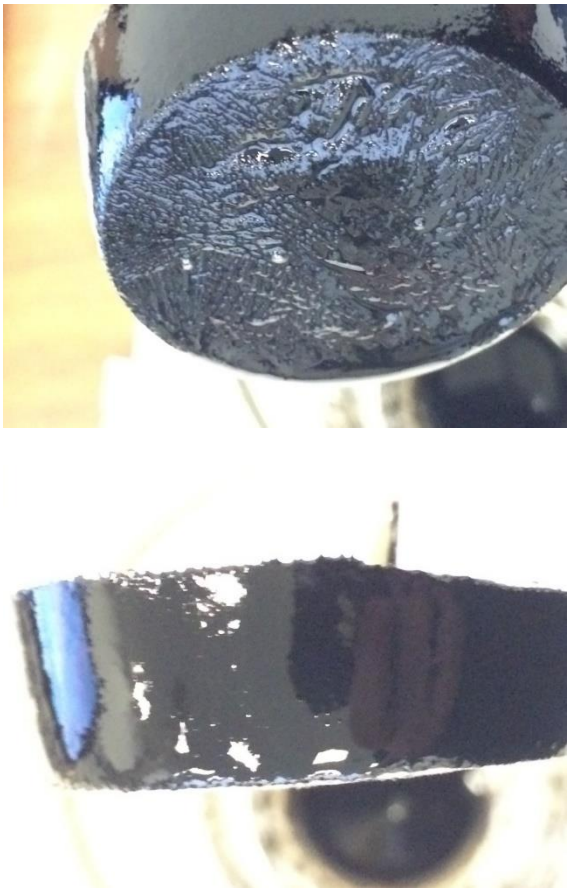

Figure 2-10: Photo of a frozen sample of Nanofluid with 0.3 wt% CNT showing the homogeneity of CNT distribution.

Figure 2-11 depicts photos taken of the samples one day after the freezing process. It can be noticed that samples cooled to the critical temperature did not show any sign of instability; however, further cooling to lower temperatures increases the tendency of Nanofluids to destabilize. Figure 2-11 shows also that adding more CNT particles increases the possibility of the Nanofluid destabilizing. This is shown by comparing the samples of 0.3 wt% and 1 wt% cooled down to a temperature of -5 ^{o}C. In that case, Nanofluid with the lower CNT concentration did not destabilize while the higher concentration showed a beginning of instability and agglomeration is clear near the surface. Further cooling to -10 ^{o}C shows that both Nanofluids are instable due to the probable failure of GA to withstand low temperatures as explained earlier.

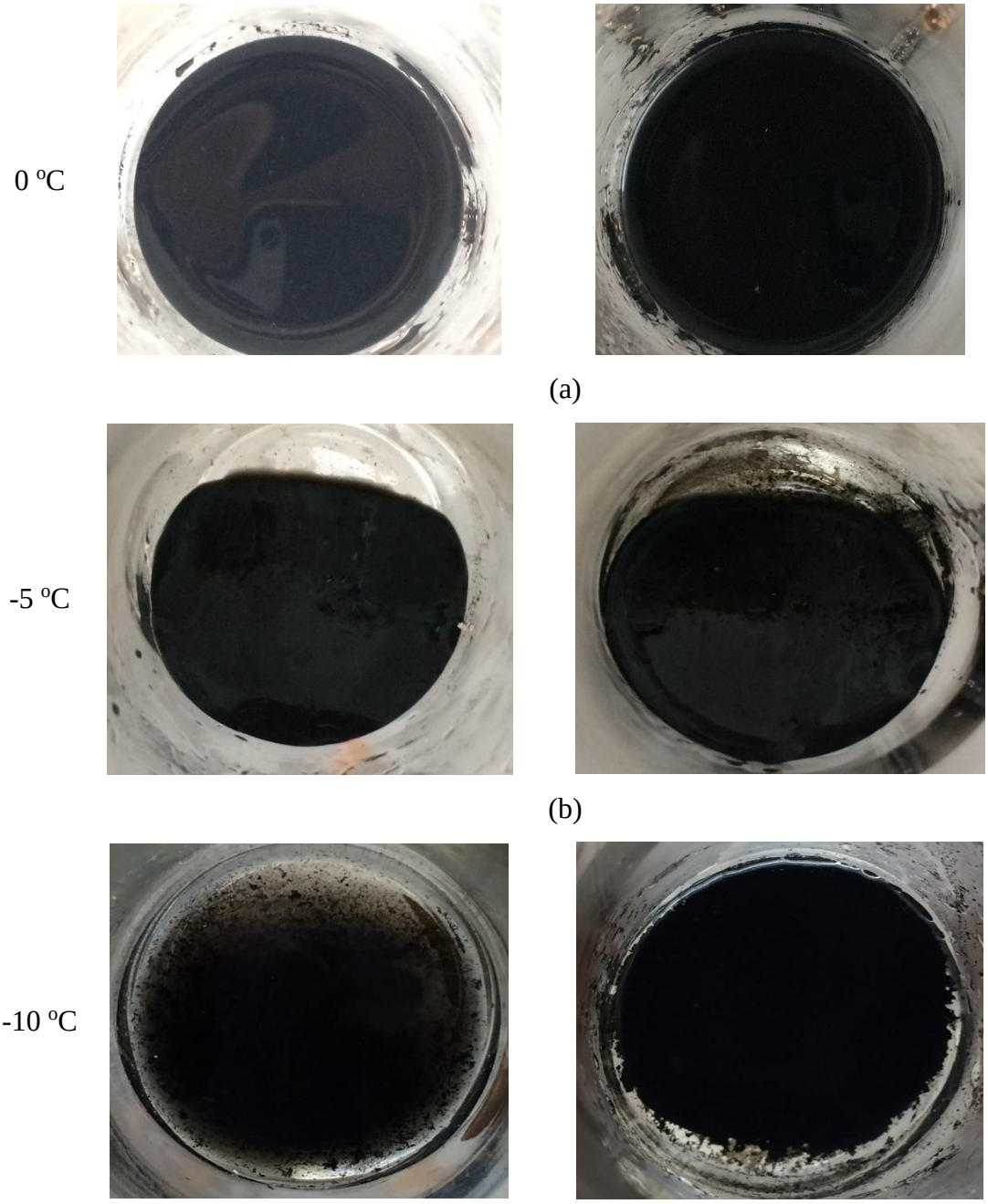

Figure 2-11: Photos of the tested samples one day after the freezing to temperatures of (a) critical temperature, (b) -5 ºC and (c) -10 ºC.

CHAPTER 3

EXPERIMENTAL INVESTIGATIONS

In this chapter, a detailed look at the experimental work will be presented. One of the main objectives of this thesis is to investigate experimentally the freezing process of Nanofluids with and without the existence of natural convection. Therefore, an experimental set-up was made in order to study the effect of different aspects on the freezing process. In the following sections, discussions and details of the problem formulation, experimental set-up and instrumentation, experimental procedure, and finally results are presented.

3.1 Design of Experiment

It is important that prior to performing any experimental measurements that the experiment is well designed in order to optimize both time and effort. In this section, the problem is first formulated clearly highlighting the main parameters to be studied. Then, the experimental set-up as well as instrumentation are discussed.

3.1.1 Problem introduction

As can be noticed from the literature review, there is a lack of experimental information in the topic of Nanofluids freezing, especially CNT-water Nanofluids. It is therefore intended to study this topic in detail. In addition, it was discussed that the fact that using conventional PCM in latent heat thermal energy storage has many shortcomings. One of the main disadvantages is the supercooling phenomenon that prolongs the nucleation initiation. The supercooling phenomenon becomes less pronounced as natural convection takes place, as discussed earlier. In this thesis, the freezing phenomenon of CNT-water Nanofluid is going

to be observed experimentally with and without the existence of natural convection in order to highlight the effect of the existence of nanoparticles on the freezing process of the new-made NePCM.

A three dimensional box was made where CNT-water Nanofluid is in its cavity side. The main characteristic of this box is that it can be used to introduce or suppress natural convection in the Nanofluid as it is being frozen. Natural convection can be introduced if one vertical wall is kept at a temperature lower than the freezing temperature introducing a temperature gradient between the liquid initially and the freezing front leading to natural convection circulations in the test cell. The suppression of natural convection can be made by making the cooled wall at the bottom of the cavity. Another characteristic of the test cell is that it allows easy visualization of the freezing front as it advances in the Nanofluid. Furthermore, temperature measurements, in the direction of the freezing front movement, were taken at different locations inside the test cell.

3.1.2 Problem formulation

It is very important to design every experiment before starting the runs. Designing the experiment starts by knowing exactly what the objectives of the experiment are. In this thesis, the objective of the experimental work is to know the effect of CNT concentration in the Nanofluid on the freezing process. This aspect is going to be tested with and without the existence of natural convection. In order to test different CNT concentrations, synthesizing different CNT-water Nanofluids was one task of this thesis work, and it was discussed in a previous chapter.

The second important aspect in performing experiments is to know exactly the dependent variables that are going to be observed upon changing the aforementioned parameter, i.e. CNT concentration as an independent variable. In this experiment, it was intended to observe the temperature readings at different locations in the test cell. Moreover, a side task of this thesis was to visualize, using a high resolution camera, the freezing front at different times of the experiment. However, only photos of water freezing were possible because the Nanofluid used is black which made it impossible to take photos.

3.1.3 Experimental set-up and instrumentation

The experimental work focused on studying the freezing of CNT-water Nanofluids in a box with and without the existence of natural convection. For that purpose to be accomplished an experimental set up was made and it can be seen in Figure 3-1. The set up consists of a cubical test cell and a refrigeration unit with necessary hose connections. The arrangement of the entire experimental setup is shown as a schematic diagram in Figure 3-2.

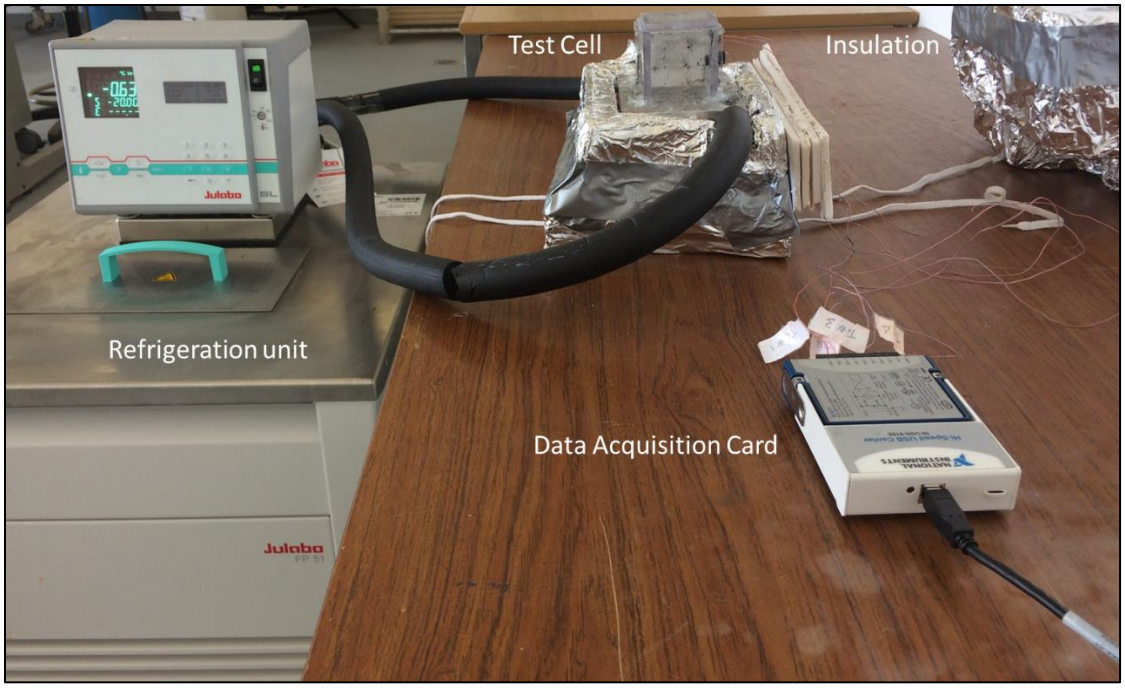

Figure 3-1: Photograph of the experimental set-up arrangement and instrumentation

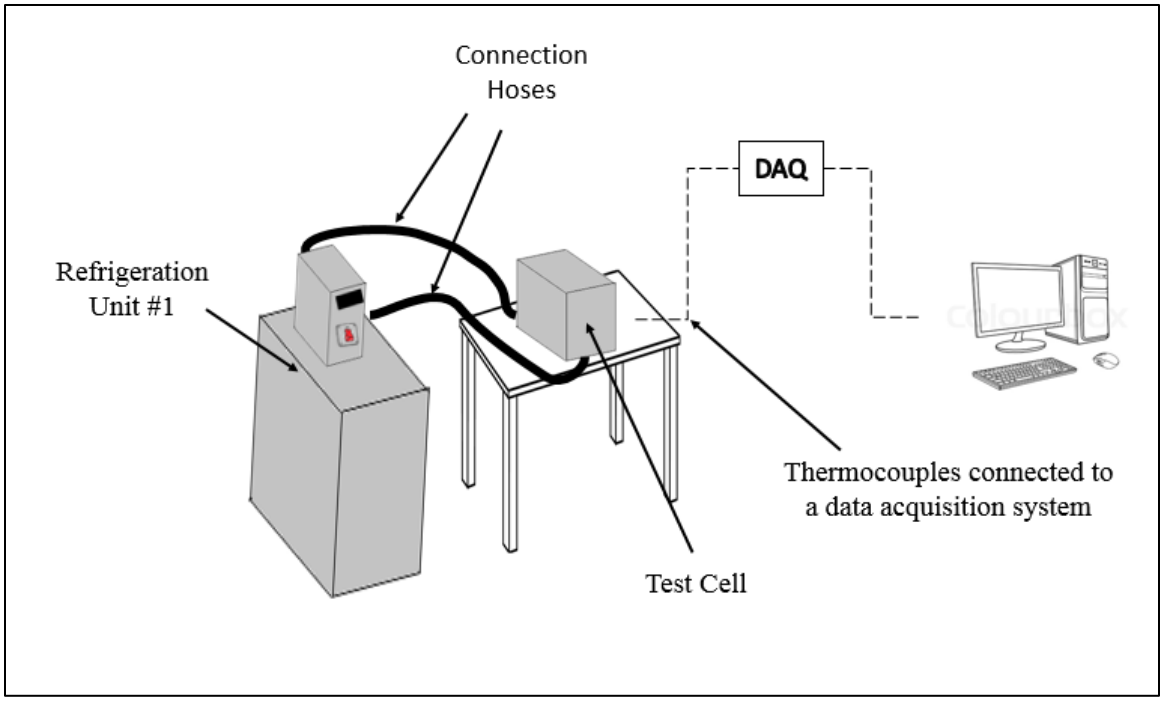

Figure 3-2: Sketch of the experimental set-up and instrumentation.

The test cell was made of one cooling plate and five windows, as can be seen in Figure 3-3. The dimensions of the test cell cavity are 5 cm × 5 cm × 6 cm, corresponding to a volume of 150 mL. Those dimensions were chosen such that a two dimensional freezing process takes place.

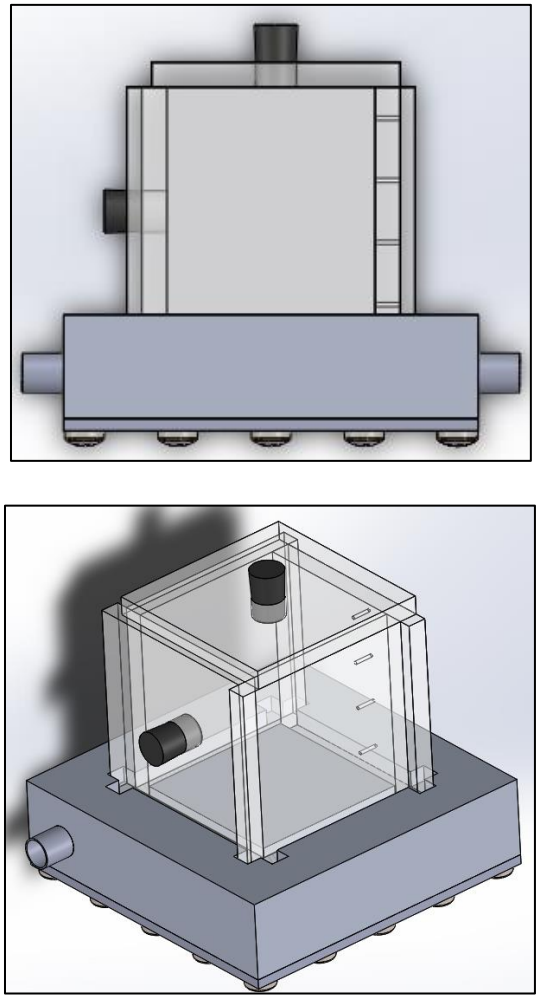

Figure 3-3: Three-dimensional view of the designed test cell with details indicated.

The cooling plate was made of an Aluminum bar, to ensure good thermal conductivity and lightweight for easy handling. As depicted in Figure 3-4, nine 6-mm-wide channels were milled using a CNC machine for the coolant to flow through, i.e. establishing a constant temperature on the cooling plate.

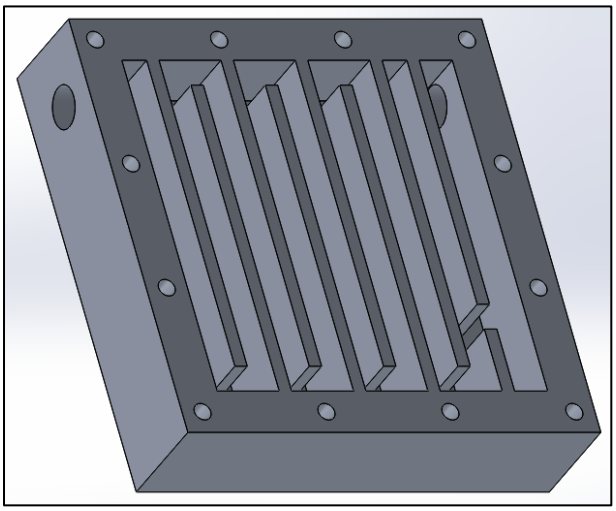

(a)

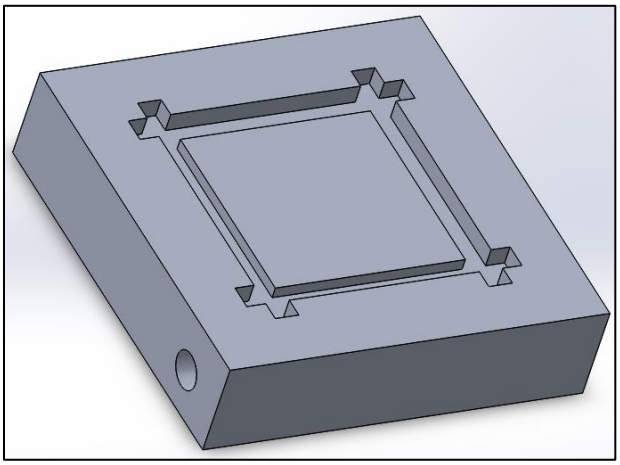

(b)

Figure 3-4: General View of the two sides of the cooling plates; (a) Channels side and (b)Cavity side, respectively.

The coolant was supplied with a reasonable flow rate from a refrigeration unit to ensure a better thermal uniformity of the cooling plate. The refrigeration unit is new and claimed to have a thermal stability of 0.05 ^{o}C. On the other side of the cooling plate, with which the Nanofluid or water are in contact, slots were made for the windows to be placed in. The test cell was designed such that it gives the capability to investigate the freezing process both by thermocouples and visually by observing the freezing front. Four windows were made of Plexi-glass of 6 mm thickness to have a better visualization of the freezing front of water. Compressed Styrofoam with a thickness of 6 cm was used as an insulation of the test cell. The insulation was removed occasionally for a short time to take photos if needed. From the literature review made, it is evident that freezing front or solid-liquid interface is present in such cases. Hence, one of the Plexi-glass windows was utilized for observing the freezing front as it advances in the tested liquid. Another Plexi-glass window was used to measure the temperature distribution at specific locations as the freezing process takes place. Four 1-mm holes were drilled in that Plexi-glass in a direction perpendicular to the cooling plate, at distances of 5.5 mm, 20.5 mm, 35.5 mm, and 50.5 mm, respectively, shown in Figure 3-5. The reason of making those holes is to be able to read temperature in the direction of the freezing front movement, which will help in predicting the position of the solid-liquid front. Two-dimensional drawings of the detailed specification of the test cell can be found in Appendix A.

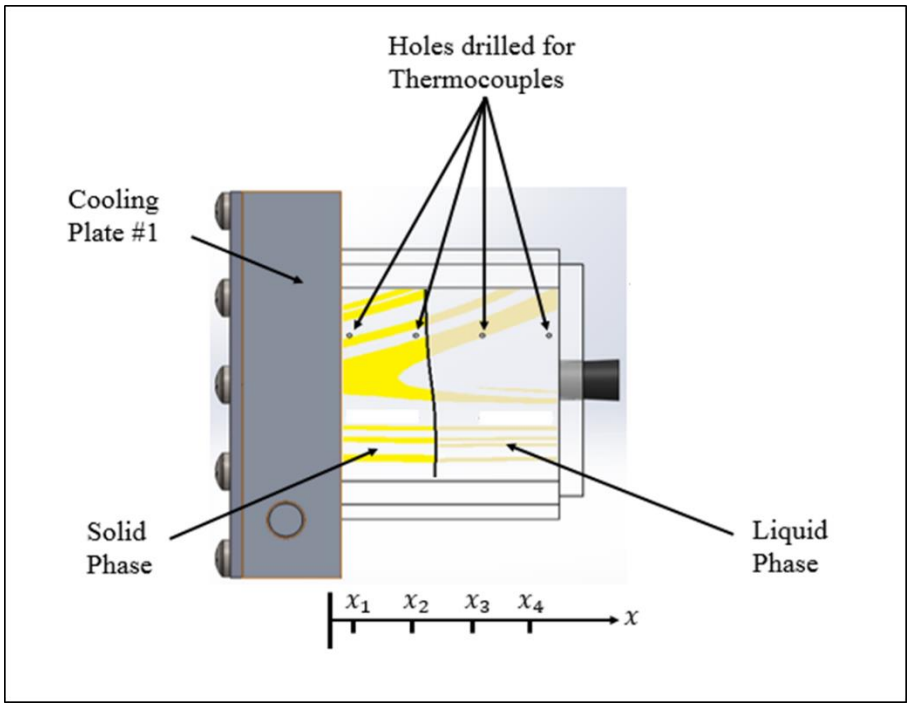

(a)

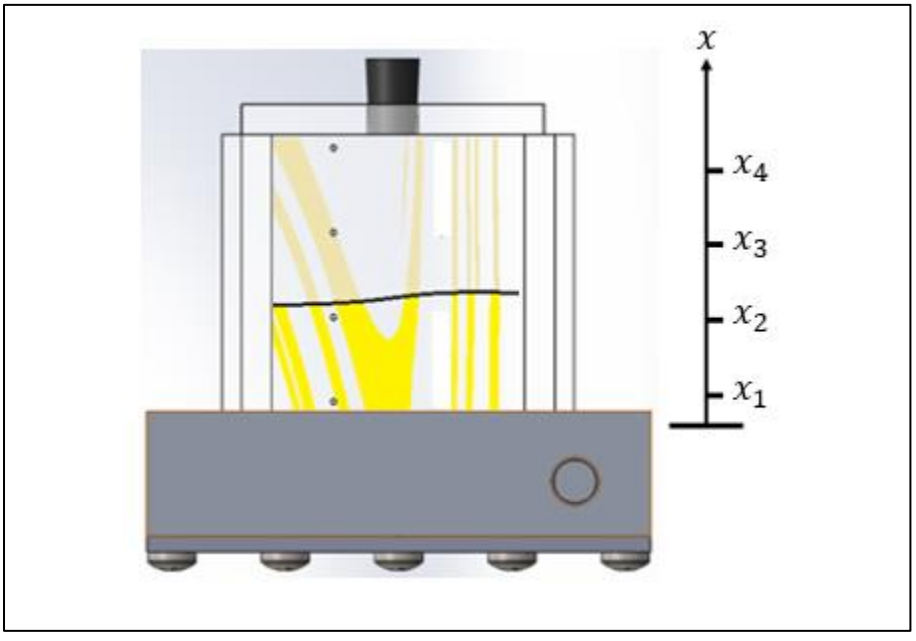

(b)

Figure 3-5: Simple sketches of the test cell at the two tested freezing processes with: (a) natural convection existing and (b) natural convection suppression.

Four thermocouples were inserted into the holes that were drilled onto the Plexi-glass. The thermocouples were inserted such that it is about one millimeter away from the Plexi-glass into the cavity side of the test cell. Silicon paste was applied to the base of the thermocouples. A sketch of a single thermocouple is given in Figure 3-6 and a photo of two thermocouples is shown in Figure 3-7. The four thermocouples were calibrated carefully prior to mounting on the test cell and uncertainty for temperature readings was determined to be ± 0.6 ^{o}C, review Appendix B. A channel data acquisition (DAQ) unit (NI 9162, National Instruments, Austin, TX), which has a built-in cold junction compensation circuit, was used to log the thermocouples readings. The DAQ unit was connected to a personal computer and was operated by a LabVIEW-based virtual instrument (VI), details can be found in Appendix C.

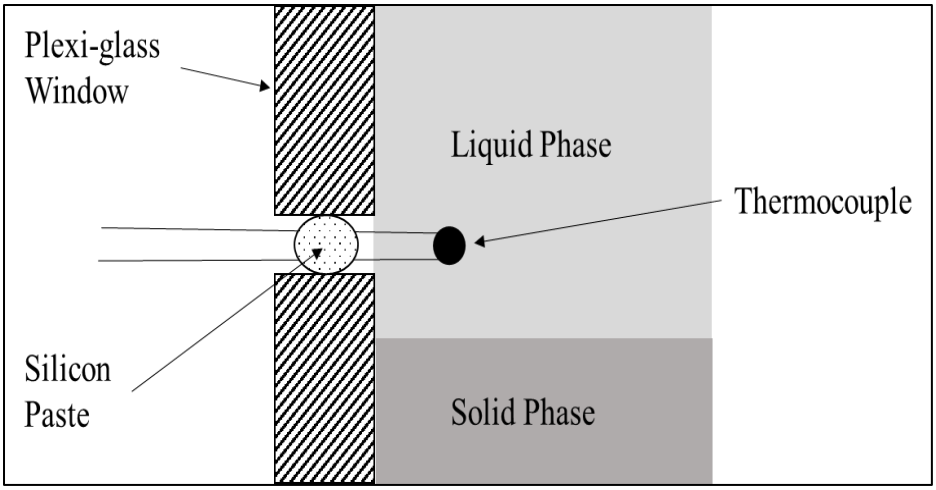

Figure 3-6: Sketch of the thermocouples insertion method.

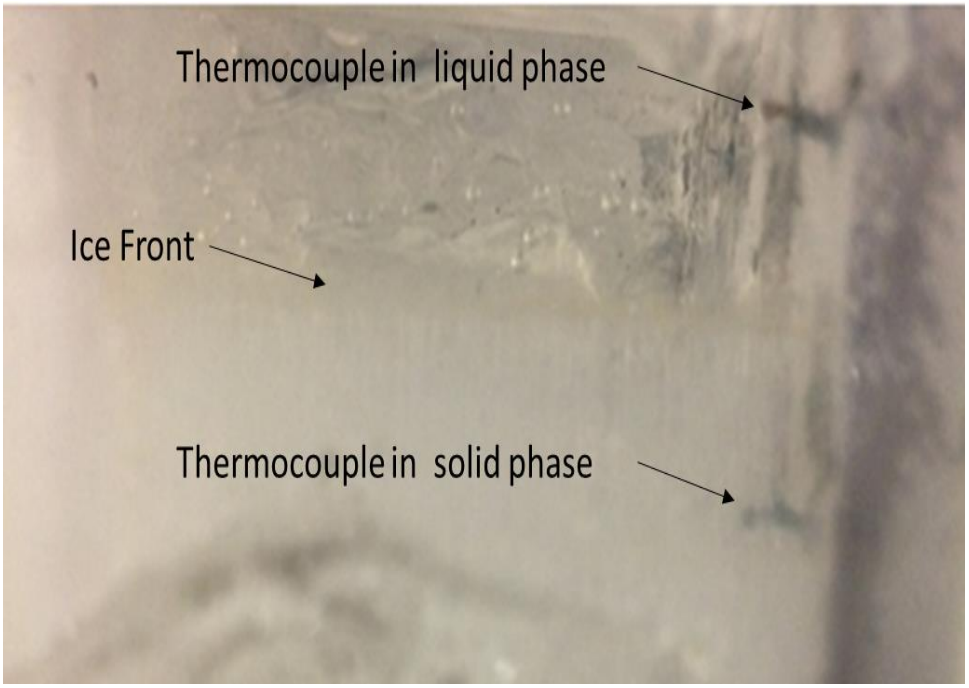

Figure 3-7: Real photo of the position of the thermocouples in the test cell

The uncertainty analysis of the experimental data is presented in Appendix D. Furthermore, an estimation analysis of the time response of the thermocouples is provide in Appendix E. The experimental setup was placed in an air-conditioned room that was kept at about 23^{o}C ±2^{o}C during the entire experiment, for all runs. During the experimental runs, the refrigeration unit was connected to the cooling plates by means of well-insulated hoses. The refrigeration unit was set to a temperature (-20^{o}C), a pumping pressure (~0.4 bar) and a flow rate (~22 L/min). Those settings showed a temperature uniformity of about 0.5^{o}C on the cooling plate, after 1 minute from running the refrigeration unit. The temperature readings were logged every 6 seconds corresponding to a sampling rate of 0.167 Hz. Continuous readings were started before running the refrigeration unit to show the initial temperature of the liquid in the cavity. The growth of the solid phase was indirectly determined by the temperature variations at various locations along the freezing front movement direction. Photographic capturing were made using a simple phone camera (iPhone 5, Apple, California, United States).

3.1.4 Experimental procedure

As discussed above, the freezing process was investigated in this thesis with and without the existence of natural convection. The experimental procedure is exactly similar for both; however, the cooling plate orientation is different, i.e. at the bottom for suppression of natural convection and on the side for inducing natural circulations, see Figure 3-5.

The test cell was first filled fully with the studied liquid. In every experiment, the test cell was evacuated and new liquid sample was poured in. It is important to mention that the liquid expands or contracts because of the density change while cooling. To allow the liquid to do so, the pouring opening at the top of the test cell was left unclosed. DAQ unit is then started to record temperature values at the four thermocouples, after pouring the liquid. The initial temperature is recorded for 10 minutes, allowing accurate measurements to be obtained and allowing the liquid to settle if any movement existed because of the pouring mechanism. At the same time, the refrigeration unit was turned on with an internal circuit, not flowing through the cooling plate channels yet. After 10 minutes, the refrigeration unit reaches to a steady state of -20^{o}C. At that point, the refrigeration unit is turned off, connected to the test cell, and turned on within five minutes. DAQ unit is still reading temperature while doing all the above procedure. Photos are taken for the water experiments at different times.

Three samples of each liquid is tested in different days with randomized testing conditions. The liquids tested are tap water and CNT-water Nanofluid having a weight percentage of 0.3 wt%, and 1 wt%. The reason of the limited number of samples is an availability issue. However, those two samples were enough to draw some good conclusions.

3.2 Experimental Results

In this section, the experimental results are presented and discussed. This section is subdivided into five subsections, corresponding to four different experiments and an additional subsection dedicated to describe the phenomenon. First, the phenomenon description is presented in order to have a better understanding of the following results. Then, the experiment of freezing the water sample from below, i.e. suppressed natural convection is discussed thoroughly. After that, the experiment of freezing water from the side is presented and compared to the previous experiment. In order to refer to the two experiments easily, the suppressed natural convection experiment is called a stratified freezing experiment. On the other hand, the experiment with natural convection is called a non-stratified freezing experiment. Finally, results of the freezing of the prepared Nanofluid samples are later presented and compared to those of the water experiments. Some other parameters were obtained by a MATLAB code included as Appendix F: those are the ice front location and speed as functions of time. In addition, the heat rate being drawn from the cooling plate is obtained and presented for each experiment.

3.2.1 Description of freezing phenomena

It is desirable, before presenting the results, to describe the transient process that occurs inside the test cavity as the liquid is being cooled down and being frozen. If a small volume of liquid is placed in an environment with a lower temperature than the freezing point, it exhibits a transient temperature variation similar to the one presented in Figure 3-8. Figure 3-8 illustrates a regular cooling curve showing that the temperature of the liquid sample decreases due to the cooling action of the environment until reaching the freezing

point. At the freezing point, latent heat is taken out of the liquid volume at a certain time interval, corresponding to the quantity available to be frozen. If latent heat of fusion of the liquid is taken out, the liquid will solidify and temperature can then drop below the freezing point.

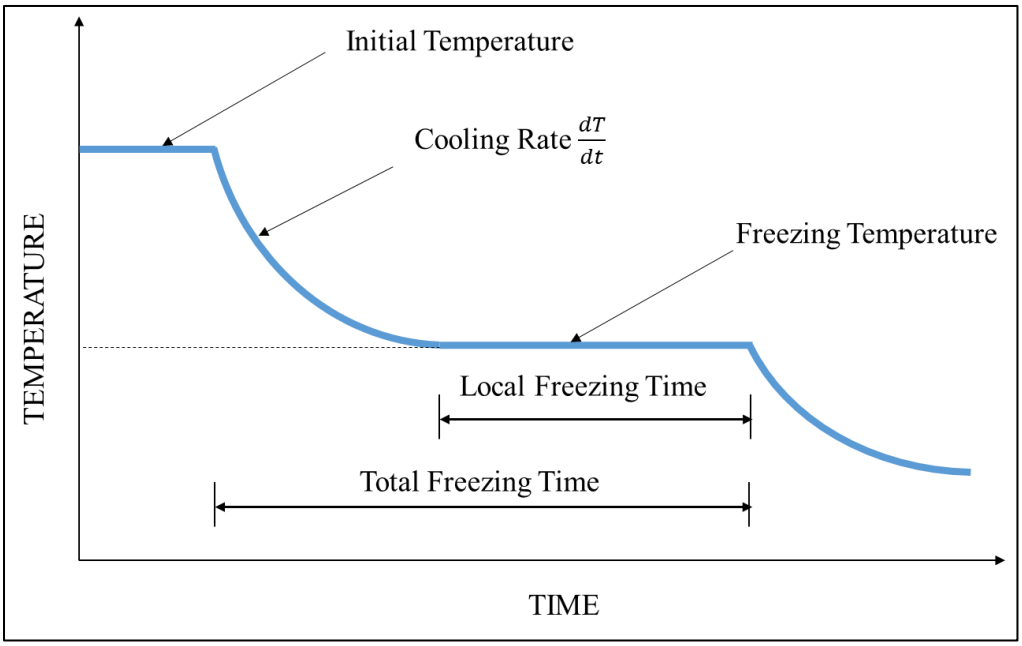

Figure 3-8: Normal cooling curve of liquids describing the transient freezing process.

However, this is not the case in most situations. It was observed in literature that a supercooling degree is encountered before freezing starts. The supercooling effect is a subject of research for many decades and still is. Figure 3-9 depicts the phenomenon of supercooling. As the cooling starts from an initial temperature, the liquid temperature drops below its freezing temperature without being frozen. Temperature keeps dropping until a point where it suddenly jumps back to the freezing point and the previous freezing process is continued. It was discussed in the literature review that the supercooling degree is affected by the cooling rate, such that high supercooling degrees are associated with high cooling rates. In addition, supercooling degree can be reduced by intruding mechanical stirring of the liquid or in the form of natural or forced convection.

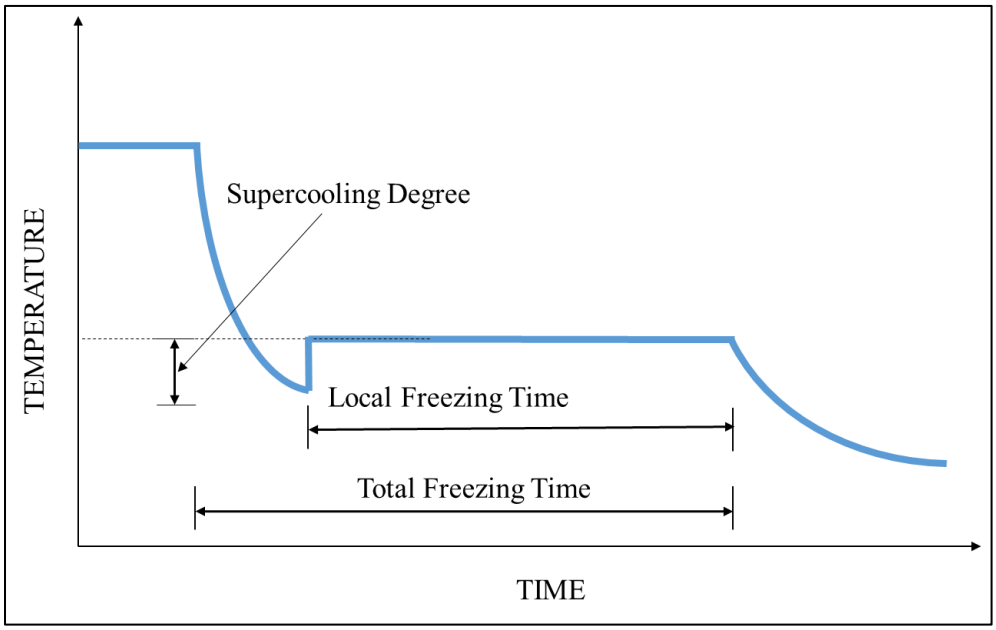

Figure 3-9: Cooling curve of liquids describing the phenomenon of supercooling.

The previous description of the freezing process is valid if a small quantity of liquid is observed, however, small volumes of liquid is impractical to study. Most applications concerning freezing processes require large amount of liquids to be frozen. It is therefore intended to study the freezing process of 150 mL of fluid in this work. As illustrated previously, the temperature is going to be measured at different locations of the test cell, along the freezing front movement direction. Normally, cooling curves are similar to the described ones; however, it is important to keep in mind that freezing of liquid would take place locally rather than homogenously, as compared to small volumes.

3.2.2 Experiment 1: Freezing of water from below (Stratified Experiment)

In this experiment, the cooling plate was placed at the bottom. This experiment works as the basis to which all other similar experiments are compared. Natural convection is caused by density variation and buoyancy forces that result in the sinking of the heavier liquid and the rising of the lighter part. By placing the cooling plate at the bottom, the liquid near the plate is cooled down, thus made denser than the other part of the liquid occupying the upper part of the cavity. Since denser liquid is at the bottom, a stratified-like fluid is existing and diffusion is the dominant mode of heat transfer. The aforementioned experimental procedure is performed and temperature is read for around four hours continuously.

Figure 3-10 shows the transient temperature readings of the four thermocouples for a sample experimental run. All four thermocouples exhibit a smooth decay of temperature initially, showing the absence of natural convection. The smoothness of the temperature decay continues for the first two thermocouples until freezing takes place and temperature then drops below the freezing point.

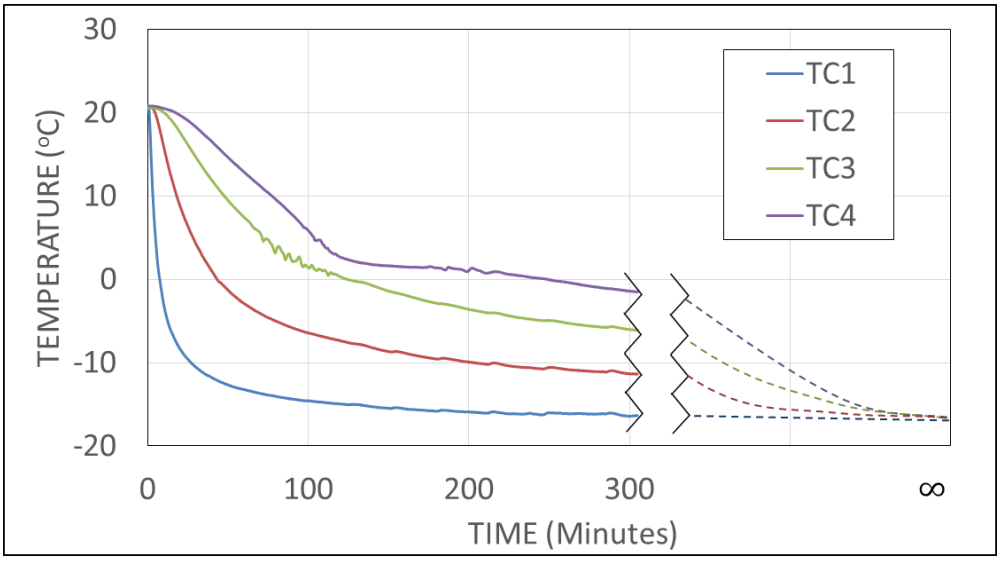

Figure 3-10: Transient temperature readings of Experiment 1.

Figure 3-11 shows a zoomed-in plot of the temperature readings at the thermocouples. It is apparent that the third thermocouple is showing a fluctuation in temperature readings starting from a time of about 70 minutes after cooling begins resulting from the onset of natural convection caused by the fact that Rayleigh number has reached the critical value for natural convection to take place, i.e. Rayleigh number of 1000 [91]. A similar behavior is observed for the last thermocouple, however, weaker in magnitude.

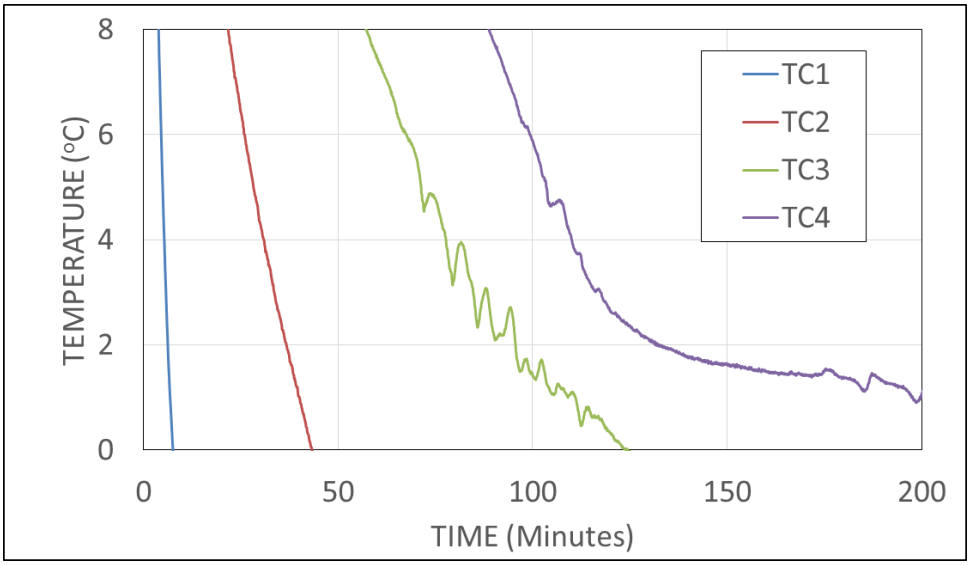

Figure 3-11: Zoomed-in plot of the temperature readings in experiment 1 to show the natural convection fluctuations.

The reason of these fluctuations in temperature readings is a weak natural convection developing at that time. Natural convection is caused by the fact that water has a density inversion point at a temperature of 4℃. Figure 3-12 shows the density variation of water as a function of temperature. At the point of density inversion, the density reaches a maximum of about 1000 kg/m^3. Upon further cooling, temperature drops as well as density, causing an opposite phenomenon to the one inspected previously that natural convection would not develop because of the stratified-like density behavior of water. It can be noticed clearly from Figure 3-11 that natural convection occurs when the average liquid temperature is between the maximum density point (4℃) and the freezing point; however, gets weaker as temperature is approaching the freezing point. One may notice also that the temperature fluctuation magnitudes is less than 1℃. Natural convection does not vanish by the end of the fluctuations but continues with smaller magnitudes until solidification takes place.

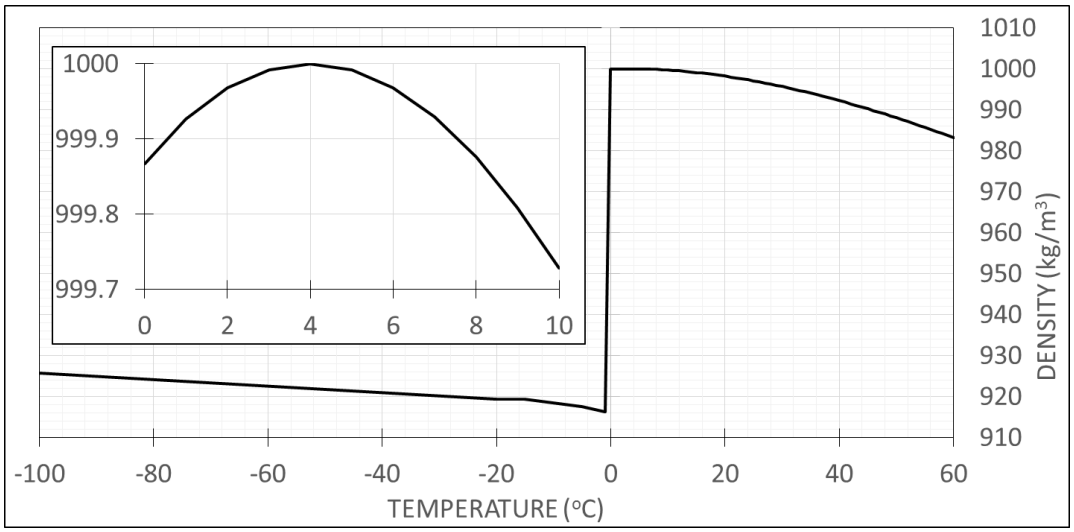

Figure 3-12: Water density variation at different temperatures, indicating the density inversion point.

A MATLAB code was generated to easily analyze the experimental data and obtain some other parameters that give further insights on the problem at hand, Appendix F. The freezing front arrival time is one of the code's outputs. The code determines the beginning of the cooling process and checks the ice-front arrival time at every thermocouple, then determines the time taken for the ice front to move from one thermocouple to the other. The code as well as Figure 3-10 show that the ice-front arrival times at thermocouples one, two, three, and four are 8, 46.1, 136.64, and 265.58 minutes, respectively.

Figure 3-13 shows the solid-liquid front position as a function of time elapsed after the cooling process begins. Since the problem could be compared to Stefan problem, discussed in Chapter 2, the solid-liquid front is proportional to the square root of the elapsed time, as Stefan concluded. Using a backward differencing derivation of the previous figure, Figure 3-14 depicts the estimated speed of the ice front as a function of time. It is evident that the ice front starts by a high magnitude and that speed reduces as time advances.

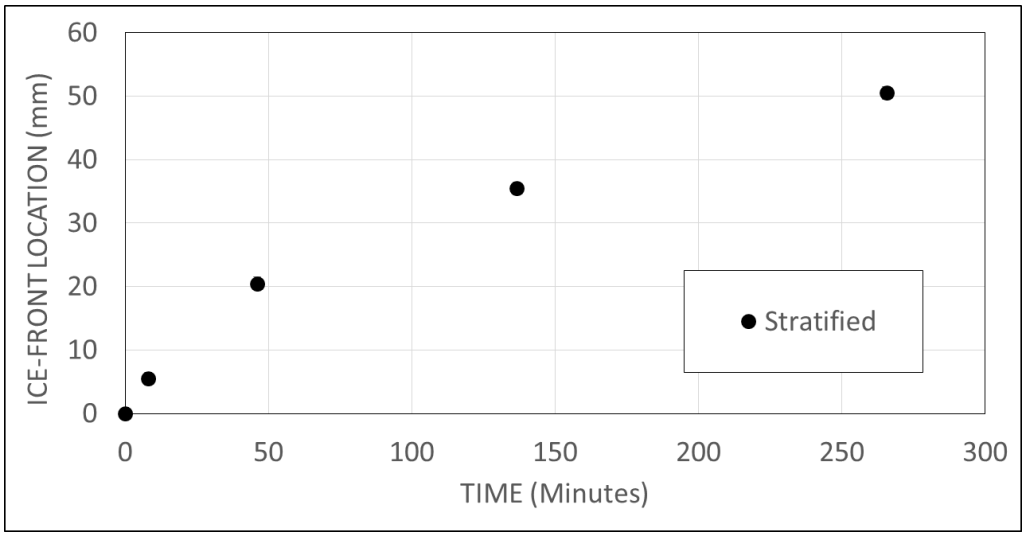

Figure 3-13: Plot of the Ice-front estimated location for experiment 1, indicating the thermocouples locations.

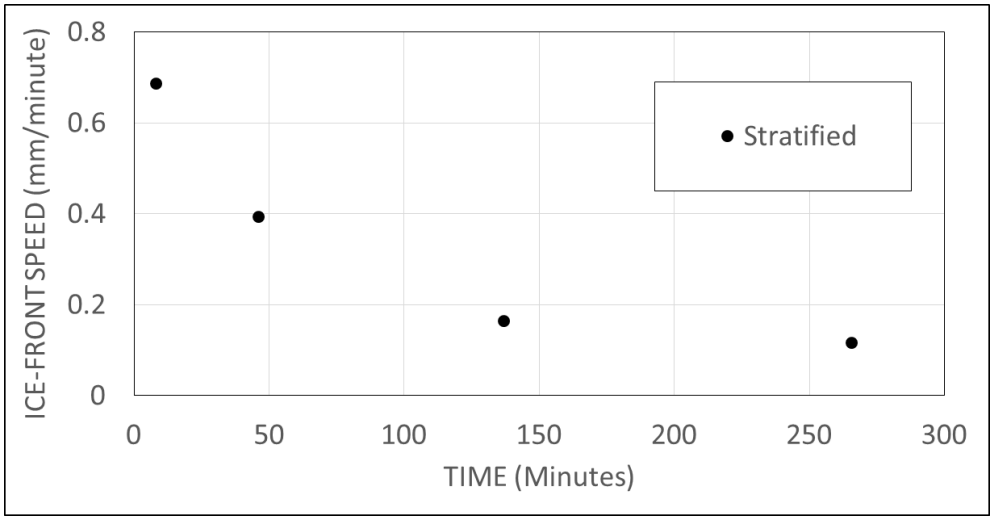

Figure 3-14: Plot of the Ice-front estimated speed for experiment 1, indicating the overall average speed.

Figure 3-15 shows an estimated value of the heat rate at the wall. The value of the heat rate was measured by assuming that the temperature gradient between the wall and the first thermocouple, located at 5.5 mm away, is constant. That is the temperature takes a linear profile from the wall to the first thermocouple. The following equation was used as the basis of Figure 3-15

$$Heat\ Rate = -kA_{wall}\frac{dT}{dx} = -kA_{wall}\frac{\Delta T}{\Delta x} \quad (3\text{-}1)$$

Where k stands for average thermal conductivity of the volume bound by the wall and the first thermocouple. Measurements of thermal conductivity shows that ice has a thermal conductivity of 2.2 W/m-K, thus this value was used. The area of the cooling plate is taken as 25 cm^2. The heat rate starts by a large value corresponding to the initiation of the freezing process. However, this value tends to decrease in magnitude until it reaches to a value of zero at steady state, not shown in the figure.

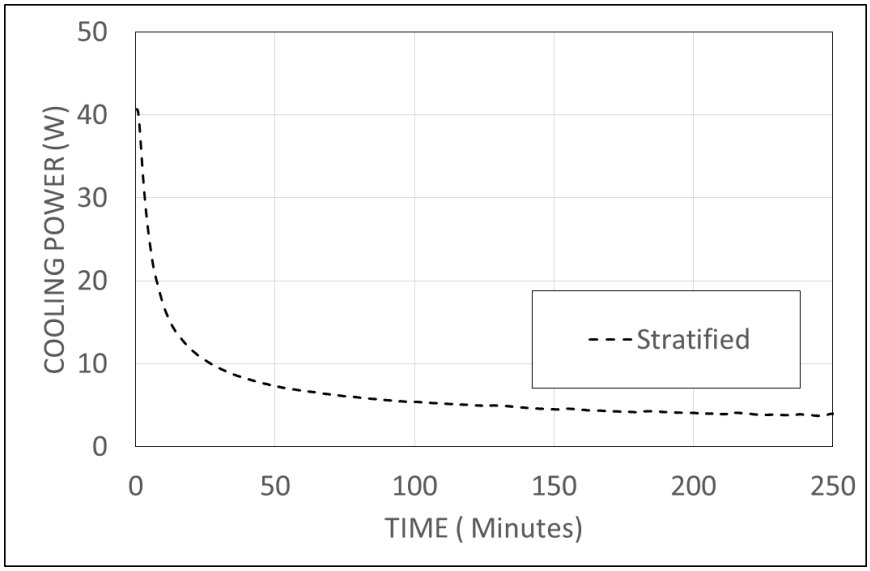

Figure 3-15: Plot of the estimated heat flux at the cooling wall for Experiment 1.

3.2.3 Experiment 2: Freezing of water from a vertical side (Non-stratified Experiment)

In the second experiment, the cooling plate is placed at one vertical side. As the temperature of the cooling plate is brought down to -20^{o}C, the liquid adjacent to the wall gets cooler than the part further away. Density of the cooler part of the liquid is greater in magnitude than that of the warmer part; hence, natural convection would exist from the beginning of the cooling process.

Figure 3-16 shows the transient temperature readings of the four thermocouples for a sample experimental run. All four thermocouples exhibit a steeper decay of temperature compared to the previous experiment presented in Figure 3-10. The rapid decrease of temperature is elaborated in Figure 3-17, which shows individual plots of temperature readings at the four thermocouples, comparing the two experiments, i.e. with and without natural convection.

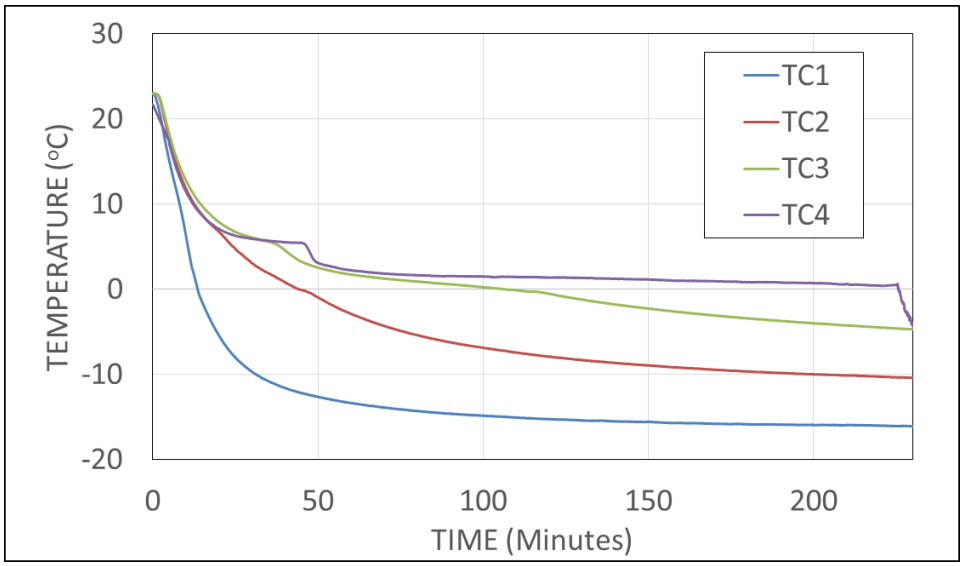

Figure 3-16: Transient temperature readings of experiment 2.

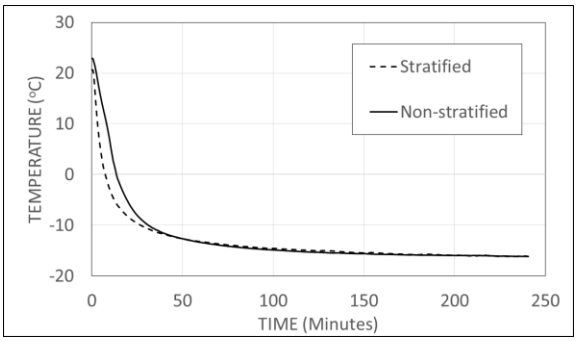

(a)

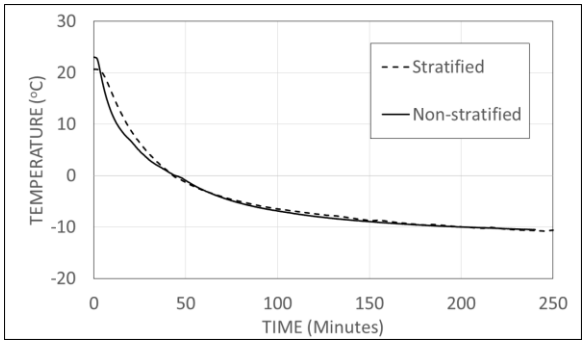

(b)

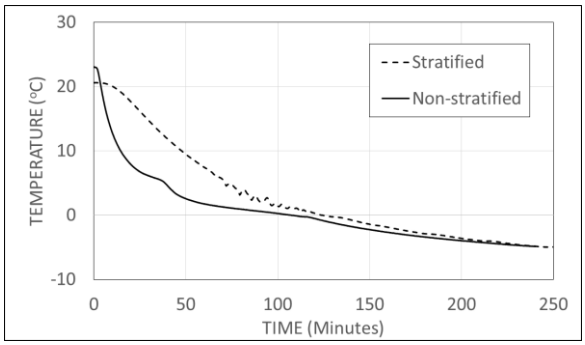

(c)

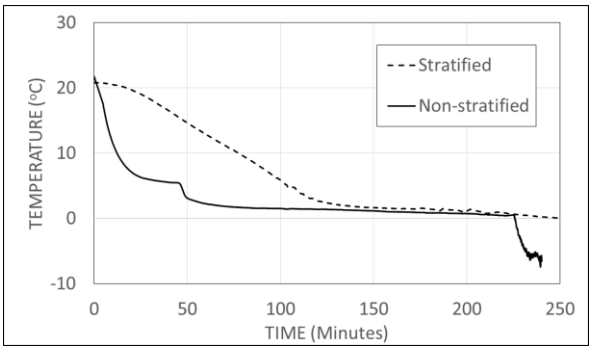

(d)

Figure 3-17: Temperature readings of Experiment 1 and 2 at; (a) Thermocouple 1, (b) Thermocouple 2, (c) Thermocouple 3, and (d) Thermocouple 4.

Figure 3-17-(a) shows that the case of natural convection tends to delay the freezing initiation at the beginning of the freezing process. An average of 14 minutes were taken for the freezing front to move from the wall to the first thermocouple in the presence of natural convection. The time taken in the absence of natural convection was about 8 minutes, showing a fact that natural convection delays the ice-front arrival time to the first thermocouple by 6 minutes. In the absence of natural convection, the cooling power caused by the cooling plate is utilized to decrease the temperature of a local vicinity of water and to extract the latent heat out of it. On the other hand, the existence of natural convection tends to widen the affected vicinity. As an attempt to illustrate this fact, the temperature readings of the second, third, and forth thermocouples when the ice front arrives to the first thermocouple in experiment 1 are 17.6 ^{o}C, 20.3 ^{o}C, and 20.6 ^{o}C, respectively. On the other hand, the second, third, and forth thermocouples readings in experiment 2, where natural convection exists, are 9.3 ^{o}C, 10.3 ^{o}C, and 9.1 ^{o}C, respectively. This shows that with the existence of natural convection, the natural circulations of the liquid in the cavity tends to decrease the temperature of the liquid in the entire cavity, contrary to the diffusion-dominant mode where the effect was barely noticed on the second thermocouple. This, in fact, explains why the first thermocouple took a longer time to freeze compared to the time taken in the diffusion-dominant experiment.

The fact that natural convection tends to cool the entire cavity instead of a small vicinity is pronounced for the other thermocouples, shown in Figure 3-17. The last three plots of the figure as well as Figure 3-18 show that the time taken for the ice front to arrive the three thermocouples are decreased by a noticeable difference. To be precise, the ice front arrives the second, third, and fourth thermocouples at 48.1, 119.5, and 226.27 minutes, respectively. This shows a decrease of about 39.31 minutes for overall freezing process in the case of existing natural convection.

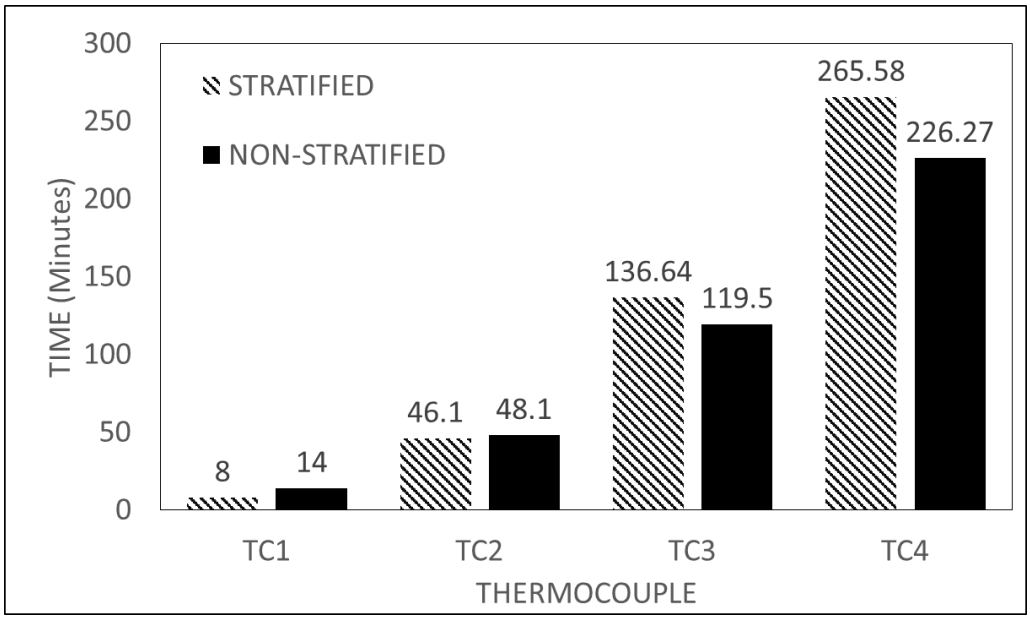

Figure 3-18: Summary of the solid-liquid front arrival times at the four thermocouples for experiment 1 and 2.

Figure 3-19 shows a zoomed-in plot of temperature readings at the thermocouples. A sudden drop of temperature in a region similar to that noticed in the previous experiment is noticed. In the case of the diffusion-dominant experiment, there existed temperature fluctuations caused by the density-inversion point, discussed earlier, at a temperature of around 4°C. However, in this experiment the density-inversion point tends to enhance the heat transfer by further strengthening the already-existing natural convection. Furthermore, no fluctuations were noticed in this experiment.

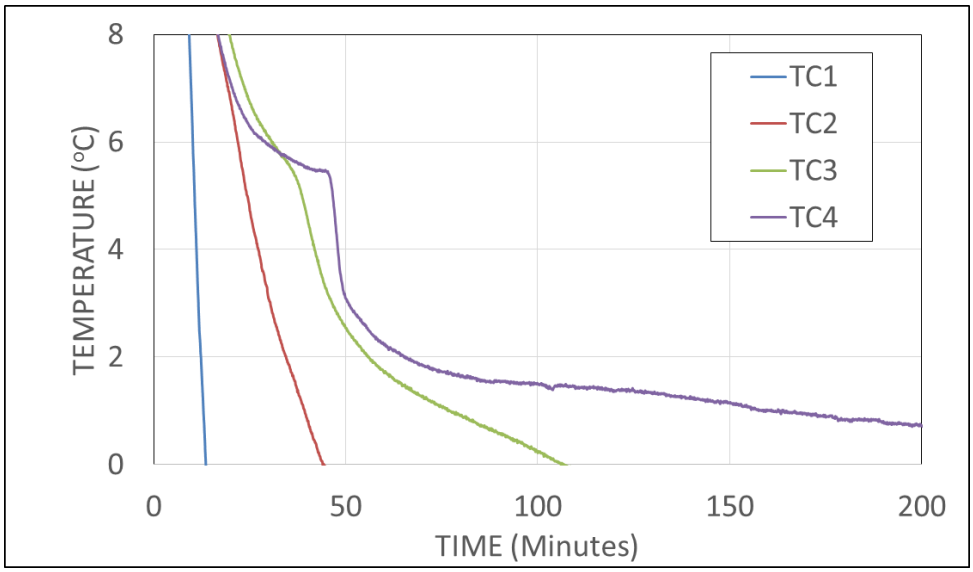

Figure 3-19: Zoomed-in plot of the temperature readings in experiment 2 to show the natural convection onset effect.

Figure 3-20 presents the ice front location as a function of time of this experiment and the diffusion-dominant experiment. The solid-liquid front location as a function of time in this experiment is similar to that of the previous experiment, except for the distortion occurring at the beginning of time. Both experiments show a relatively similar front advancement time at first; however, the time difference is enlarged as freezing front advances. The main reason is that in the non-stratified experiment, the cooling power needs to extract the latent heat of the liquid only, opposite to the stratified case where sensible and latent heats need to be extracted.

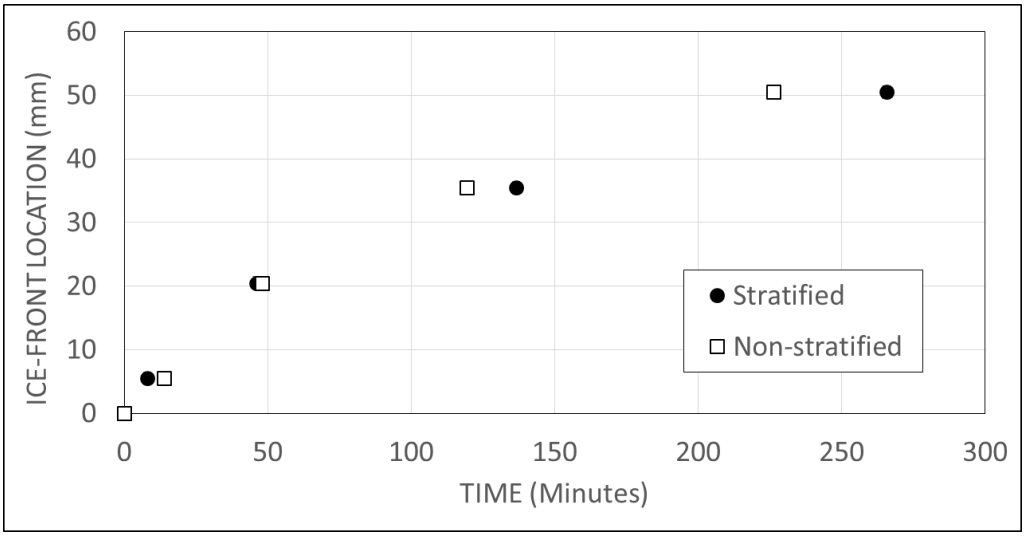

Figure 3-20: Plot of the Ice-front estimated location for experiment 1 and 2, indicating the thermocouples locations.

Figure 3-21 is showing the solid-liquid front estimated velocity of this experiment, as well as the previous experiment. The velocity of the ice front begins with a higher velocity than that at later times. The reason of the increased front velocity is the existence of natural convection at the beginning of the cooling process. The ice front velocity decreased at later times because of the weakened natural convection with elapsed time. Figure 3-21 shows also that the existence of natural convection delayed the freezing initiation compared to the high front speed in the case of diffusion-dominant experiment. However, the speed of fronts of both cases seem to coincide later.

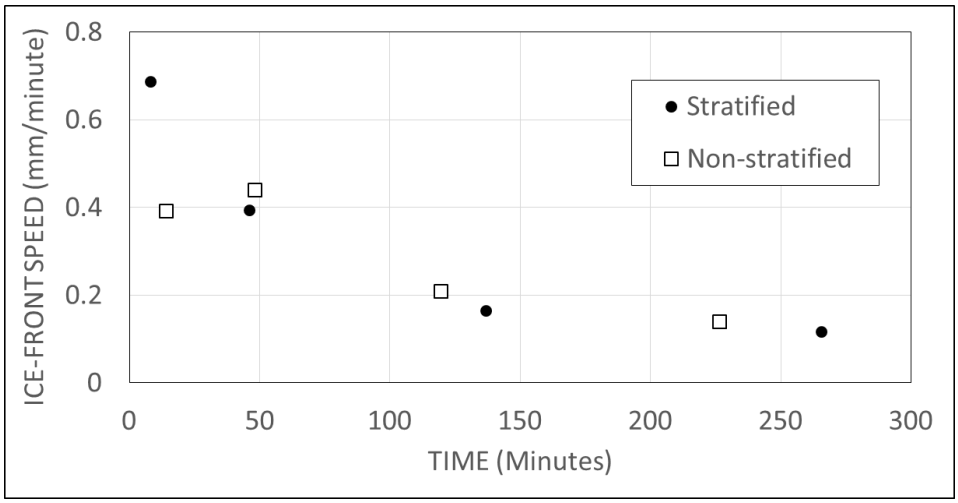

Figure 3-21: Plot of the Ice-front estimated speed for experiment 1 and 2.

Figure 3-22 shows the cooling power extracted from the cooling plate for this experiment and the previous experiment. It is showing that even though existence of natural convection has an advantage of decreasing the time of the freezing process, it requires a higher cooling energy to freeze the same amount of liquid at early times, 8.9 kJ higher to be specific. This amount of energy is consumed in inducing natural convection during the freezing process. Later, the cooling power needed to freeze water is the same with and without the existence of natural convection. Table 3-1 depicts real photos of the solid-liquid front locations as a function of time at different times for the two experiments discussed above.

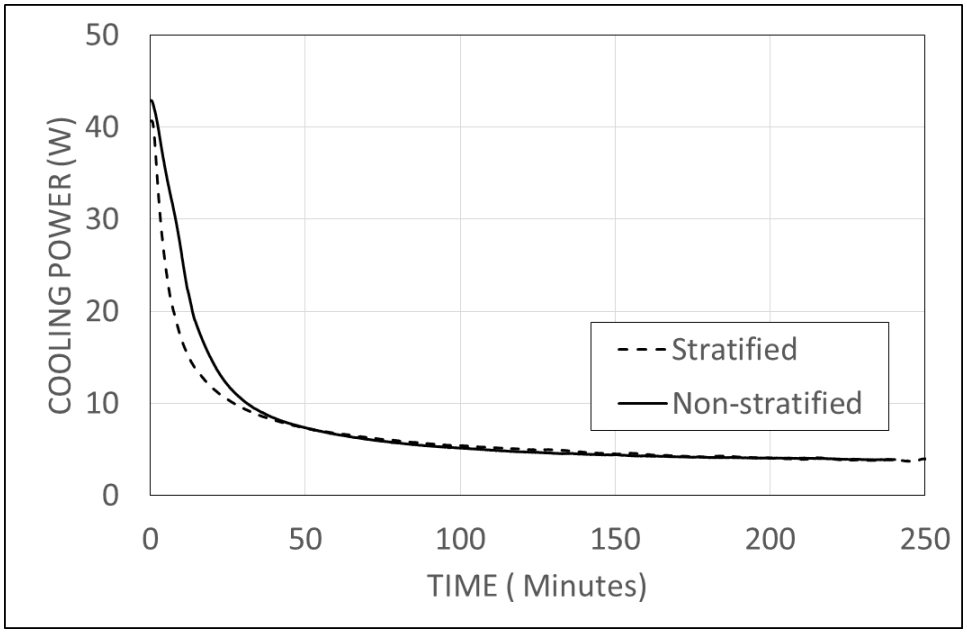

Figure 3-22: Plot of the estimated cooling power at the cooling wall for experiment 1 and 2.

Table 3-1: Photos to visualize the solid-liquid front at different times corresponding to time arrival at (a) thermocouple 1 (b) thermocouple 2 (c) thermocouple 3 (d) thermocouple 4, Figures (e) summarize the front arrival times, and (i) and (ii) correspond to stratified and non-stratified experiment, respectively.

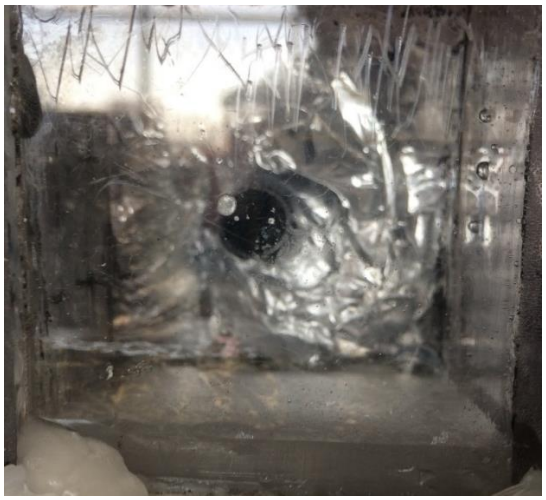

(a-i)

(a-ii)

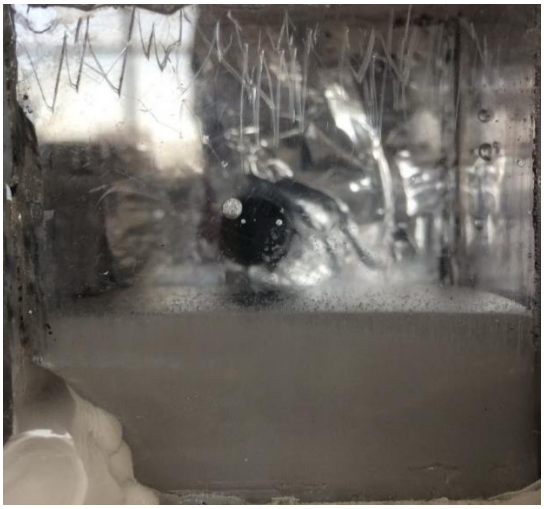

(b-i)

(b-ii)

(c-i)

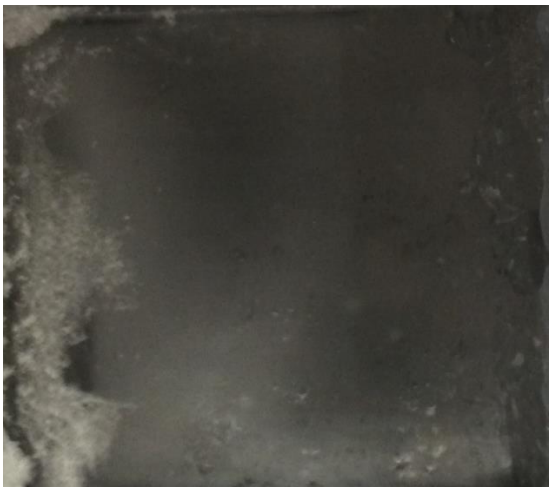

(c-ii)

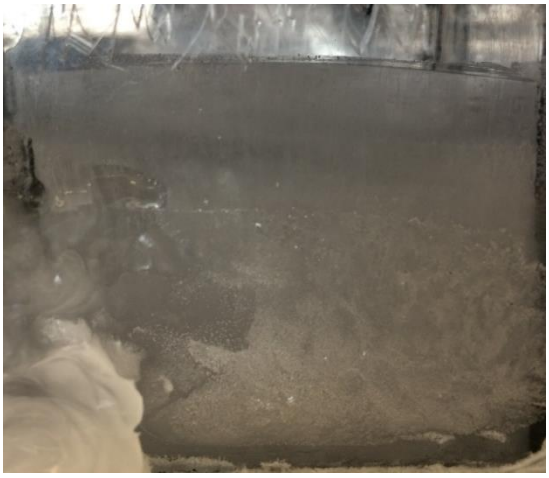

(d-i)

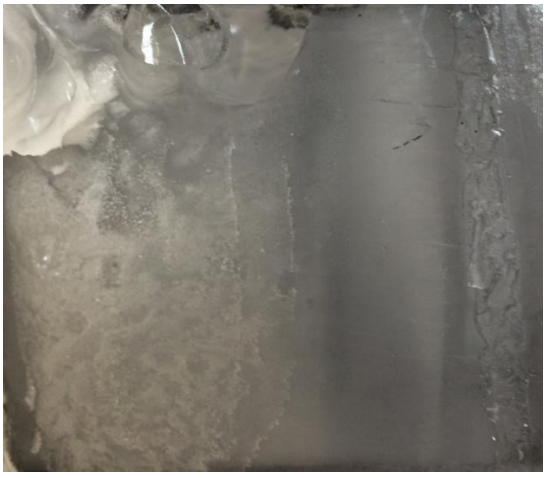

(d-ii)

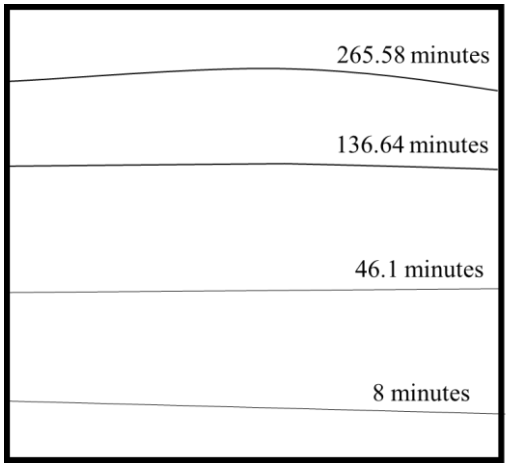

(e-i)

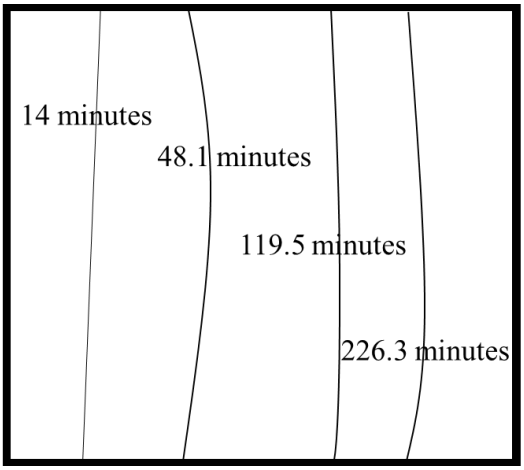

(e-ii)

3.2.4 Freezing of CNT-water from below (Stratified Experiments)

This experiment is similar to Experiment 1; however, the working liquids are CNT-Water Nanofluids with different CNT concentrations. Two concentrations were used for the purpose of showing the improvement of the freezing process namely, 0.3 wt% and 1 wt%. Similar procedure was followed and temperature is recorded at the same thermocouple locations.

Figure 3-23 presents the temperature readings at the four thermocouples of different CNT concentrations. The first thermocouple readings show that all tested Nanofluids exhibit similar temperature variation; however, the difference is clearer for the other thermocouples. Two reasons are hypothesized as the reasons why temperature of the three samples were distinct. The first reason is thought to be the initial temperature of the samples. This hypothesis was tested and presented in the last section of this chapter as one source of results discrepancies. In that section, it is proven that initial temperature is not significant to change the cooling process by great extent. Thus, the second hypothesis is believed to be the reason of the difference in freezing front advancement. The second hypothesis is that the different CNT concentrations result in different freezing processes, hopefully better.

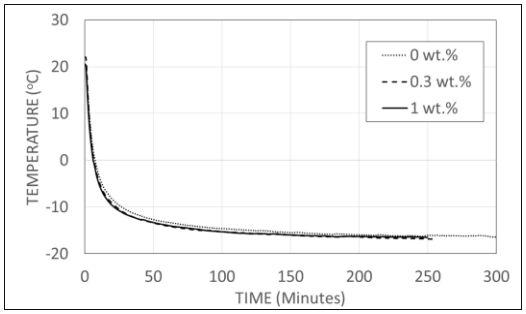

(a)

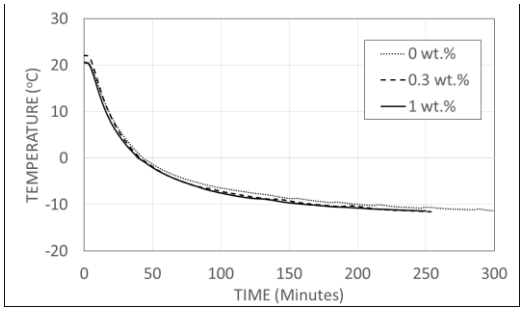

(b)

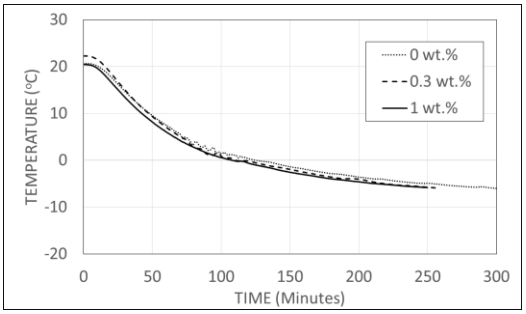

(c)

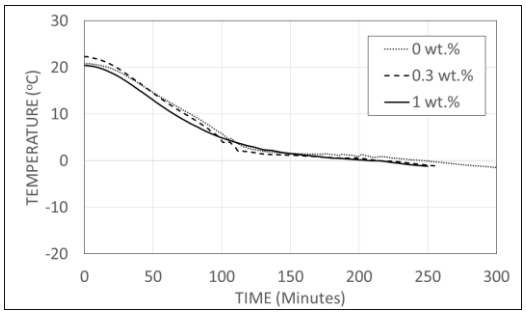

(d)

Figure 3-23: Temperature readings of Experiments with different CNT concentrations in the absence of natural convection at; (a) Thermocouple 1, (b) Thermocouple 2, (c) Thermocouple 3, and (d) Thermocouple 4.

Figure 3-25 and Figure 3-26 depict zoomed-in plots of the temperature readings at the third and fourth thermocouples, respectively, in order to illustrate the effect of CNT concentration on the natural convection fluctuations. One can notice from both plots that fluctuations are reduced by increasing CNT concentration. As discussed previously, natural convection enhances heat transfer, therefore, Figure 3-26 shows that adding more CNT particles decreases the strength of natural convection and that reduces the enhancement of temperature drop of the liquid, in turn. The main reason is that adding more CNT particles increases the viscosity of Nanofluids, which acts to suppress natural convection.

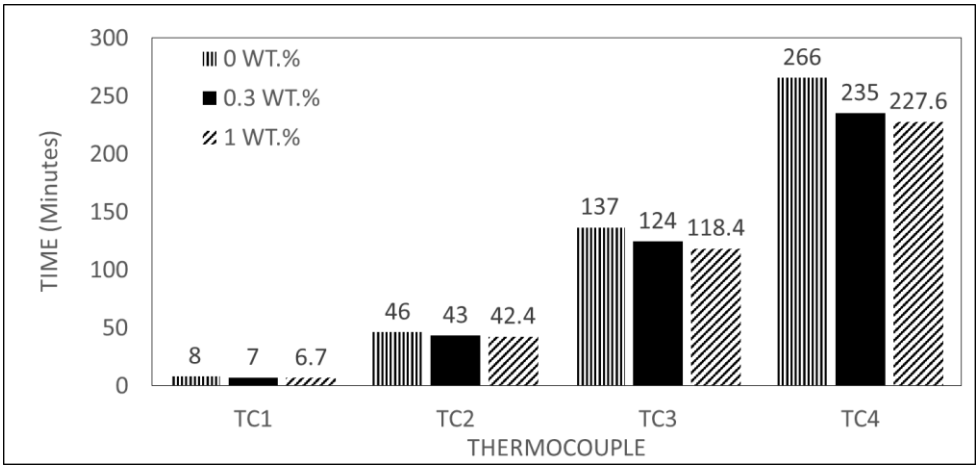

Figure 3-24: Summary of the solid-liquid front arrival times at the four thermocouples for all tested liquids in the absence of natural convection.

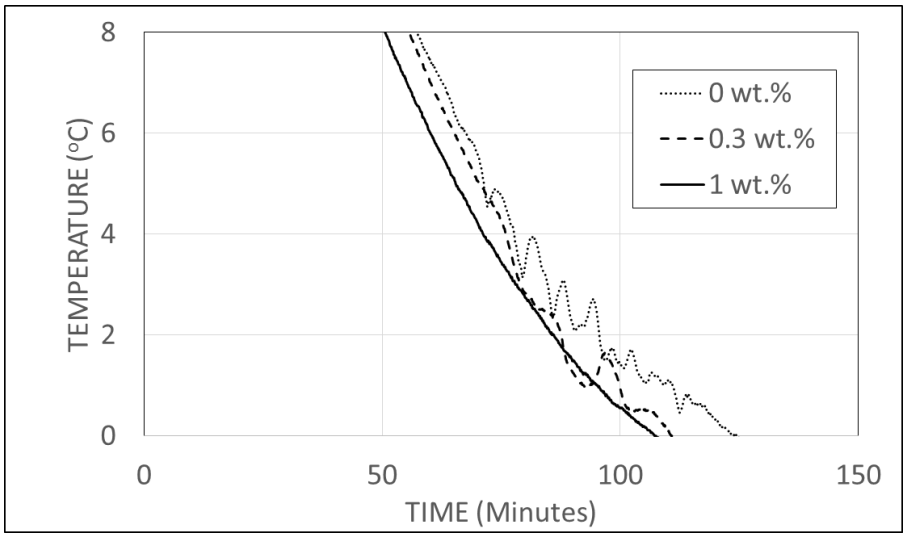

Figure 3-25: Zoomed-in plot of the temperature readings at the third thermocouple for different CNT concentrations in the absence of natural convection.

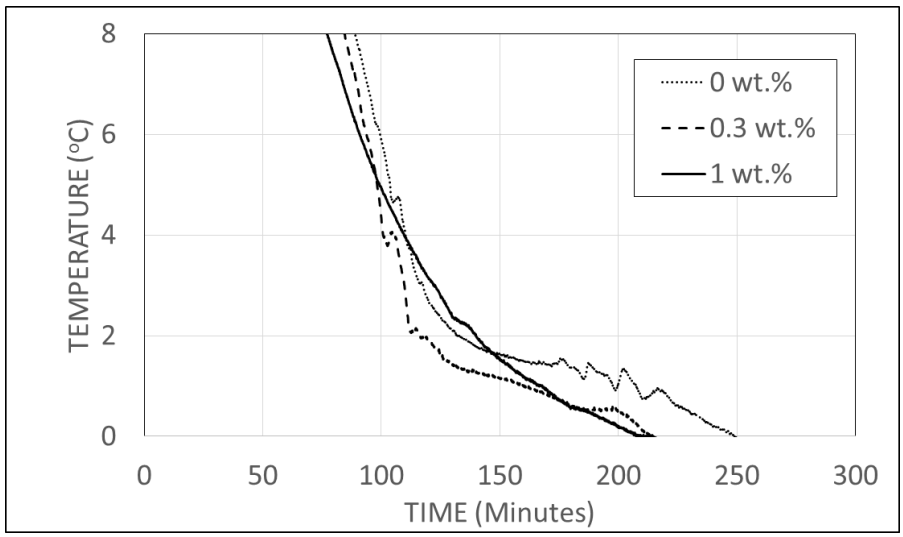

Figure 3-26: Zoomed-in plot of the temperature readings at the fourth thermocouple for different CNT concentrations in the absence of natural convection.

The solid-liquid front locations at different times can be seen in Figure 3-27. The front location is directly proportional to the square root of the elapsed time, similar to experiment 1; however, the location of the front differs between the three tested fluids. Adding CNT particles to the base fluid seem to decrease the time of front arrival at all thermocouples. The solid-liquid front arrives the third thermocouple 18.6 minutes earlier for the case of 1 wt.% CNT concentration and 13 minutes earlier for the case of 0.3 wt% CNT concentration compared to the case of the base fluid, i.e. water. The time difference was further reduced upon reaching the fourth thermocouple, where the time difference was about 31 minutes and 38.4 minutes for the cases of 0.3 wt% and 1 wt% CNT concentrations compared to the freezing time of tap water.

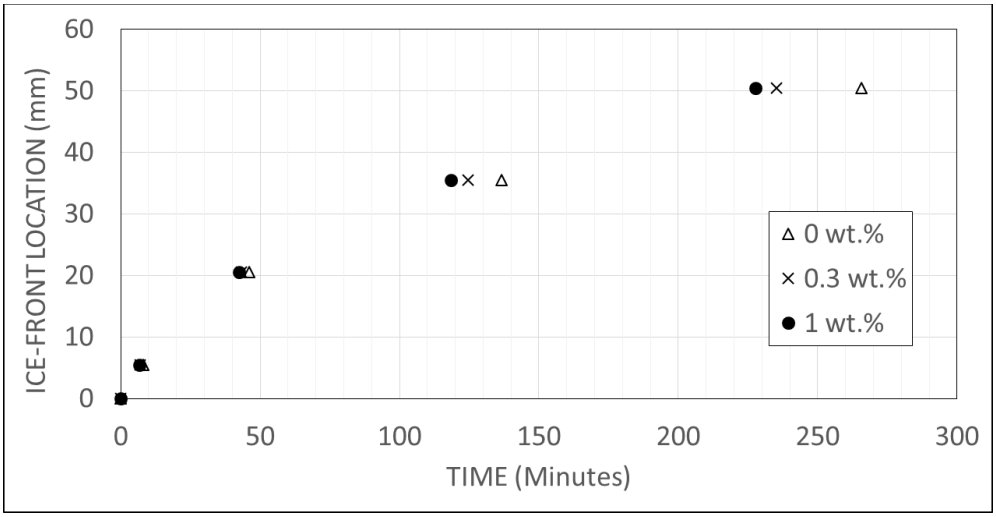

Figure 3-27: Plot of the Ice-front estimated location for different Nanofluids in the absence of natural convection.

Figure 3-28 illustrates the speed of the solid-liquid front for the three tested fluids. It is evident that at the beginning Nanofluids tend to have a higher front speed than the base fluid. Later, the solid-liquid front speeds coincide and reach to an asymptotic value.

Figure 3-29 shows than there is no significant difference in the cooling power between all tested liquids.

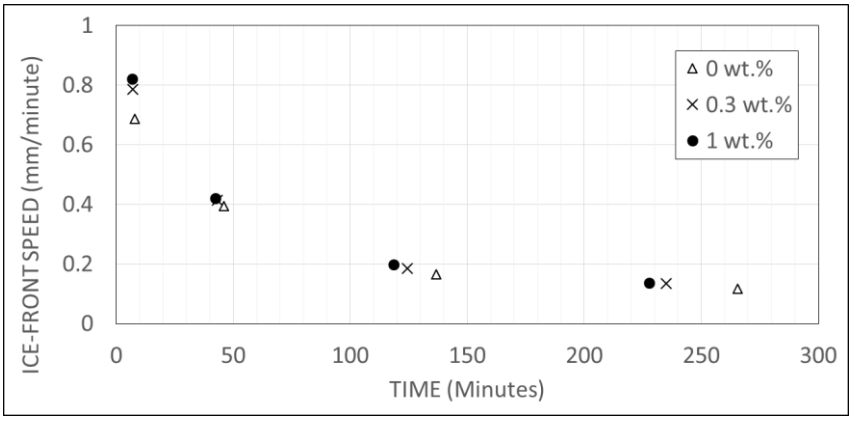

Figure 3-28: Plot of the Ice-front estimated speed for different Nanofluids in the absence of natural convection.

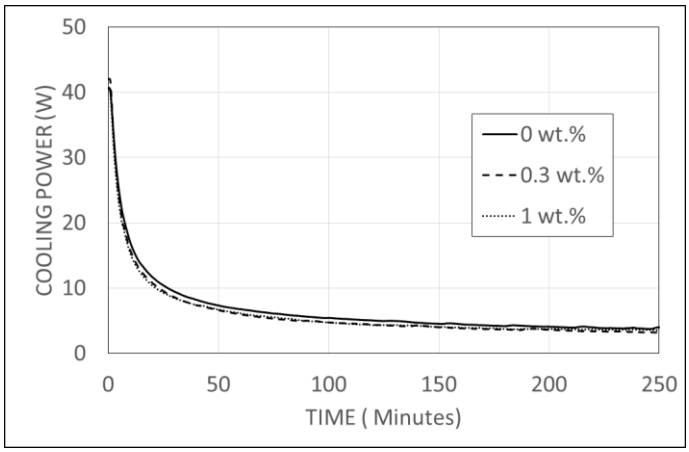

Figure 3-29: Plot of the estimated cooling power at the cooling wall for all tested liquids in the absence of natural convection.

3.2.5 Freezing of CNT-water from a vertical side (Non-stratified Experiments)

Experiment 2 was repeated with different CNT concentrations added to water, 0.3 wt% and 1 wt% to be specific. Similar procedure and experimental setup was followed as in Experiment 2.

Figure 3-30 illustrates the temperature readings at the four thermocouples of different CNT concentrations. The first two-thermocouple readings show that all tested Nanofluids exhibit similar temperature variation; however, the difference is clearer for the other thermocouples. Water and 0.3 wt% CNT-water Nanofluid seem to have no big differences in temperature measurements, even though the Nanofluid's temperature is always higher than that of water before freezing takes place. A huge difference is clear upon adding 1 wt% CNT to water. Temperature readings in Figure 3-30-(c) and Figure 3-30-(d) show that the Nanofluid has a much higher temperature than that of other tested liquids at some critical point, corresponding to the onset of natural convection at the density-inversion point. Only 1 wt% CNT Nanofluid shows a delay in reaching the density-inversion point compared to the base liquid and the other Nanofluid sample. An average of 23 minutes were the time delay in reaching the density inversion point for Nanofluid with 1 wt% CNT concentration. This delay in time is caused by the fact that adding more CNT particles tend to increase the viscosity of the working liquid, which suppresses natural convection and thus reducing the heat rate. This fact can be observed in Figure 3-31 and Figure 3-32.

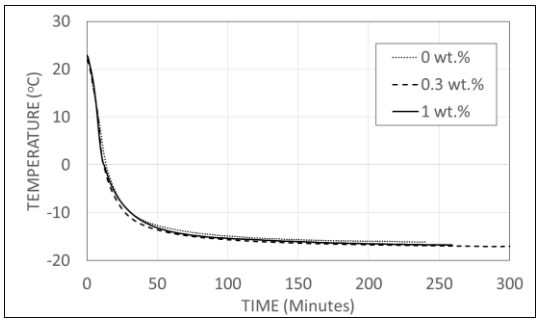

(a)

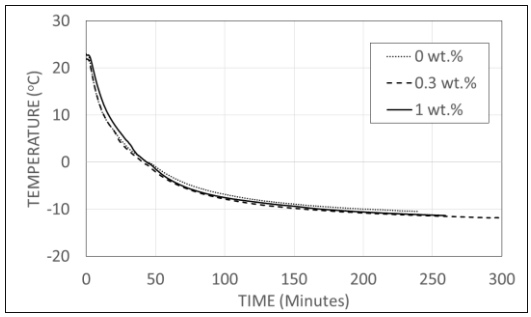

(b)

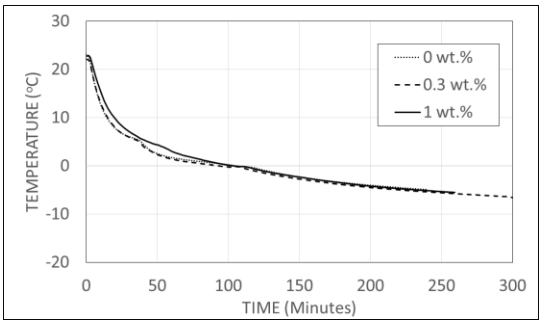

(c)

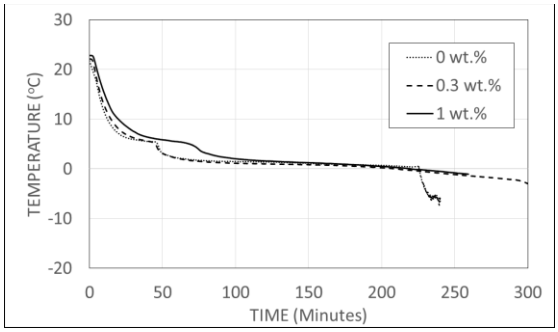

(d)

Figure 3-30: Temperature readings of Experiments with different CNT concentrations in the presence of natural convection at; (a) Thermocouple 1, (b) Thermocouple 2, (c) Thermocouple 3, and (d) Thermocouple 4.

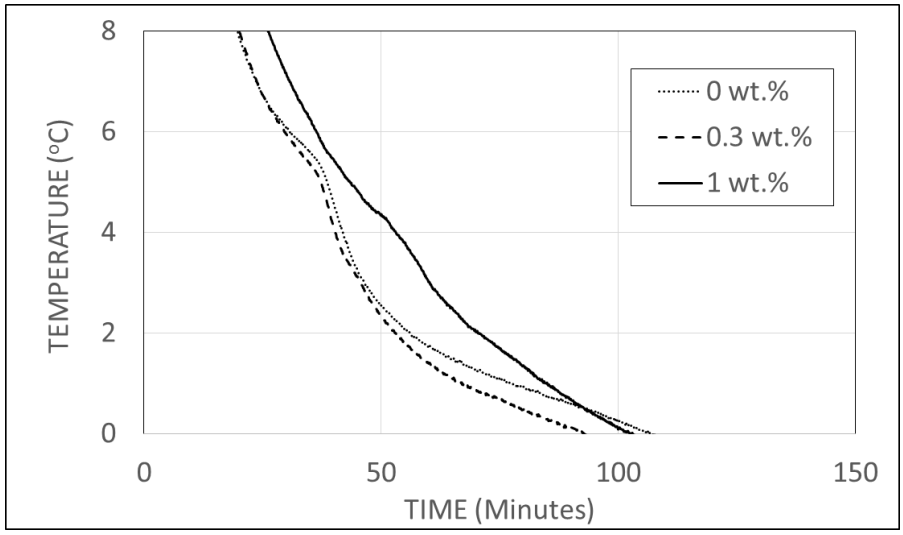

Figure 3-31: Zoomed-in plot of the temperature readings at the third thermocouple for different CNT concentrations in the presence of natural convection.

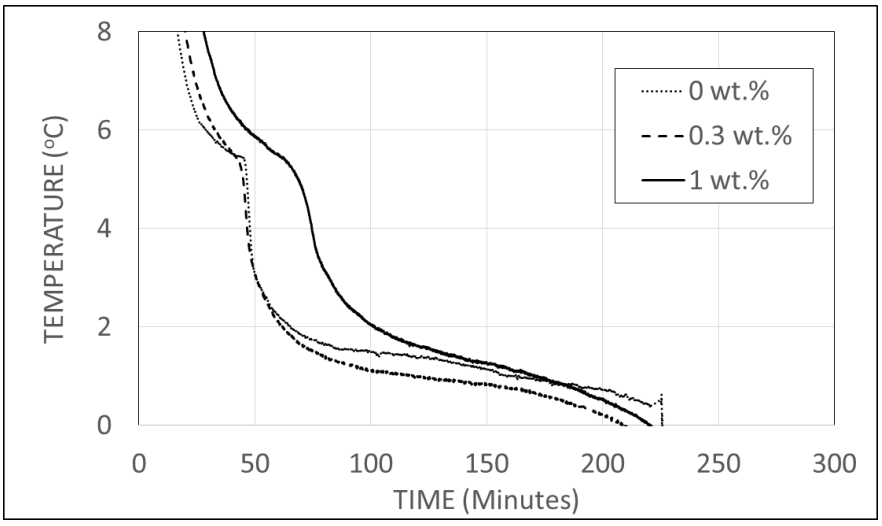

Figure 3-32: Zoomed-in plot of the temperature readings at the fourth thermocouple for different CNT concentrations in the presence of natural convection.

The solid-liquid front locations at different times can be seen in Figure 3-33. The front location is directly proportional to the square root of the elapsed time, a similar behavior observed in both experiments; however, with a little distortion in the convection-dominant situations. Adding more CNT particles to the base liquid seem to increase the time of front arrival at the fourth thermocouples, while the effect is not pronounced at the first, second and third thermocouples. The solid-liquid front arrives the fourth thermocouple 1 minute later and 14 minutes later than the base liquid arrival time for the cases of 0.3 wt% and 1 wt.% CNT concentration, respectively. This, in fact, is opposite to the previous experiment where diffusion was the dominant mode of heat transfer. The main reason is that adding more CNT particles reduces natural circulation strength and thus approaching the stratified freezing experimental results, which took longer times of complete freezing compared to the non-stratified situations. The solid-liquid arrival times can be seen in Figure 3-34.

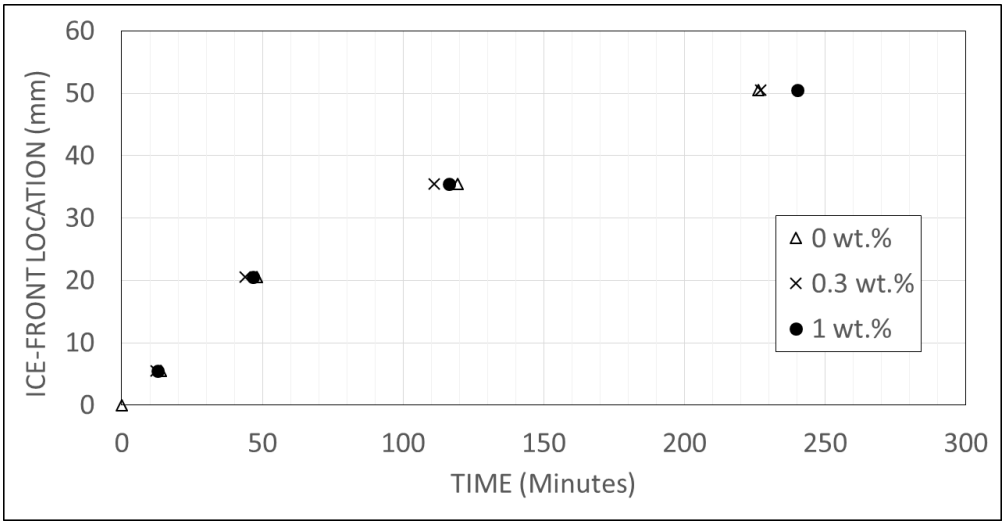

Figure 3-33: Plot of the Ice-front estimated location for different Nanofluids in the presence of natural convection.

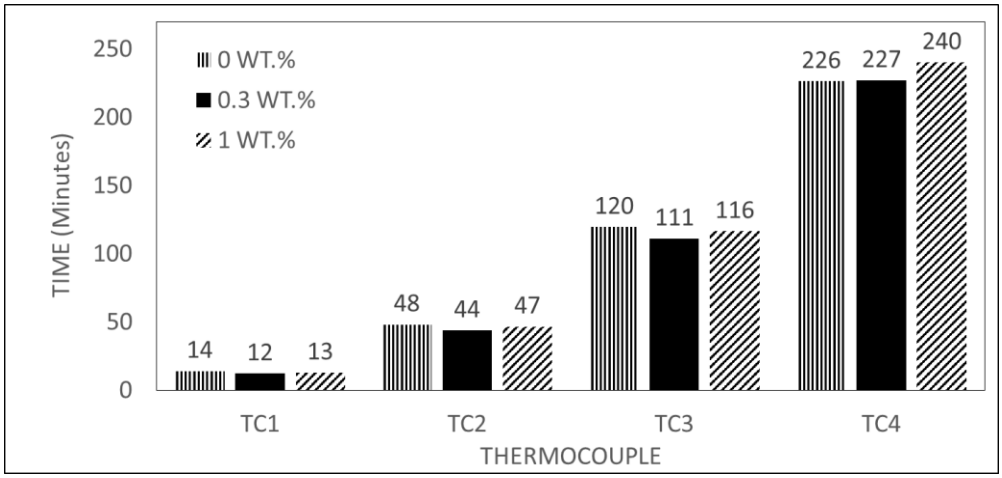

Figure 3-34: Summary of the solid-liquid front arrival times at the four thermocouples for all tested liquids in the presence of natural convection.

Figure 3-35 shows the speed of the solid-liquid front for the three tested fluids. Nanofluid with 1 wt% CNT concentration proves to be the slowest solid-liquid speed compared to other tested liquids.

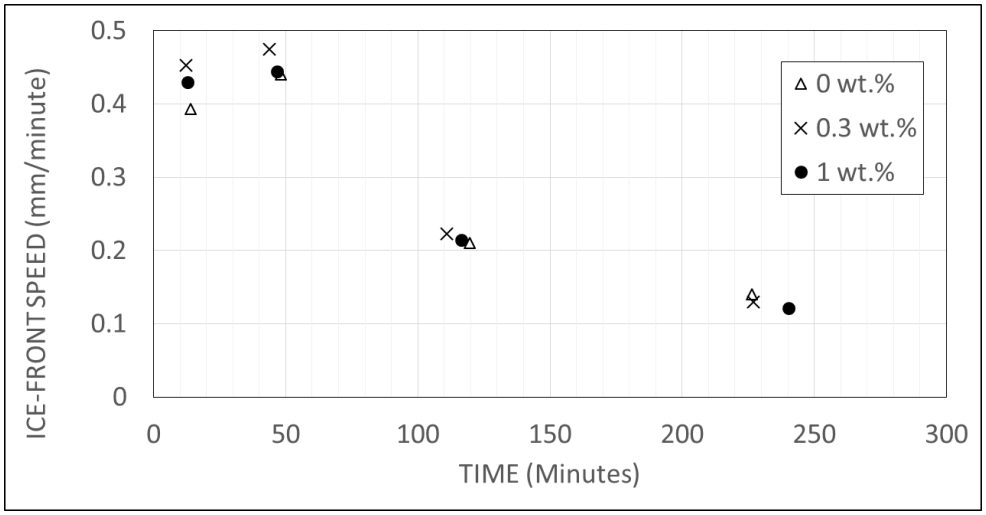

Figure 3-35: Plot of the Ice-front estimated speed for different Nanofluids in the absence of natural convection.

Figure 3-36 depicts the cooling power extracted out of the tested liquids. There is no big difference in the cooling energies between the tested liquids, except the largest CNT concentration, which consumed about 2 kJ more than the others.

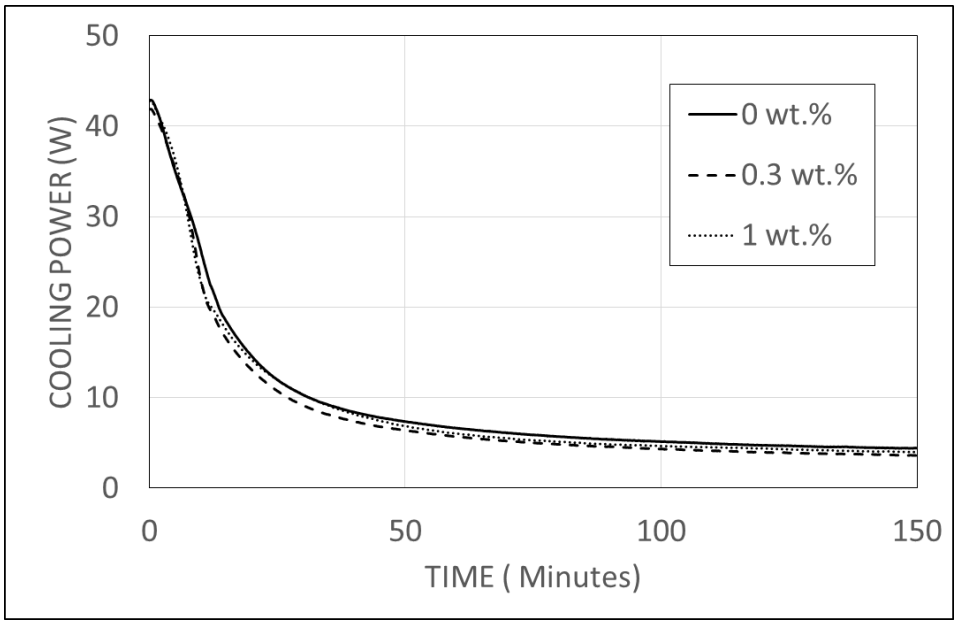

Figure 3-36: Plot of the estimated cooling power at the cooling wall for all tested liquids in the presence of natural convection.

3.3 Sources of Discrepancies

In this section, two sources of discrepancies in the experimental results are discussed namely thermal insulation as well as initial liquid temperature. The uncertainty of the time measurement is calculated corresponding to an uncertainty in temperature measurements of 0.6 ^{o}C. The time uncertainty is calculated to be 4 minutes. It is worth mentioning that this uncertainty is resulting from the calibration of the used thermocouples. There exist other uncertainty error sources such as that made by the uncertainty of initial liquid temperature. Since the uncertainty of initial temperature is about 2 ^{o}C, the corresponding time uncertainty is calculated in a similar manner as 12 minutes. Hence, the total uncertainty of time measurements is taken as 14 minutes.

The thermal insulation used in the experimental set-up was placed to cover the entire test cell and was made of 6-mm thick Styrofoam that was covered by aluminum sheets to reradiate surrounding temperature. To assess the effectiveness of the insulation, Figure 3-37 shows a comparison of two real photos of the solid-liquid front taken with and without insulation. It is clear that without thermal insulation the front takes a distorted shape, closer to a reversed C shape, in contrary to the shape made by thermally insulated freezing experiment. The reason of the reversed C shape is that the assumed-insulated walls of the test cell is participating in supplying heat from the surroundings and thus preventing the liquid; water in this case, to be frozen effectively.

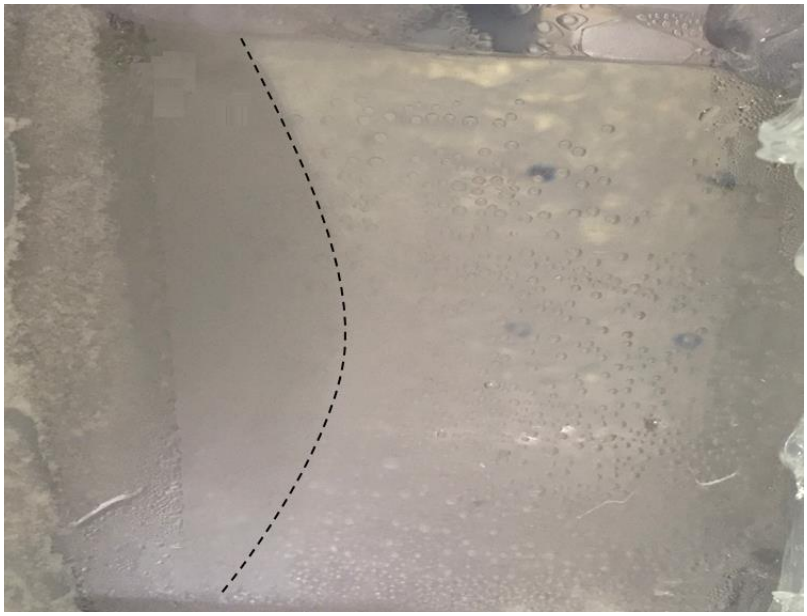

(a)

(b)

Figure 3-37: Photos of the experimental test cell at the same relative freezing time for the cases of (a) non-existing thermal insulation and (b) existing thermal insulation.

CHAPTER 4

NUMERICAL FORMULATION

As discussed in the previous chapters, this thesis investigates a two dimensional freezing problem. In this chapter, the same problem was investigated numerically by first constructing a computational fluid dynamic (CFD) model then validating it with the experimental results obtained earlier. In order to accomplish this task, the problem is first formulated, and then the numerical equations to be solved are introduced and discussed in details along with introducing the numerical technique used in solving those equations.

The CFD model requires solving several partial differential equations (PDEs) that are highly coupled. The equations are the mass, momentum, and energy conservation equations. The solution of those equations are difficult and computationally expensive due to the non-linearity when coupling the equations and due to the need of solving them simultaneously.

The equations of continuity, momentum, and energy equations are analytically solved for many simplified situations. However, the majority of heat transfer applications are complex in nature and numerical approach is needed. Many attempts were tried to simulate phase-change problems, especially solidification problems. The mathematical models of phase-change problems can be classified into two methods; moving-grid and fixed-grid methods. A general description of both methods can be found in [92].

In the moving-grid method, the governing conservation equations are solved for each phase separately. An additional equation is added to take care of the heat transfer at the solid-

liquid interface. However, in this method the solid-liquid interface position needs to be fed to the CFD code in order to evaluate the velocity and temperature fields.

In the fixed-grid method, only one set of conservation equations are solved for the entire domain, i.e. liquid phase, solid phase, and solid-liquid interface. The conservation of mass, momentum, and energy at the interface is taken care of by introducing suitable source terms. This method is going to be used in this work because it is already integrated in the software to be used.

4.1 Problem Formulation

The problem to be modeled herein is similar to that of the experiment. Figure 4-1 shows a two dimensional schematic diagram of the problem. The geometrical model is a rectangular cavity of a width (W_i) and a height (S) filled with liquid at an initial temperature of T_i, i.e. variable initial temperature. The temperature of left wall is dropped suddenly 20 degrees below the freezing point of water and the other walls are assumed adiabatic, i.e. corresponding to the insulated Plexi-glass walls in the experimental set up. The working fluids used in this research are water, as the base fluid, and CNT-water Nanofluids with different concentrations namely 1 wt%, and 2 wt%. It is intended, as well, to study the effect of the cavity size and the initial temperature of the freezing process. Both temperature and velocity fields are examined thoroughly.

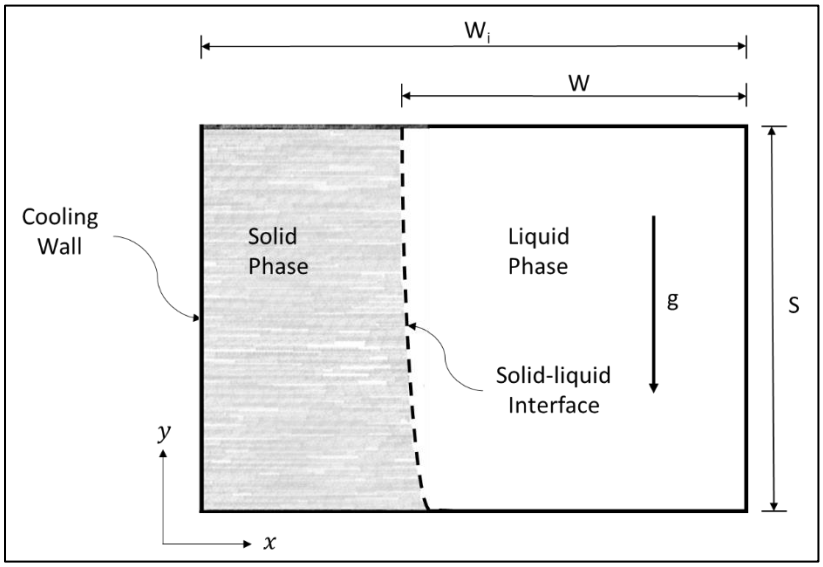

Figure 4-1: Schematic diagram of the physical model of the two dimensional solidification problem.

4.2 Governing Equations

In this section, the governing equations of the two-dimensional flow and temperature fields are presented. The working liquid, especially Nanofluid samples are treated as single homogenous fluids. In addition, the flow is assumed Newtonian, incompressible, and laminar. The transient mass, momentum and energy equations can be formulated as follows;

(a) Conservation of mass (Continuity) equation:

$$\frac{\partial \rho}{\partial t} + \rho \frac{\partial (v_x)}{\partial x} + \rho \frac{\partial (v_y)}{\partial y} = 0 \qquad (4\text{-}1)$$

Where ρ is the density, $v_x \; and \; v_y$ are the superficial velocities in the x- and y-directions, respectively.

(b) Conservation of momentum (Navier-Stokes) equations:

$$\frac{\partial (\rho v_x)}{\partial t} + v_x \frac{\partial (\rho v_x)}{\partial x} + v_y \frac{\partial (\rho v_x)}{\partial y} = -\frac{\partial p}{\partial x} + div(\mu \; grad \; v_x) + S_x \qquad (4\text{-}2)$$

$$\frac{\partial (\rho v_y)}{\partial t} + v_x \frac{\partial (\rho v_y)}{\partial x} + v_y \frac{\partial (\rho v_y)}{\partial y} = -\frac{\partial p}{\partial y} + div\left(\mu \; grad \; v_y\right) + S_y + S_b \quad (4\text{-}3)$$

Where p is pressure, μ is the liquid viscosity, and S_x , S_y and S_b are source terms which are defined later on.

(c) Conservation of energy equation:

$$\frac{\partial (\rho h)}{\partial t} + v_x \frac{\partial (\rho h)}{\partial x} + v_y \frac{\partial (\rho h)}{\partial y} = div\left(\kappa / c_p \; grad \; h\right) - S_e \qquad (4\text{-}4)$$

Where h is the sensible enthalpy, κ is thermal conductivity, and S_e is the energy source term, which is defined in the next paragraphs.

4.2.1 Source terms definition

The previously discussed governing equations are in a general format suggested by Patankar [93] for the numerical solution of fluid flow and heat transfer problems. The governing equations included a transient term, a convective term, a diffusive term, and source terms. In this format, Patankar stated that any problem could be modeled by defining suitable source terms. The model used in this work is called the enthalpy-porosity method developed first by Voller and Prakash [94]. It is important to note that the methodology used to model phase-change problems is by assuming the entire cavity as a porous medium, where the porosity is a function of temperature such that its value is unity in the liquid phase, allowing free movement of liquid, and zero in the solid phase, stopping the particle movements in solid phase. In the following paragraphs, the necessary source terms for that purpose to be accomplished are defined.

(a) S_x and S_y source (momentum sink) terms:

The way of coupling the momentum and energy equations lies in determining the best momentum sink terms. This way should guarantee that if the temperature of any fluid particle approaches the solidification temperature, the velocity of that fluid particle is zeroed. There are three existing techniques to implement this method. These are switching-off technique, Darcy law method, and variable viscosity method.

The switching-off technique states that if the temperature of a cell in the domain reaches the solidification temperature, the velocity in that cell should be switched off to zero and momentum equation is no longer solved for that cell, i.e. only energy equation is solved. On the other hand, if the temperature of a cell is higher than the solidification temperature, the momentum equation is solved along with the energy equation.

The variable viscosity technique, however, states that if the temperature of a cell reaches the critical temperature, the viscosity of that cell is increased to a very large number reducing the velocity in that cell to zero.

The method used in this work, which is used in the available software, is the Darcy law technique. It treats the domain as a porous medium with a temperature dependent porosity. It states that initially the domain has a unity porosity, corresponding to a full liquid phase. When the temperature solution of a cell reaches the critical temperature, the porosity of that cell is decreased to a very low value, supressing the fluid flow. The software used in this work is developed to simulate the solidification of alloys as well as pure substances. Compound alloys solidifies at a range of temperatures and a mushy zone exists between the two phases where the temperature distribution might not be linear. In order to simulate any type of material, the solidification phase change is assumed to take place between two temperatures, i.e. T_s and T_l those are called solidus and liquidus temperatures, respectively. In the case of simulating pure liquids both temperatures are equal and no mushy zone would exist. In general, the porosity of liquid particle with temperatures between the two temperatures varies linearly according to the following relation

$$\lambda = \begin{cases} 0, & T \leq T_s \\ (T - T_s)/(T_l - T_s), & T_l < T < T_s \\ 1, & T \geq T_l \end{cases} \qquad (4\text{-}5)$$

As clearly indicated in this relation, if a cell in the domain is at a temperature higher than the liquidus temperature, the porosity has a unity value. The porosity in this method is equivalent to the liquid fraction in the cell; hence, the term porosity is replaced by liquid fraction in the remaining part of this writing, for easy referring to the topic.

Starting from Darcy's Law and following the derivation of Voller and Prakash, the momentum sink terms are written as

$$S_x = -A\,v_x \tag{4-6}$$

$$S_y = -A\,v_y \tag{4-7}$$

Where A has the following form

$$A = -\frac{C(1-\lambda)^2}{(\lambda^3+\varepsilon)} \tag{4-8}$$

Where ε is a very small number to avoid division by zero in numerical solution, and C is a mushy-zone constant, which depends on the morphology of the porous medium in cells where the temperature is between the solidus and liquidus temperatures. In the case of modelling solidification problems, the value of this factor is a very large number generally in the range of 10^4 to 10^7.

In a solidification problem, the effect of the momentum sink terms is as follows. In the liquid part of the domain, corresponding to a liquid fraction of unity, the source terms have a value of zero hence the velocity obtained are those obtained by the ordinary momentum conservation equations. In the mushy zone, the value of A increases with decreasing the liquid fraction; hence, starting to overcome the other terms of the momentum conservation equations. In the solid part of the domain, corresponding to a liquid fraction of zero, the source terms dominate all other terms in the momentum conservation equations and force the velocities in the corresponding cells to values close to zero. The limiting value of A, i.e. $-C/\varepsilon$, should be as high as possible to supress fluid velocities in the solid part.

(b) S_b (body force) source term:

This source term is in the y-direction momentum conservation equation and is used to induce natural convection in the cavity, which stems from the variation of density with temperature variation. The body force source is written in general as

$$S_b = \rho g \tag{4-9}$$

Where ρ is density variation, which is a function of temperature. Assuming Boussinesq approximation to be valid in treating the flow process, i.e. density is independent of temperature except for a gravity source term where density varies with temperature as the following equation

$$\rho = \rho_o + \rho_o \beta (T - T_o) \tag{4-10}$$

Then, Substituting Equation 4-10 into Equation 4-3, the body force source term can be rewritten as

$$S_b = \rho_o g [1 + \beta (T - T_o)] \tag{4-11}$$

Where ρ_o is a reference density, g is the gravitational acceleration, i.e. 9.81 m/s^2, β is a thermal expansion coefficient of the fluid, and T_o is a reference temperature. This term is valid if the temperature difference in the domain is small and density change is not significant.

(c) S_e (energy) source term:

An important aspect in phase change processes is the fact that as the liquid solidifies, a latent heat of diffusion is released and that has to be taken care of in modelling such problems. Therefore, it is customary to express the total enthalpy by the following relation

$$H = h + \Delta H \tag{4-12}$$

i.e. the sum of sensible enthalpy, $h = c_p T$, and latent heat of fusion ΔH. The latent heat is a function of temperature. In the case of solidification problems where a mushy zone exists, it is given by

$$\Delta H = \begin{cases} 0, & T < T_s \\ \lambda L, & T_l < T < T_s \\ L, & T > T_l \end{cases} \tag{4-13}$$

This equation suggests that in a solidification process, the phase is originally liquid and the total heat is composed of the sensible heat added to the latent heat. However, as temperature of a cell approaches the solidus temperature, the latent heat is released and thus the total enthalpy equals to only the sensible enthalpy.

Voller suggested using the following energy equation formulation of convection-diffusion phase change problems

$$\frac{\partial(\rho H)}{\partial t} + v_x \frac{\partial(\rho H)}{\partial x} + v_y \frac{\partial(\rho H)}{\partial y} = div(\kappa \, grad \, T) \tag{4-14}$$

Note, the energy equation suggest above is in terms of the total enthalpy rather than the sensible enthalpy presented in Equation 4-4. Substituting Equation 4-11 and comparing the resulting equation with Equation 4-4, proves that the energy source term is given by

$$S_e = \frac{\partial(\rho \Delta H)}{\partial t} + v_x \frac{\partial(\rho \Delta H)}{\partial x} + v_y \frac{\partial(\rho \Delta H)}{\partial y} \tag{4-15}$$

For isothermal solidification problem, or a very small mushy zone problem, the convective part is neglected, because of the small values of velocity magnitudes.

4.2.2 Non-dimensional form of the governing equations

In order to understand the physics behind the problem at hand, the governing equations are non-dimensionalized. The governing equations in this new form are in form of dimensionless parameters that, then, can be generalized for many situations. The derivation is obtained by adopting the following dimensionless parameters

$$\tilde{x} = \frac{x}{W_i} \qquad \tilde{y} = \frac{y}{S} \qquad \widetilde{v_n} = \frac{v_n}{k/(\rho C_p S)}$$

$$\tilde{p} = \frac{p}{k^2/(\rho C_p^2 S^2)} \qquad \tilde{t} = \frac{t}{(\rho C_p S^2)/k} \qquad \tilde{T} = \frac{T - T_{cr}}{T_i - T_{cr}} \tag{4-16}$$

$$\widetilde{\Delta H} = \frac{\Delta H}{L}$$

Where subscript i stand for initial value, subscript n stands for directions x and y, and T_{cr} is critical temperature of freezing, because it is the temperature of the solid-liquid front at all times and it is the cause of natural convection. The resulting mass, momentum, and energy equations are as follows, in respective order

$$(AR)\frac{\partial(\widetilde{v_x})}{\partial\tilde{x}} + \rho\frac{\partial(\widetilde{v_y})}{\partial\tilde{y}} = 0 \tag{4-17}$$

$$\frac{\partial(\widetilde{v_x})}{\partial\tilde{t}} + (AR)\widetilde{v_x}\frac{\partial(\widetilde{v_x})}{\partial\tilde{x}} + v_y\frac{\partial(\widetilde{v_x})}{\partial\tilde{y}} = -(AR)\frac{\partial\tilde{p}}{\partial\tilde{x}} + \frac{1}{(Pr)}[(AR)^2\frac{\partial^2\widetilde{v_x}}{\partial\tilde{x}^2} + \frac{\partial^2\widetilde{v_x}}{\partial\tilde{y}^2}] + \tilde{A}\widetilde{v_x} \tag{4-18}$$

$$\frac{\partial(\widetilde{v_y})}{\partial\tilde{t}} + (AR)\widetilde{v_x}\frac{\partial(\widetilde{v_y})}{\partial\tilde{x}} + v_y\frac{\partial(\widetilde{v_y})}{\partial\tilde{y}} = -\frac{\partial\tilde{p}}{\partial\tilde{y}} + \frac{1}{(Pr)}\left[(AR)^2\frac{\partial^2\widetilde{v_y}}{\partial\tilde{x}^2} + \frac{\partial^2\widetilde{v_y}}{\partial\tilde{y}^2}\right] + \tilde{A}\widetilde{v_y} + (Ra)(Pr)\tilde{T} \tag{4-19}$$

$$\frac{\partial(\tilde{T})}{\partial\tilde{t}} + (AR)\widetilde{v_x}\frac{\partial(\tilde{T})}{\partial\tilde{x}} + \widetilde{v_y}\frac{\partial(\tilde{T})}{\partial\tilde{y}} = (AR)^2\frac{\partial^2\tilde{T}}{\partial\tilde{x}^2} + \frac{\partial^2\tilde{T}}{\partial\tilde{y}^2} - \frac{1}{(Ste)}\frac{\partial\widetilde{\Delta H}}{\partial\tilde{t}} \tag{4-20}$$

It is important to note here that an important assumption was made during the derivation of the previous equations, which is the applicability of assigning constant thermophysical properties for each phase, i.e. solid phase can have different properties than liquid phase. The applicability of Boussinesq approximation was assumed valid in the derivation for simplification purposes. The most important note of Equations 4-17 through 4-20 is the appearance of five dimensionless numbers; those are aspect ratio (AR), Prandtl number (Pr), Rayleigh number (Ra), Stefan number (Ste), and porosity modified factor ($\tilde{A}$). The definition of those numbers are given as

$$AR = {S}/{W_i} \qquad Pr = {\mu C_p}/{k}$$

$$Ra = \frac{\rho_l^2 g \beta C_{p,l}(T_i - T_{cr})S^3}{\mu K_l} \qquad Ste = \frac{C_{p,s}(T_i - T_c)}{L} \tag{4-21}$$

$$\tilde{A} = \frac{A}{\mu/S^2}$$

One may notice that aspect ratio, Rayleigh number, and porosity-modified factor depend on the geometry of the domain as well as the initial temperature of the working liquid. The influence of the temperature of the cooling plate shows up as a factor affecting Stefan number because of the need to find the heat capacity at an average temperature between the critical and the plate temperatures. Prandtl number depends solely on the initial temperature of the working fluid. In this work, different Rayleigh numbers and aspect ratios were investigated to obtain a better understanding of the freezing process. Note that the non-dimensional form of governing equations are not referred to anymore, since they served their purpose stated at the beginning of this section.

4.2.3 Control volume discretization

The previous governing equations are constructed for a two dimensional flow. The solution of those equations are obtained using various techniques, such as finite difference, and finite volume methods. In this thesis, a brief overview of the finite volume method is presented. The reason of using this method is that a CFD software is used to solve those equations. The software used is FLUENT, which uses a finite volume approach to solve the mass, momentum, and energy equations. A fully implicit advancement in time and upwind in space differencing schemes are adopted in this work. Patankar in 1980 [93] developed the finite volume method used in this work.

To illustrate the method used by Patankar, the energy equation, i.e. equation 4-4, is solved for a finite domain. The finite domain is first discretised into finite volumes, i.e. areas in a two dimensional domain. Following the notations in Patankar's work, and referring to Figure 4-2, the energy equation is rewritten as

$$a_P h_P = a_E h_E + a_W h_W + a_N h_N + a_S h_S + a_P^o h_P^o + b \qquad (4\text{-}22)$$

Where the a's refer to the coefficients representing the convective and diffusive fluxes in the pth control volume, and the subscripts $P, E, W, N,$ and S indicate the nodal locations relative to the pth control volume. The superscript o represents that this term is evaluated at the previous time step, and the term b represents the discretized form of the energy source term. The discretization of the momentum equation is similar. However, with an important addition of the staggered grids to avoid the zigzagging problem of the pressure field [93].

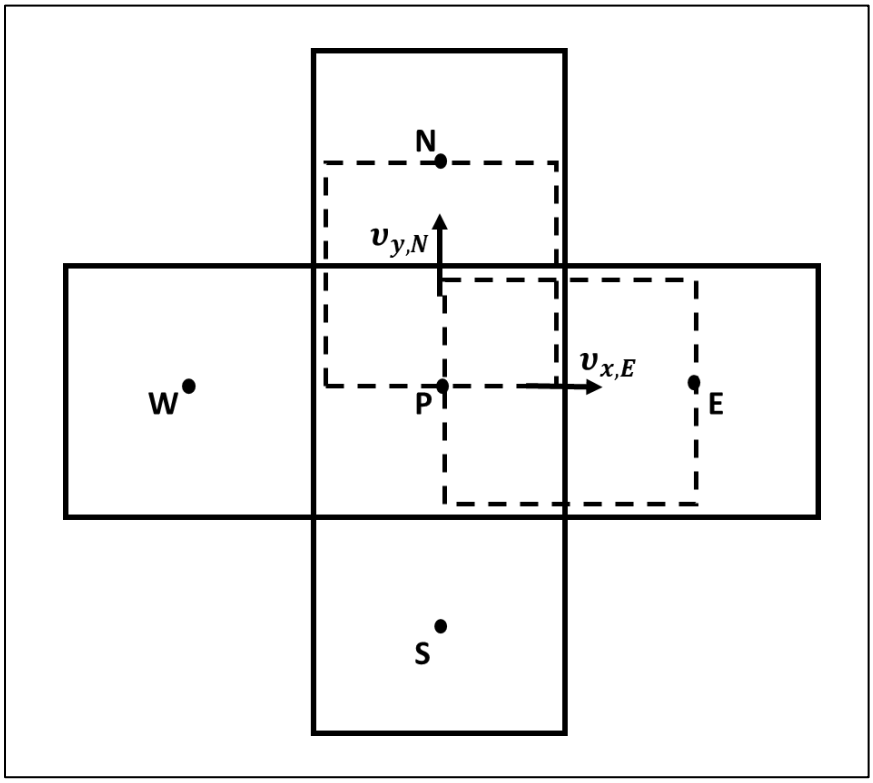

Figure 4-2: control volume discretization of a two dimensional flow domain, indicating the staggered grids.

4.3 Numerical Solution Methodology

In this thesis, FLUENT 15 is used and the following necessary settings are followed in simulating the CFD model. The solidification/melting model was enabled and a mushy zone constant C was set to 10^5 , i.e. the default value suggested by FLUENT. The SIMPLE algorithm was used to solve the governing equations. The momentum and energy equations were solved using the QUICK differencing scheme. The pressure correction equation was solved using the PRESTO scheme. The problem at hand is nonlinear so the use of under-relaxation factors is important for the solutions to converge. The under-relaxation factors for the pressure correction, momentum, liquid fraction, and energy were set to 0.3, 0.7, 0.9 and 0.6, respectively. The residual convergence criteria were set to 10^{-7} for continuity and momentum, and 10^{-9} for thermal energy. To satisfy that, the number of iteration under each time step is set to be 100. Extrapolation of future results was allowed while solving the governing equation for better convergence or results.

In order to induce natural convection in the test cell, the density was allowed to vary with temperature in a gravity source term. A trial to simulate variable density in the closed cavity failed to give good results due to the fact that mass cannot be conserved in a closed domain if the density is varied by a great amount. A modified Boussinesq approximation was used, in which the gravitational source term included a variable thermal expansion coefficient, taking into account the density inversion point. Results showed good matching between the experimental and numerical temperature and flow fields. The subroutine of the modified Boussinesq approximation is given in Appendix H.

4.4 Solution Independency Tests

It is important to understand that there are two types of errors in numerical analysis; those are numerical error and true error. The *numerical error* can be checked by first applying a certain grid size or time step and obtaining the solution. Then, another solution is obtained by refining the grid size or time step. The new solution corresponding to the new grid size or new time step is compared to the previous solution and the relative error is obtained. If the relative error is found to be low in magnitude, then the previous grid size or time step is sufficient to be used with minimum numerical error. Bearing in mind that using finer grid sizes and time steps is computationally expensive and time consuming. The other type of errors is the *true error*, which is defined as the relative error between the numerically obtained value and the actual experimental value. This error is high in nature, since numerical solution is just a simplification of the actual physical situation with simplifying assumptions. Grid size and time step independency tests were performed and discussed in the following sections. In order to obtain a general grid size and time step, the experimental results are used as they present the highest Rayleigh number to be simulated.

4.4.1 Solution independency of grid size

The results of Experiment 2 was simulated using the aforementioned numerical procedure. The width and height of the cavity were set to 6 cm and 5 cm, respectively. The initial liquid temperature was set to 295 K. The cooling wall was suddenly dropped to a temperature of 253 K. A fine time step was used in order to obtain good representative comparison, i.e. a time step of one second was used.

It is important that the solution be optimized while giving accurate temperature and flow fields. In order to observe the error involved with different grid sizes in the temperature field, Figure 4-3 shows the temperature and vertical velocity profiles at two horizontal lines in the tested cavity namely, y/S=0.25 and y/S=0.75. The table show the profiles after a time interval of 900 seconds. The grid structure tested is of a mapped type where the domain is divided into squares of side dimensions of 1 mm, 0.5 mm, 0.25 mm, and 0.125 mm.

It can be noticed that grid sizes of 0.5 mm, 0.25 mm, and 0.125 mm can be used to obtain the temperature field with low errors involved. However, for velocity field a grid size of 0.25 mm and 0.125 mm or lower should be used. In this work, a grid size of 0.25 mm was chosen, as numerical error involved is considered minimal for this application of heat transfer problems.

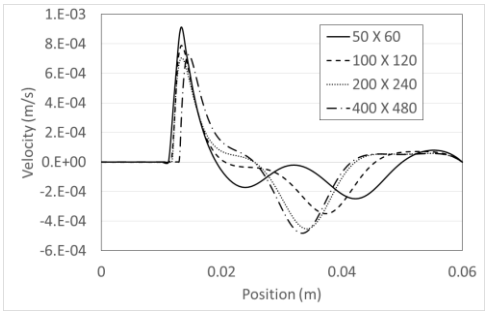

(a)

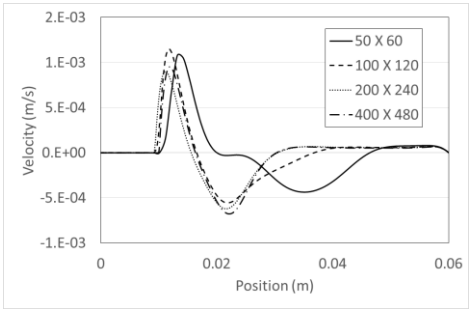

(b)

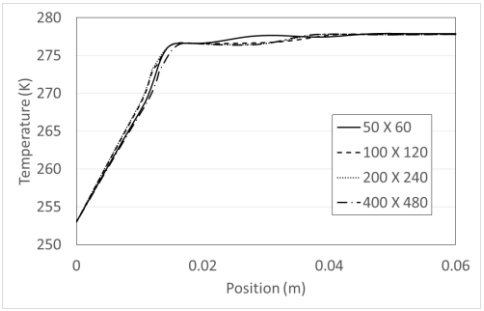

(c)

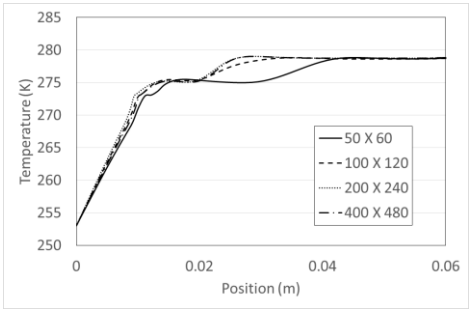

(d)

Figure 4-3: Grid-size independency tests of vertical velocity and temperature profiles at a time of 900 seconds: (a) vertical velocity at y/S=0.25 (b) vertical velocity at y/S=0.75 (c) temperature at y/S=0.25 (d) temperature at y/S=0.75

4.4.2 Solution independency of time step

In order to observe the error involved with different time steps in the temperature and flow fields, Figure 4-4 shows the temperature and vertical velocity profiles at two horizontal lines in the tested cavity namely, y/S=0.25 and y/S=0.75. The table shows the profiles after a time interval of 900 seconds. The time steps tested were 20 seconds, 10 seconds, 5 seconds, and 1 second. The grid size used was that obtained from the previous section, i.e. 0.25 mm square cells.

It can be noticed that using a time step of either 5 seconds or 1 second would give similar results with low numerical errors. In this work, a time step of 5 seconds was chosen as numerical error involved is considered minimal for this application of heat transfer problems.

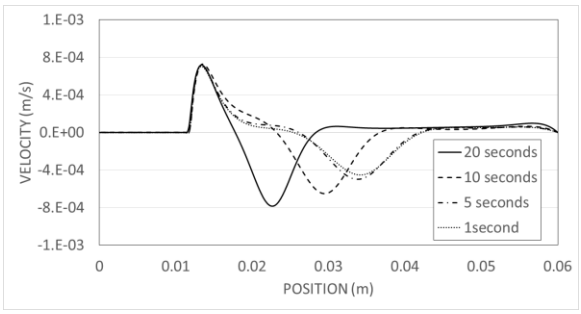

(a)

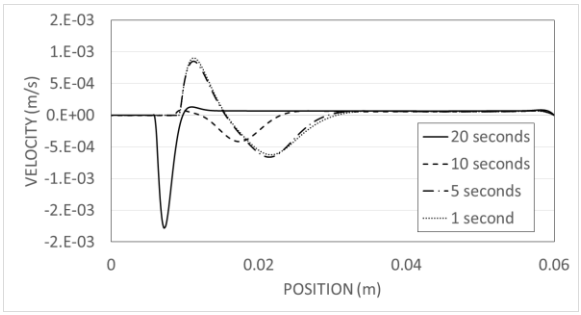

(b)

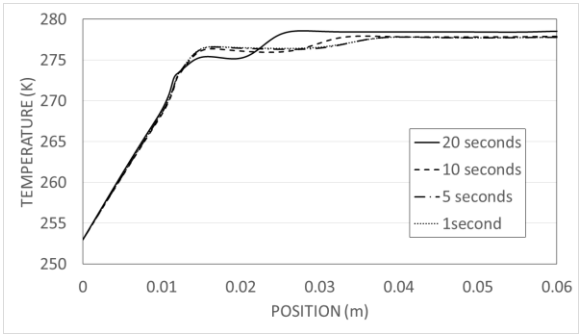

(c)

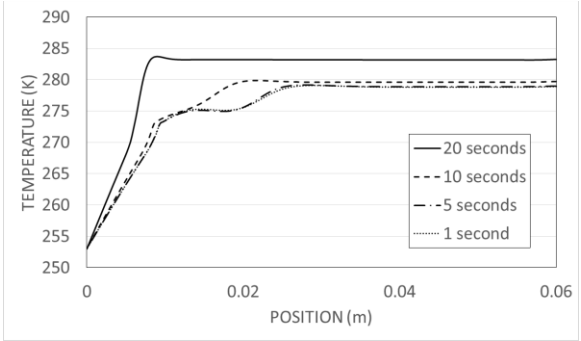

(d)

Figure 4-4: Vertical velocity and temperature profiles for comparison between different time steps at a time of 900 seconds: (a) vertical velocity at y/S=0.25 (b) vertical velocity at y/S=0.75 (c) temperature at y/S=0.25 (d) temperature at y/S=0.75

4.5 Validation against Experimental Results

In this section, the CFD model is validated against other published results as well as the experimental results obtained in this work. First, the solidification of water is going to be simulated using the CFD model and compared to the results obtained in the previous chapter. Next, the model is validated against the work of Gau and Viskanta [95],in which they performed a melting experiment of pure Gallium. Their work has been a benchmark of many research papers that simulate phase-change problems [86].

Figure 4-5 and Figure 4-6 represent the temperature readings at different points in the test cavity. Those points are made such that they represent the position of the four thermocouples placed in the experimental work. Figure 4-5 depicts the case of stratified freezing experiment of water. The numerical model seem to estimate the temperature reading at the first thermocouple. However, the reading of the second thermocouple was not perfectly estimated. The imperfection occurs in the region where natural convection cause by density-inversion point. Similarly, the third and fourth thermocouples where estimated by the numerical model, however, with an over-estimation of the strength of natural convection caused by the density-inversion point. Figure 4-6 indicates the temperature readings for the case of non-stratified freezing experiment of water. Similar to the stratified experiment, temperature were estimated to a good extent by the CFD model with an over-estimation of the strength of natural convection, especially in the density-inversion vicinity. However, for all cases the freezing front were estimated with an error of less than 20%. A successful trial to solve the problem was performed by increasing the viscosity of the working liquid to weaken the natural convection effect.

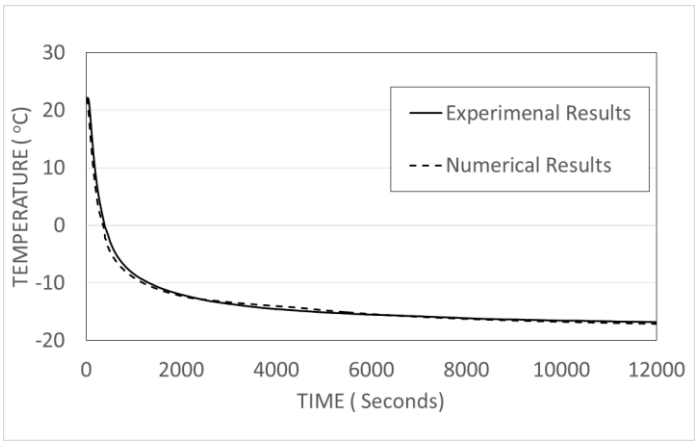

(a)

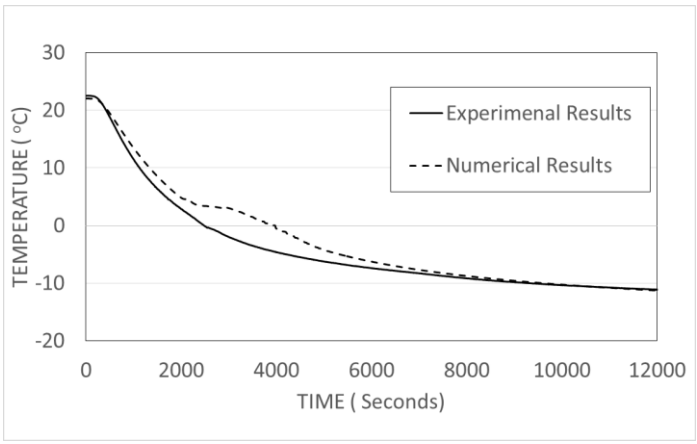

(b)

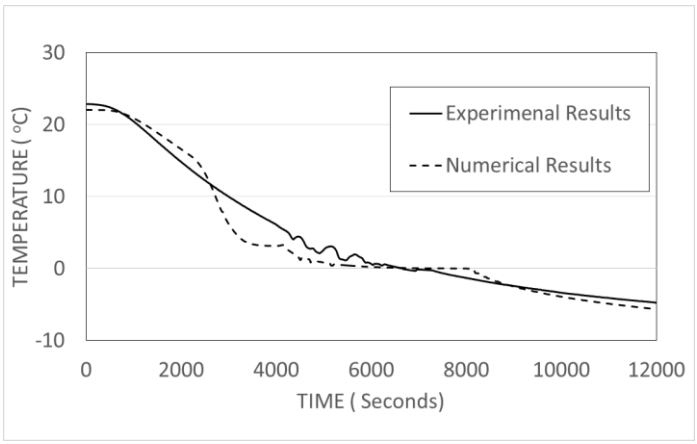

(c)

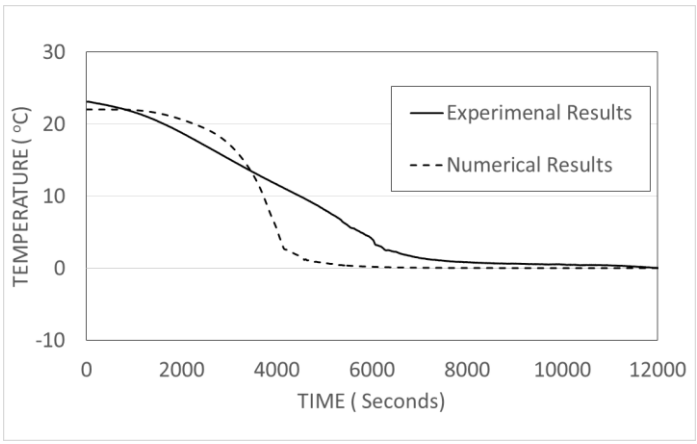

(d)

Figure 4-5: Validation of CFD model against experimental results for the case of stratified freezing of water at (a) Thermocouple 1 (b) Thermocouple 2 (c) Thermocouple 3 (d) Thermocouple 4.

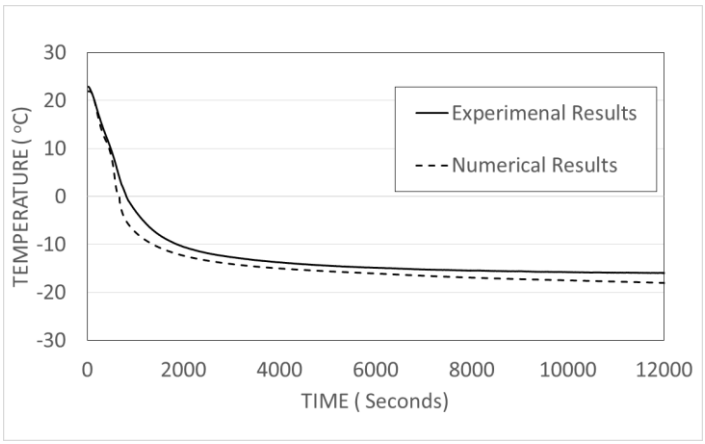

(a)

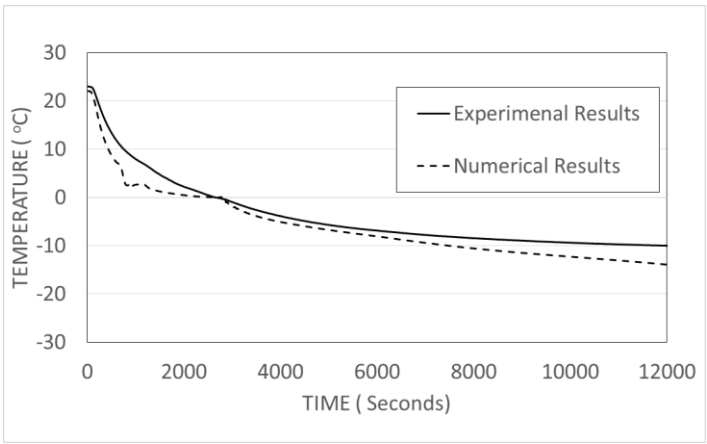

(b)

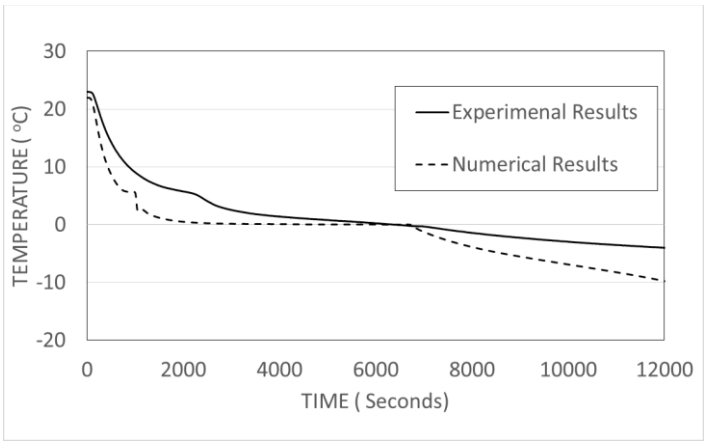

(c)

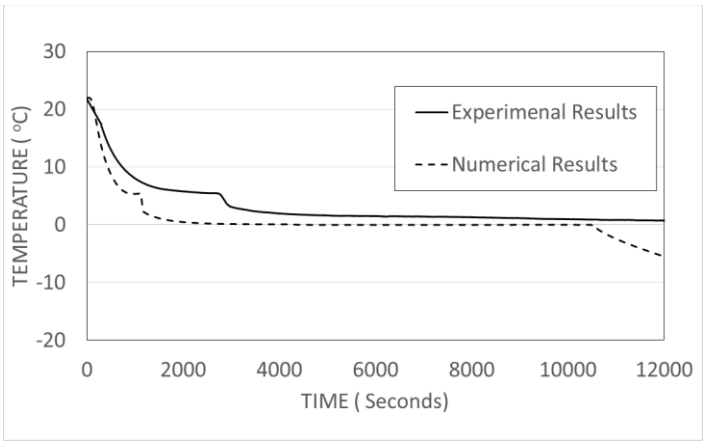

(d)

Figure 4-6: Validation of CFD model against experimental results for the case of non-stratified freezing of water at (a) Thermocouple 1 (b) Thermocouple 2 (c) Thermocouple 3 (d) Thermocouple 4.

Second, The work of Gau and Viskanta [95] was simulated using the present CFD model and is presented in Figure 4-7. In that work, pure Gallium was present in a cavity with dimensions 6.35 cm × 8.89 cm. Gallium was placed in the cell as a solid at its critical temperature and was melted by one wall maintained at 9 degrees above the critical temperature of Pure Gallium. Figure 4-7 shows that the CFD model is able to estimate the solid-liquid front to a good extent. However, sources of discrepancy are being that properties of Gallium was inputted to the model as constants and temperature independent, which led to the problem of not matching the experimental results.

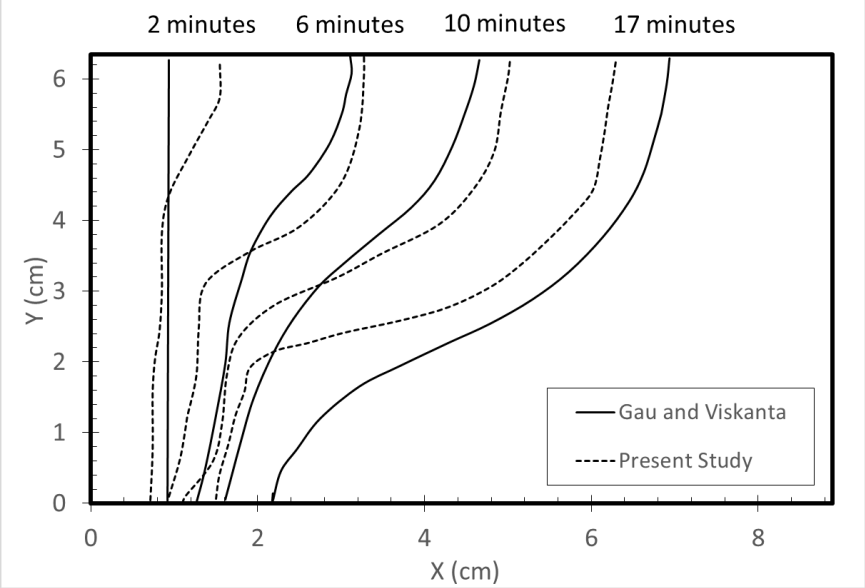

Figure 4-7: Validation of the CFD model against the work of Gau and Viskanta [95], indicating the solid-liquid front at different times of melting pure Gallium in a cavity.

4.6 Parametric Study of the Freezing Process: Results and Discussion

In this section, a discussion of different parameters that affect the freezing process is presented. Initial Rayleigh number, cavity aspect ratio, as well as CNT concentration are studied as the main parameters of this study. The use of initial Rayleigh number is because Rayleigh number in the test cavity will vary from an initial maximum value to zero at the end of the freezing process. Initial Rayleigh number and cavity aspect ratio were discussed in a previous section. In order to simplify the presentation of data, Cases of pure-water freezing is first presenting and results are discussed in details. Second, freezing of different CNT concentrations are presented for selected pairs of initial Rayleigh numbers and aspect ratios. Finally, the best cases are concluded and further recommendations are given to enhance the freezing process of PCM.

4.6.1 Freezing of pure water (Stratified Vs. Non-stratified)

Pure-water freezing in a rectangular two-dimensional box is simulated using the developed CFD model. The geometry of the simulated cases is sketched in Figure 4-1. Nine cases were made corresponding to different aspect ratios and different initial Rayleigh numbers, summarized in Table 4-1. Three aspect ratios were tested; those are two, one, as well as 0.5. The aspect ratio is defined as the ratio of the length of the cooling plate to the width of the cavity. The length of the cooling plate was held constant because varying the length of the cooling wall means changing the cooling power supplied to the system, which makes comparison of different aspect ratios useless. Rather the length of the cooling wall is held constant and the volume of the test cavity is changed according to the studied aspect ratio, then results can be normalized to a unit volume of liquid. Three different initial Rayleigh numbers were numerically simulated as well, those are 9×10^3, 5.9×10^5 and 1.12×10^6, corresponding to initial liquid temperatures of 1°C, 25 °C and 60 °C. The thesis's main objective to understand the effect of natural convection of the freezing process, hence, each simulated case is performed twice; one solving only for the energy equation (referred to as stratified cases), and the other solving for the flow and energy equations (referred to as non-stratified cases). Results of cases are compared to understand the contribution natural convection makes to the freezing process.

Table 4-1: Summary of the simulated parameters for the freezing of pure water.

No.	Temperature Difference $(T_i - T_{cr})$	Aspect Ratio AR	Initial Rayleigh number Ra_i	Prandtl Number Pr	Stefan Number Ste
1	1 K	1	9×10^3	9.52	0.006
2	25 K		5.9×10^5	6.52	0.145
3	60 K		1.12×10^6	8.03	0.348
4	1 K	2	9×10^3	9.52	0.006
5	25 K		5.9×10^5	6.52	0.145
6	60 K		1.12×10^6	8.03	0.348
7	1 K	0.5	9×10^3	9.52	0.006
8	25 K		5.9×10^5	6.52	0.145
9	60 K		1.12×10^6	8.03	0.348

Figure 4-8, Figure 4-9, Figure 4-10, and Figure 4-11 show the results of isotherms and streamlines at different freezing times for some of the studied cases. The isotherms in the figure are representative of how heat is being transferred in the test cell, such that vertically aligned isotherms are indicative of diffusion mode of heat transfer. On the other hand, distorted isotherms might indicate the existence of other heat transfer modes, such as natural convection heat transfer in this case. Figure 4-8 depicts the isotherms and liquid fractions of the first case in Table 4-1. As can be seen in this Figure 4-8-(i), isotherms are vertical and aligned at all times meaning that heat is transferred by means of diffusion only, even though a value of initial Rayleigh number of 9×10^3 is above the critical value above which natural convection is effective. The critical Rayliegh number is reported to be about 1000 [91]. There exists a weak circulation of flow shown in Figure 4-8-(ii). As the freezing process advances, natural circulations become weaker until diminishing. This case would be the basis to which CNT-water Nanofluids are compared. Similar to the experimental results presented in the previous chapter, CNT-water Nanofluids proved to be effective when diffusion alone was the mode of heat transfer.

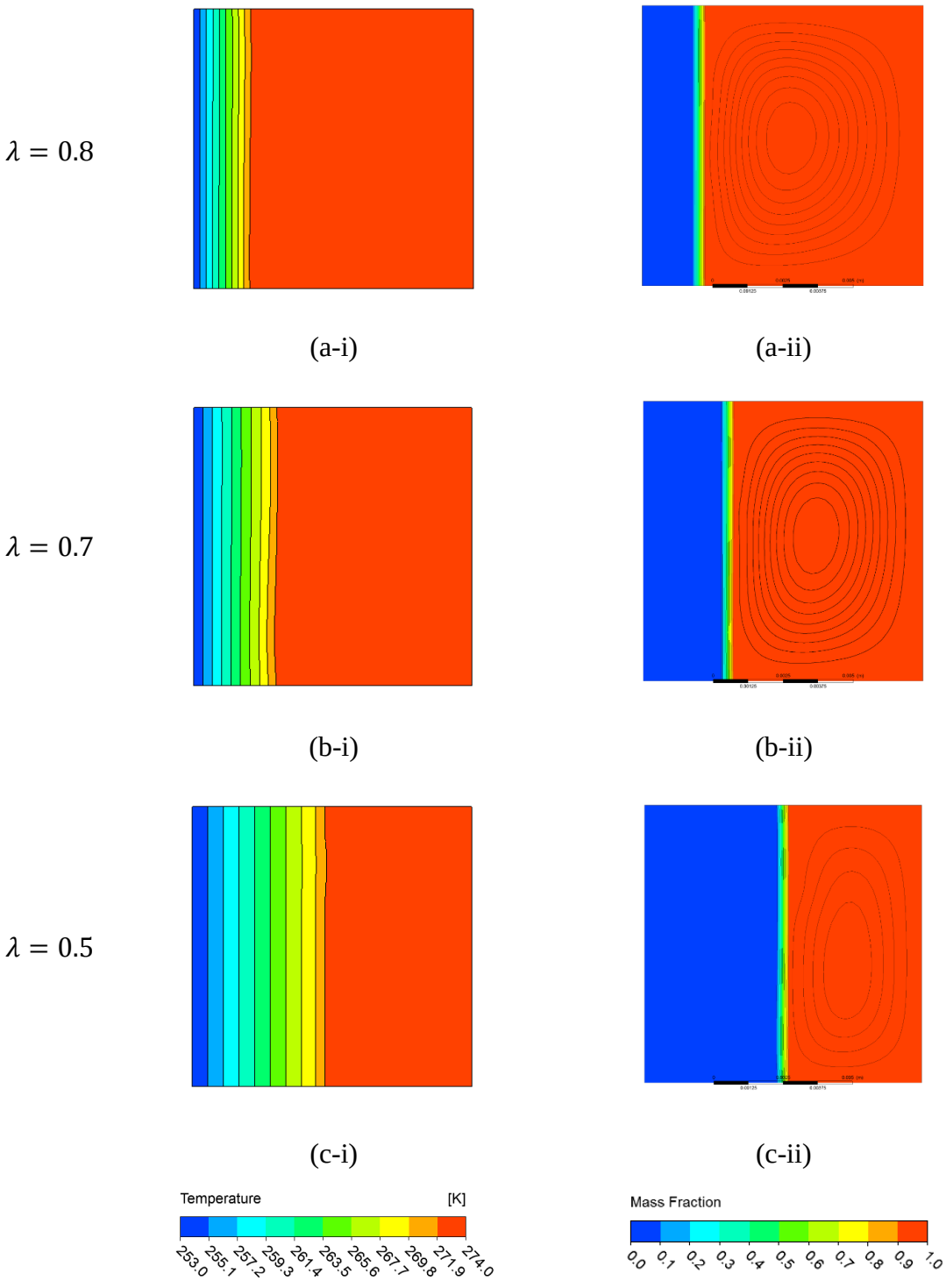

Figure 4-8: Results of simulated cases of unity aspect ratio and $Ra_i = 9 \times 10^3$, indicating (i) isotherms and (b) liquid mass fraction as well as streamlines.

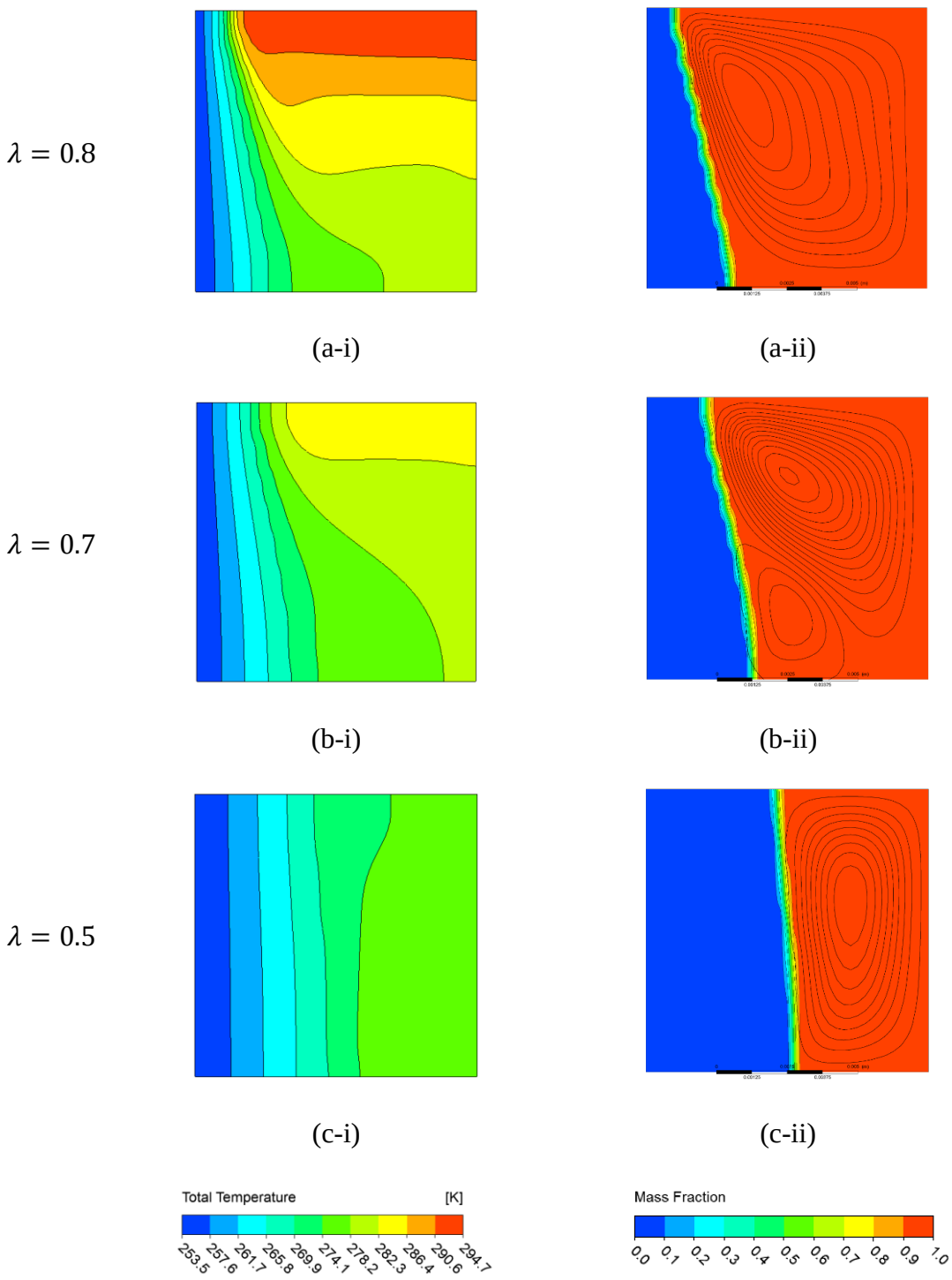

Figure 4-9: Results of simulated cases of unity aspect ratio and $Ra_i = 1.12 \times 10^6$, indicating (i) isotherms and (b) liquid mass fraction as well as streamlines.

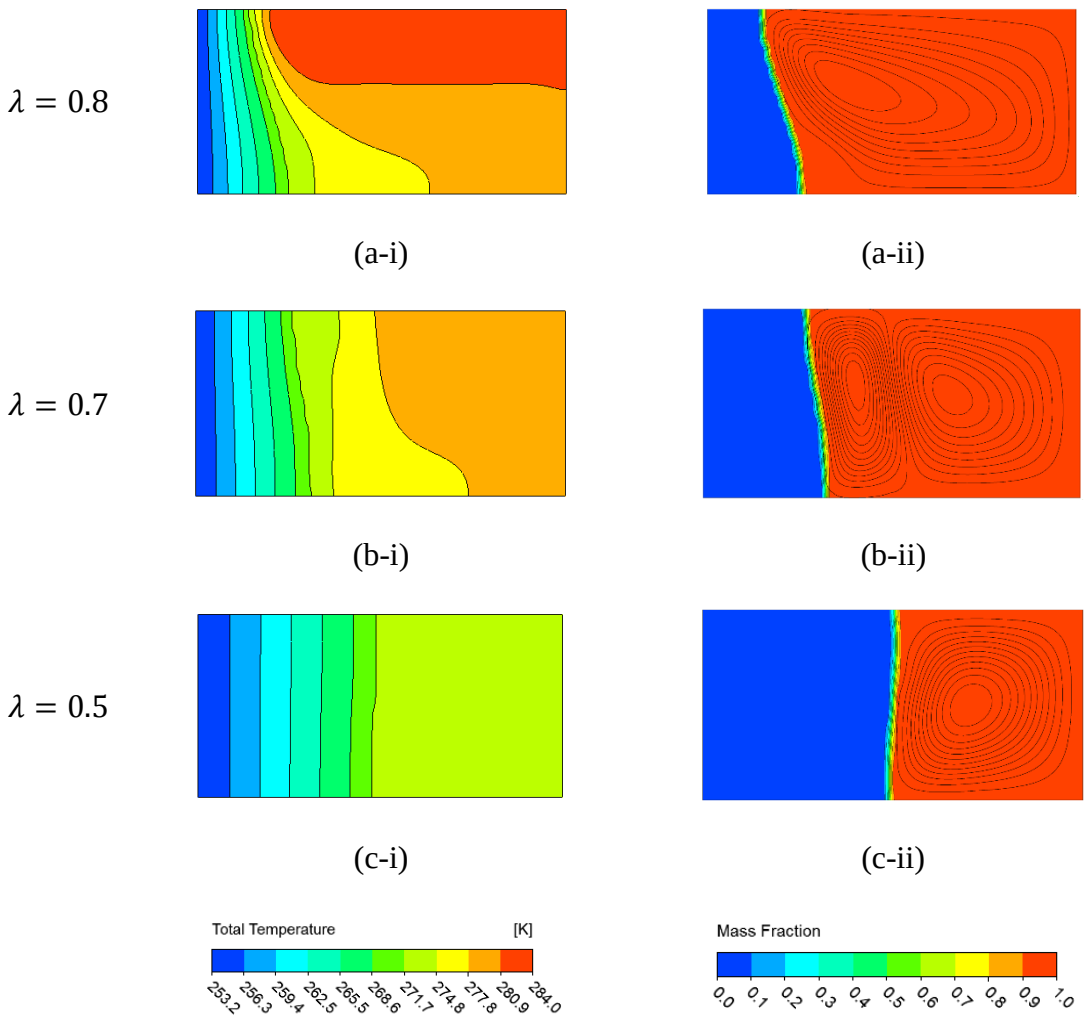

Figure 4-10: Results of simulated cases of an aspect ratio of 0.5 and $Ra_i = 1.12 \times 10^6$, indicating (i) isotherms and (b) liquid mass fraction as well as streamlines

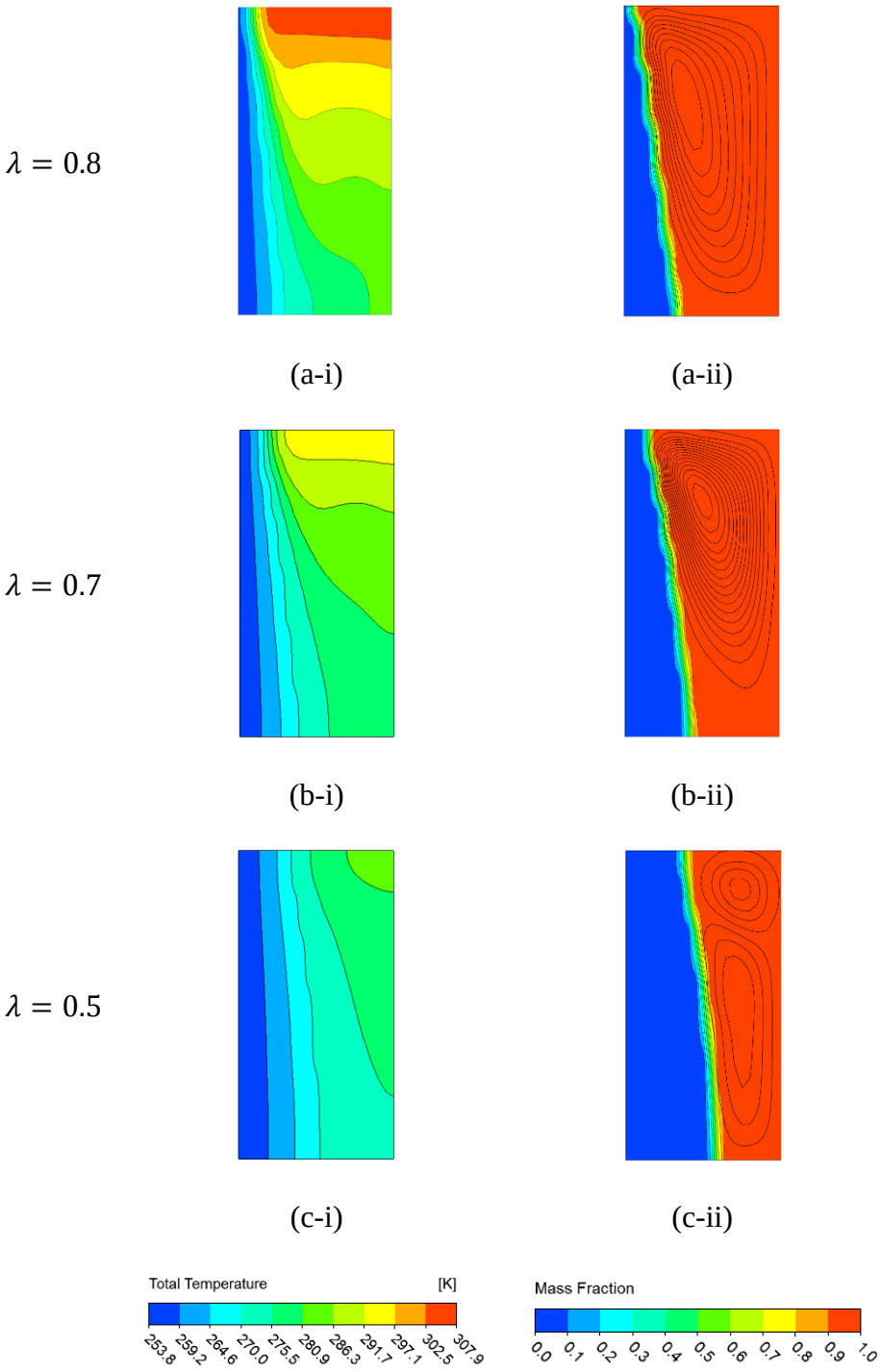

Figure 4-11: Results of simulated cases of unity aspect ratio and $Ra_i = 1.12 \times 10^6$, indicating (i) isotherms and (b) liquid mass fraction as well as streamlines.

Figure 4-9 shows the isotherms and liquid fraction of another case with a higher Rayleigh number, i.e. $Ra_i = 1.12 \times 10^6$. A glance at the isotherms of that case shows that they are distorted from being vertically aligned. This indicates the strength of the effect being exerted by natural convection caused by the density change due to temperature variation in the test cell. It can be noticed as well that the isotherms become aligned as the freezing front advances and a diffusion-dominant mode is eventually taking over. This is trivial since the value of Rayleigh number is reducing because temperature decreases as freezing progresses. The liquid mass fraction on the right side of the figure show that the solid-liquid front starts from the left wall and is advancing more in the bottom half of the cavity compared to the upper half. In order to understand the reason of this behavior Figure 4-12a shows a contour of total heat transfer in the cavity. Figure 4-12a proves that heat transfer in the upper cavity side is much higher than in the lower side because of the existence of natural convection. This result is reasonable because natural convection moves the warmer part of the liquid to the upper half of the cavity. This, in turn, makes the difference in temperature across the solid-liquid front higher in the upper half, resulting in a higher resistance to freezing in that location. The cooling power tends to force the solid-liquid fraction to move forwards, however, the high-temperature liquid acts as a melting source. The temperature difference across the front in the lower half is less, which makes the front advance more profoundly. Back to Figure 4-9, the streamlines show that natural circulations start by one large circulation. As time elapses, another smaller, weaker, and direction-opposite circulation begins to grow in size. The new circulation is because water has a density-inversion point at a temperature of 4^{o}C. This circulation becomes larger as time elapses until it dominates the flow regime in the cavity. The value of Rayleigh number

of this circulation can be calculated easily as approximately 6×10^4, which is higher than the critical value. The existence of this new circulation reverses the temperature fields such that high-temperature liquid sinks to the bottom half of the domain rather than staying at the top half. This, in fact, is the reason why the solid-liquid front flattens at higher times of the freezing process. In addition, Figure 4-12b represents a contour figure of the shear stress in the cavity. The figure shows clearly that a high stress rate exists in the upper half of the cavity near the solid-liquid front, which explains that the melting rate in the upper half is higher than that on the lower half.

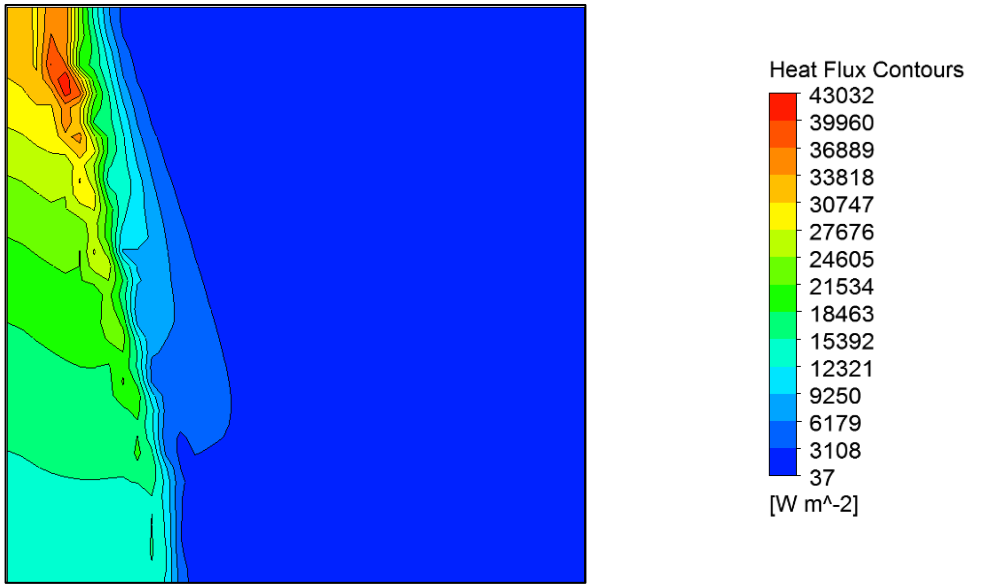

(a)

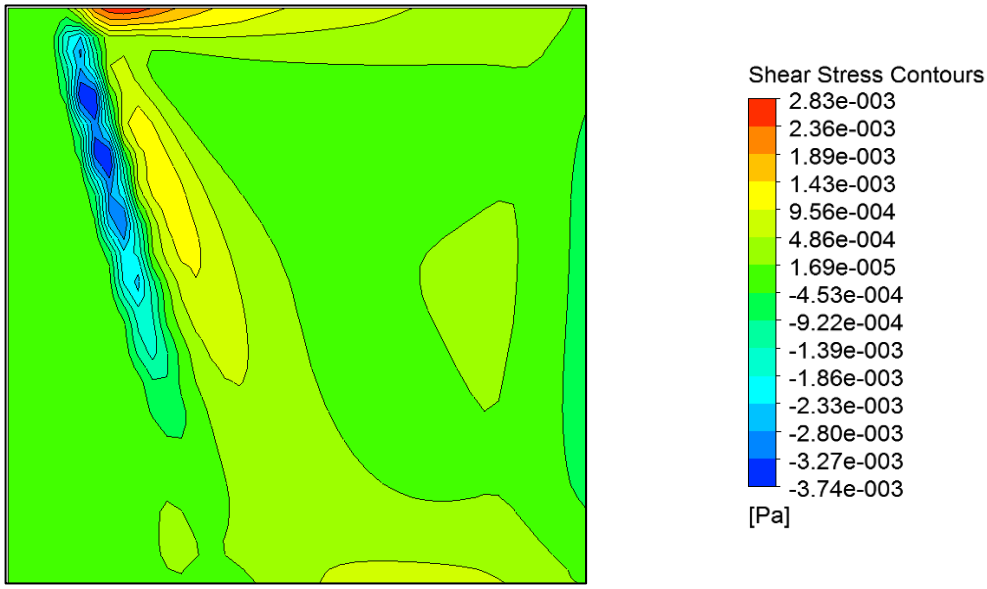

(b)

Figure 4-12: Reason of tilted solid-liquid front using contours of (a) total heat flux and (b) total shear stress.

Figure 4-10 depicts the results of a case where Rayleigh number is $Ra_i = 1.12 \times 10^6$, similar to the previous case, however, with an aspect ratio of 0.5. The temperature isotherms starts by distorted lines showing the effect of natural convection. As time elapses, the isotherms flatten and diffusion becomes dominant. However, unlike the case of unity aspect ratio, the flattening of the isotherms starts at a lower time. The reason is understood by looking at the streamlines in the same figure. At a time when 0.3 of the cavity is frozen, the weaker circulation stands between the stronger circulation and the solid-liquid front, which reduces the strong effect of natural convection. The enhancement of the freezing process due to natural convection can be related to the length of time of contact between the stronger circulation and solid-liquid front.

Figure 4-11 shows the results of a case where Rayleigh number is $Ra_i = 1.12 \times 10^6$, similar to the previous cases, however, with an aspect ratio of two. Temperature isotherms do not show any flattening for the presented times. This proves that for this aspect ratio natural convection effect is strong at all presented times. The weaker circulation starts later than the previous cases, which means that the contact time is prolonged for higher aspect ratios.

In order to understand the effect of natural convection upon changing the aspect ratio and Rayleigh number, Figure 4-13 presents the total liquid fraction in the cavity as a function of elapsed time. The total liquid fraction is calculated as

$$Liquid\ Fraction\ (t) = \int_{x=0}^{S} \int_{y=0}^{W_i} \lambda(x, y, t) dx dy\ /(S \times W_i) \qquad (4\text{-}23)$$

As discussed earlier, the cooling wall, which supplies the cooling power is assumed constant in all simulations, i.e. 1cm long and at a temperature of -20^{o}C. Testing different

aspect ratios forces the cavity size to change, thus improper comparison of freezing times. To overcome this problem, a normalizing factor is multiplied by the elapsed time in order to take care of the sample volume differences. The normalized elapsed time is calculated as

$$Modified\ Elapsed\ Time = Simulated\ Elapsed\ Time \times Aspect\ Ratio \quad (4\text{-}24)$$

In order to show the effect of natural convection on the freezing process, each simulation was performed twice, i.e. one solving only for the energy equation (referred to as stratified cases), and the other solving for the flow and energy equations (referred to as non-stratified cases), as explained earlier. Figure 4-13a depicts the liquid mass fraction for the lowest Rayleigh number tested. This case shows that the stratified and non-stratified cases are identical for all test aspect ratios. It also shows that a lower freezing time is accompanied with cavities with higher aspect ratios. This means freezing in vertically oriented thin cavities is preferred, if shorter freezing time is need, which is of great interest for PCM applications. Figure 4-13b illustrates the effect of natural convection for a higher Rayleigh number. The trend begins to show that natural convection acts to reduce total freezing times for all cases. The effect is more pronounced at lower aspect ratios, i.e. horizontally oriented thin cavities. Figure 4-13c shows results of the case with the highest simulated Rayleigh number, i.e. highest natural convection strength. It is evident that natural convection acts to reduce the time of freezing by comparing stratified and non-stratified cases. The reduction of total freezing time becomes more pronounces with increasing initial Rayleigh number as well as reducing the aspect ratio of the cavity. A reduction of about 18% in total freezing time was noticed for an aspect ratio of 0.5 and a Rayleigh number of $Ra_i = 1.12 \times 10^6$. A note similar to that faced in the experiment can be noticed at the beginning of the

freezing process. The stratified cases start with a higher freezing rate, which makes the solid-liquid front moves faster until a point where the freezing process slows down and non-stratified cases keep freezing with a higher freezing rate. The reason is that for non-stratified cases, natural circulations tend to begin by reducing the temperature of the cavity and then solidify. In contrary to that, stratified cases acts to solidify a localized vicinity without the need to reduce the entire cavity. However, at the time intersection points, natural convection in non-stratified cases brings the entire cavity to a close temperature to that of the solid-liquid front making it easier to solidify. In addition, one may notice that for Figure 4-13c, the freezing rate increases at the middle of the freezing process for all cases. This can be attributed to the density-inversion point effect.

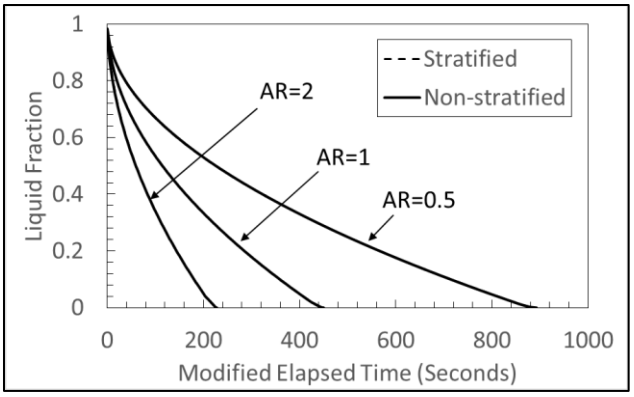

(a)

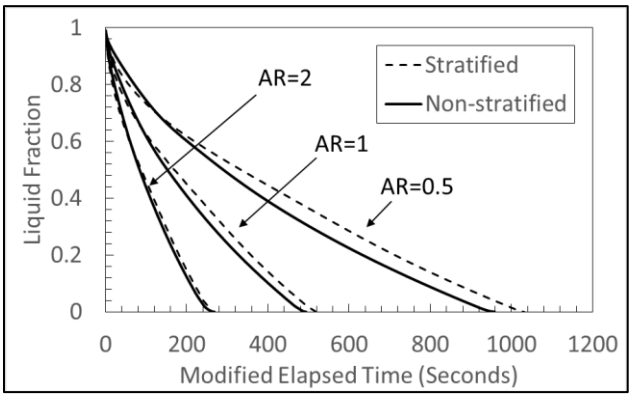

(b)

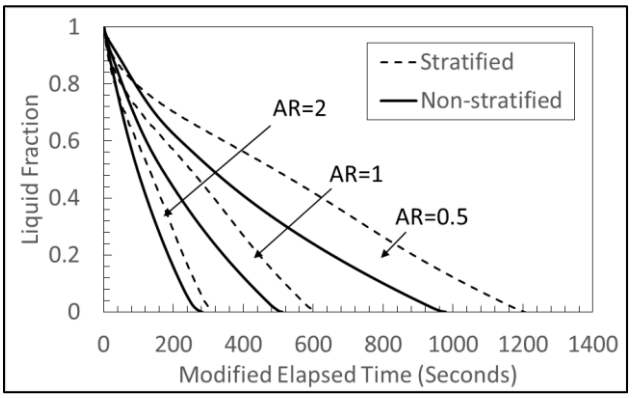

(c)

Figure 4-13: Liquid mass fraction of the simulated cases of water, indicating the effect of Rayleigh number and aspect ratio on the freezing progress for (a) $Ra_i = 9 \times 10^3$ (b) $Ra_i = 5.9 \times 10^5$ (c) $Ra_i = 1.12 \times 10^6$.

4.6.2 Freezing of difference CNT concentrations in CNT-water Nanofluids

Based on the previous section, extreme cases showing the effects of diffusion and natural convection on the freezing process are selected to compare different concentrations of CNT in Nanofluids. The cases simulated are two; one corresponding to $Ra_i = 1.12 \times 10^6$ and $AR = 0.5$, and another case with similar initial condition but with stratified freezing. The former case shows an extreme case of natural convection effect on the freezing process, while the latter shows the effect of CNT concentration on the freezing process with the existence of diffusion heat transfer as a dominant heating mode.

Figure 4-14 presents the liquid mass fraction in the test cavity as a function of modified elapsed time for different cases corresponding to CNT concentrations of 1 wt.%, and 2 wt.%. It is clear that adding CNT particles to water enhances heat transfer by lowering the freezing time for a similar volume of liquid. The maximum time reduction percentage of 27% corresponds to the highest CNT concentration in a non-stratified freezing simulation. Even though the latent heat stored is reduced by adding CNT particles, the reduction of latent heat is incomparable with the reduction of freezing time. To be exact, a reduction of latent heat was observed to be 2%, which corresponds to adding 2 wt.% of CNT particles.

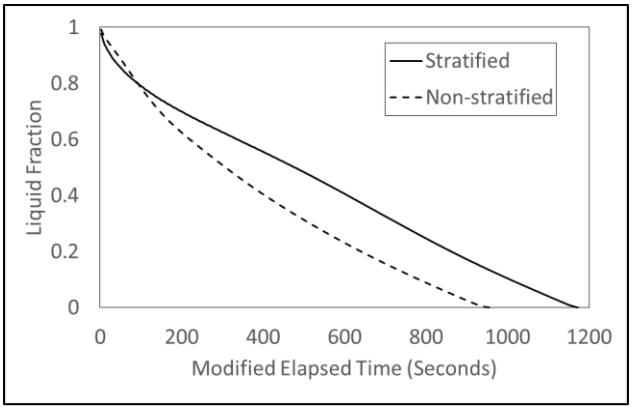

(a)

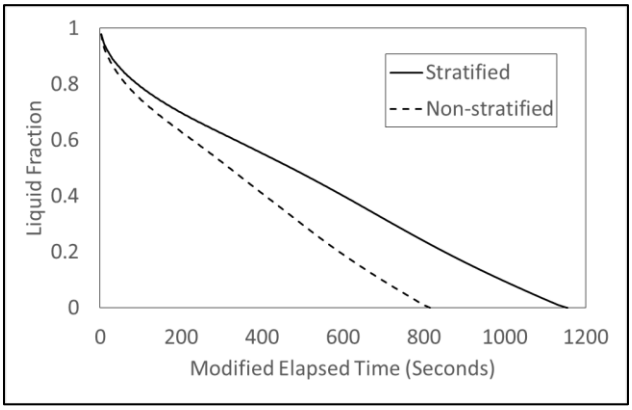

(b)

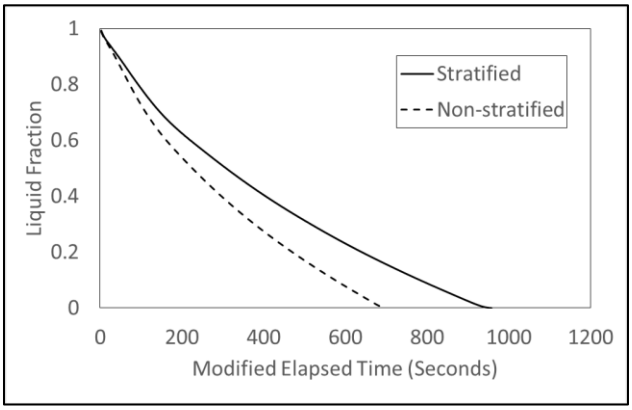

(c)

Figure 4-14: Liquid mass fraction of the simulated stratified and non-stratified freezing cases of (a) water (b) 1 wt% CNT Nanofluid (c) 1 wt% CNT Nanofluid.

Figure 4-15 depicts the total freezing time of all simulated cases with different CNT concentrations. A reduction in freezing time was noticed both stratified and non-stratified freezing processes, however, greater reduction was noticed for the non-stratified cases. The nonlinearity of time reduction is due to the fact that thermophysical properties do not change linearly rather on a power basis.

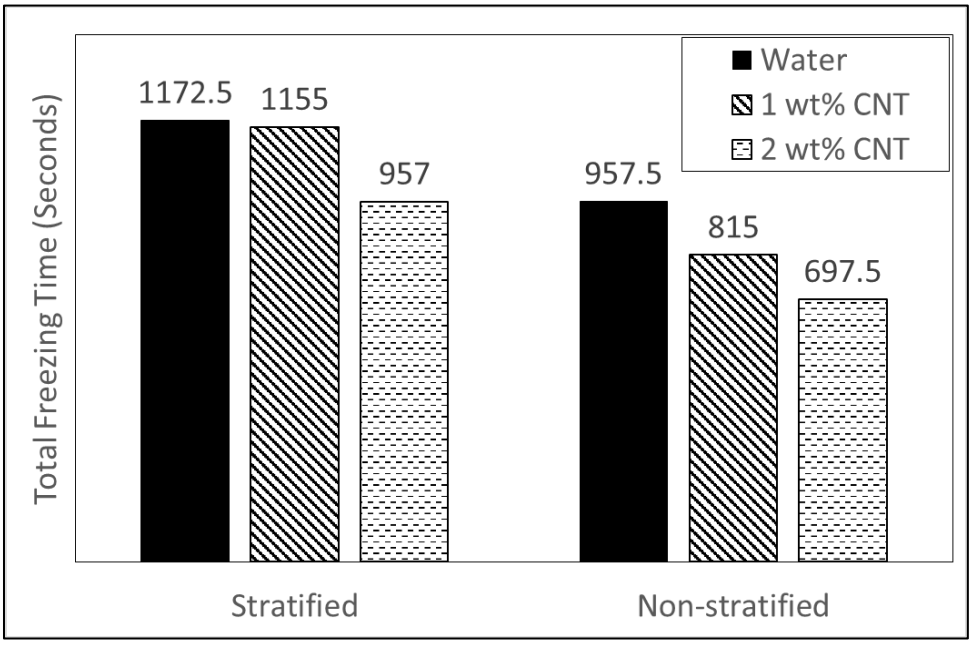

Figure 4-15: Total freezing time of the simulated stratified and non-stratified freezing cases.

In fact, the reduction in freezing time of non-stratified cases was not noticed in the experiment as clearly. This arises the question of whether this model sufficiently simulates the actual situation. In addition, it questions whether adding more CNT particles enhances natural convection or suppresses it due to the increase in viscosity. In order to answer the first question, it should be noted that the developed CFD model does not account for the agglomeration of CNT particles and instability upon freezing. Thus, the model would work assuming a low-temperature-standing surfactant is used. As for the second question, Figure 4-16 presents the vertical velocity at a centerline for different CNT loadings in the non-stratified cases at different times. Figure 4-16a shows that two circulation zones exist in all test liquids. However, because adding more CNT to water increases its viscosity, the vertical velocity magnitude is less in Nanofluids compared to that in water. In contrary, Figure 4-16b shows that vertical velocity component in the highest CNT concentration becomes higher than that of the base fluid as well as the intermediate CNT-concentration Nanofluid. This strange behavior is attributed to the fact that not only viscosity that plays a role in suppressing or enhancing natural convection but also other thermophysical properties may interfere as well. Density of studied Nanofluids increases non-linearly with adding CNT particles, which in turn increases the density difference giving further enhancement of natural convection circulations. In conclusion, natural convection enhances heat transfer to a significant extent and adding CNT particles tend to change the strength of natural convection. The change could be either negative by suppressing natural convection or positive by strengthening it. Thus, it is recommended before designing a system for thermal energy storage using CNT-water Nanofluid to study carefully the effect of all thermophysical properties on the process and a compromise is needed.

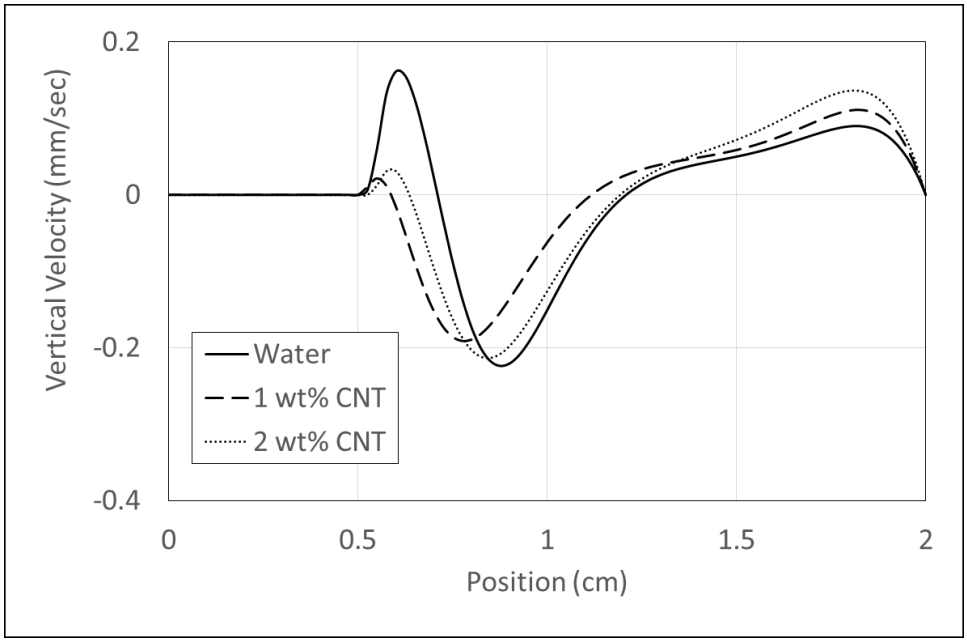

(a)

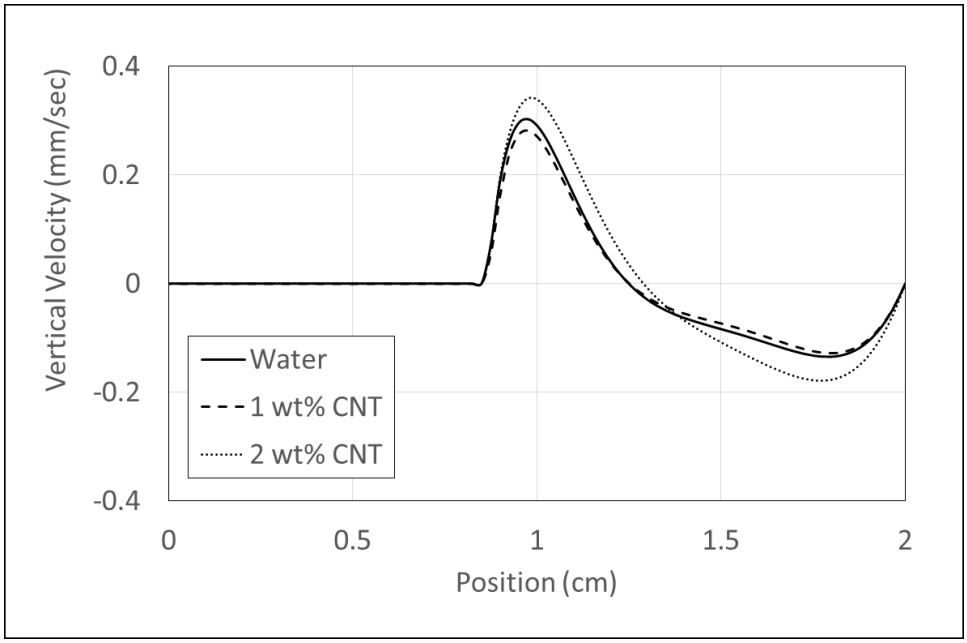

(b)

Figure 4-16: Vertical velocity component at a horizontal centerline of the cavity at different times corresponding to liquid fractions of (a) 0.78 and (b) 0.57.

CHAPTER 5

CONCLUSIONS AND RECOMMENDATIONS

In this work, numerical and experimental investigations were performed in order to obtain a good insight on the freezing process of CNT-water Nanofluids and their potential use in cold energy storage. An experimental setup was designed and built to test the total freezing time of different Nanofluids. Different stable CNT-water Nanofluids were prepared prior to making the experiments corresponding to CNT weight concentrations of 0.3% and 1%. Thermal behavior and total freezing times were tested for the aforementioned Nanofluids and compared to that of water, as it is the base liquid. This chapter is dedicated to summarize the main conclusion points of this work.

5.1 Research Conclusions

1. It was found experimentally that Nanofluids were able to reduce the total freezing time only in the absence of natural convection. A reduction in total freezing time of 11% and 14.4% was noticed upon adding 0.3% and 1% of CNT particles to water, respectively. This result benefits many industries making use of cold energy storage in reducing the charging/discharging times of ice batteries.
2. The existence of natural convection in pure water was found experimentally to reduce the total freezing time tremendously; however, upon adding CNT particles viscosity increased as well suppressing natural circulations.
3. Sudden decrease of temperature was experimentally observed after some time of the freezing process and was due to the density-inversion point. The observation was found for water as well as all tested Nanofluids.

4. Thermal conductivities of the studied Nanofluids were measured and enhancement of 4.2% was found upon adding 1% of CNT particles.
5. The reason of the failure of CNT to reduce freezing time in cases where natural convection existed was found to be due to CNT-water Nanofluid's instability and failure to withstand low temperatures.
6. Experimental tests showed that CNT-water Nanofluids with Gum Arabic could not withstand temperatures below -10 ^{o}C. While Nanofluids with CNT concentration of 0.3 wt% was capable of withstanding a minimum temperature of -5 ^{o}C.
7. Adding 0.3 wt% of CNT particles to water was found to reduce the supercooling degree of water by about 2 ℃ which saved around two minutes of total freezing time in a sample of 100 grams.
8. Numerical results showed that the flow field was characterized by two circulation zones caused by the fact that water has a density-inversion point at a temperature of 4 ^{o}C.
9. It was found numerically that adding CNT particles to water reduced the total freezing time for all studied cases. Numerical results matched the cases of diffusion-dominant freezing experiments (Stratified); however, cases with natural convection (Non-stratified) failed to match due to the lack of agglomeration information in the CFD model.
10. The CFD model was extended to simulate higher CNT concentration. A total reduction of total freezing time of 27.2% was observed upon adding 2% of CNT particles in non-stratified simulations. On the other hand, 18.4% reduction in freezing time was noticed for stratified simulations.

5.2 Future Recommendations

The following points are recommended as extension for future work:

1. Using different surfactants that could withstand low temperatures in order to enhance the stability of Nanofluids and obtain representative results.
2. Using different types of nanoparticles, especially those of high specific heats and thermal conductivities in order to increase the energy capacity for thermal energy storage systems.
3. Using Hydrogel instead of pure water so that suspended nanoparticles do not agglomerate nor precipitate. This will suppress natural convection but will increase the stability of Nanofluids when diffusion is only needed.
4. Using extended surfaces in the test cell and testing the effect of different parameters on the freezing process.
5. Introducing forced convection instead of natural convection by applying a magnetic field or rotating the test cell.
6. Using Infra-Red camera to investigate the thermal field as freezing progresses.

Appendix A: Schematic Diagrams of the Experimental Setup

In the following pages, the drawings of the experimental setup is presented.

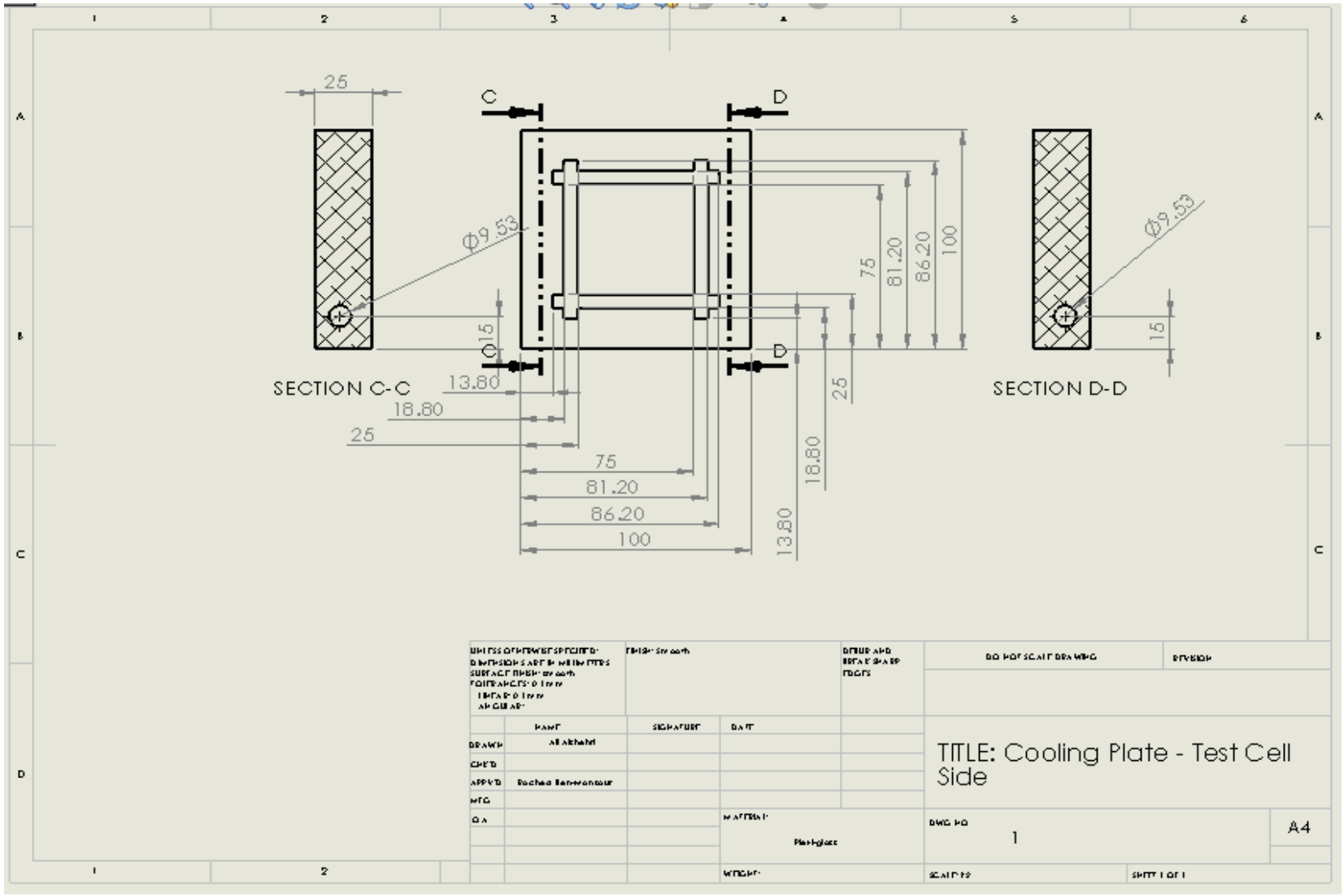
25
C
D
Ø9.53
Ø15
13.80
18.80
25
75
81.20
86.20
100
SECTION C-C
SECTION D-D
Ø9.53
15
DO NOT SCALE DRAWING
TITLE: Cooling Plate - Test Cell Side
A4
1

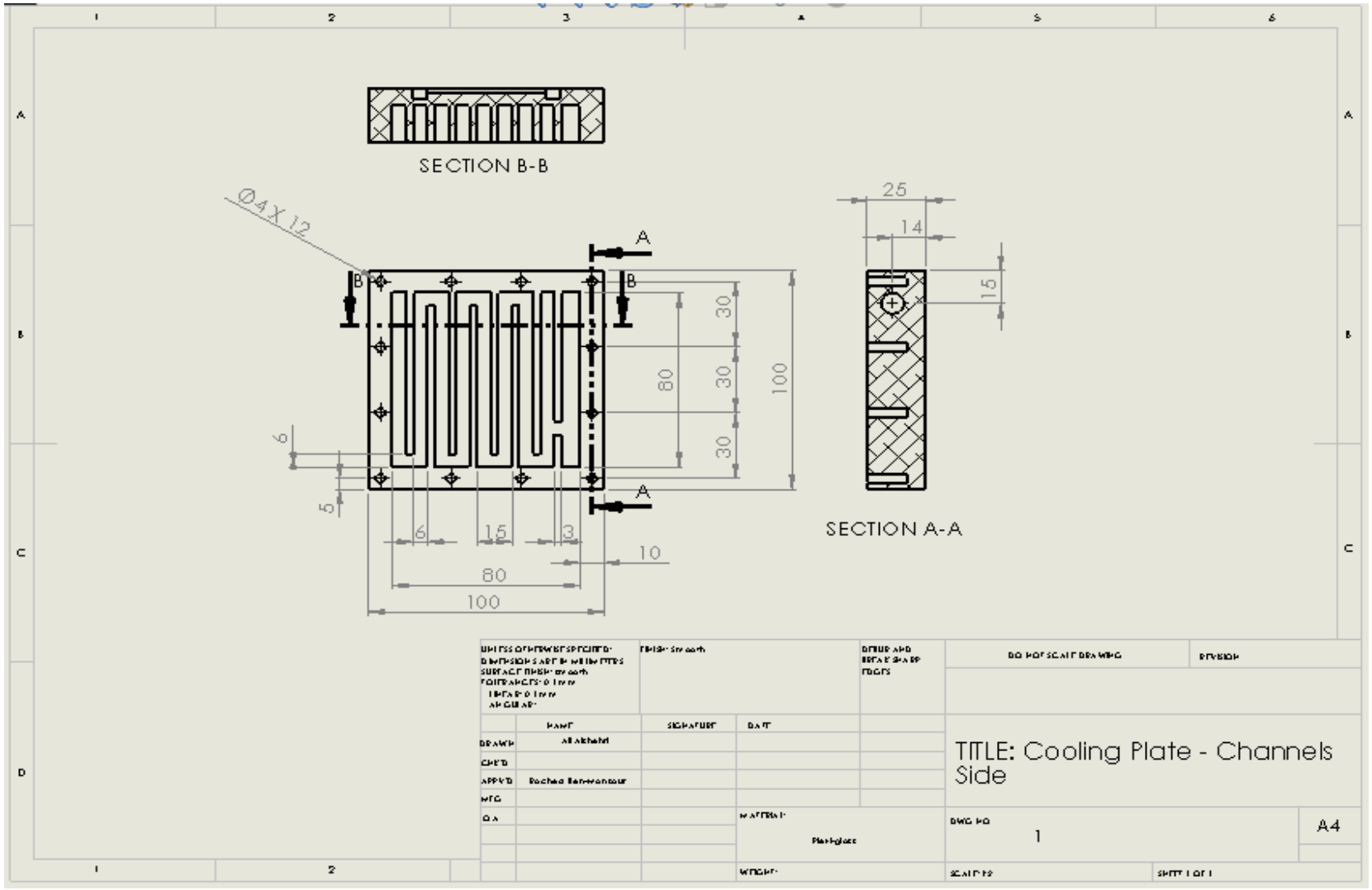
SECTION B-B
Ø4X12
A
B
B
A
30
30
30
80
100
6
5
6
15
3
10
80
100
25
14
15
SECTION A-A
TITLE: Cooling Plate - Channels Side
A4
1

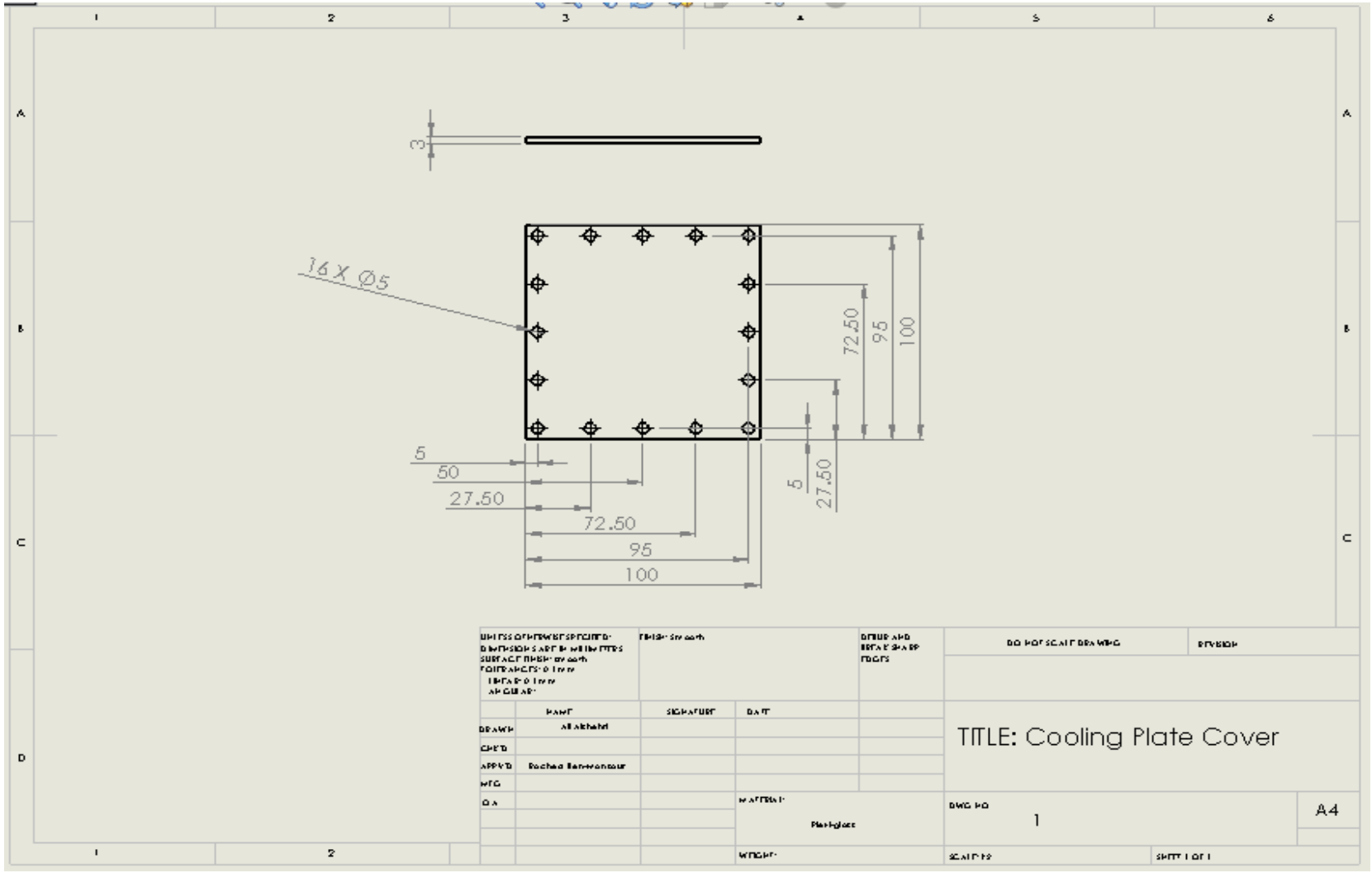
3
16 X Ø5
72.50
95
100
5
50
27.50
72.50
95
100
5
27.50
TITLE: Cooling Plate Cover
A4
1

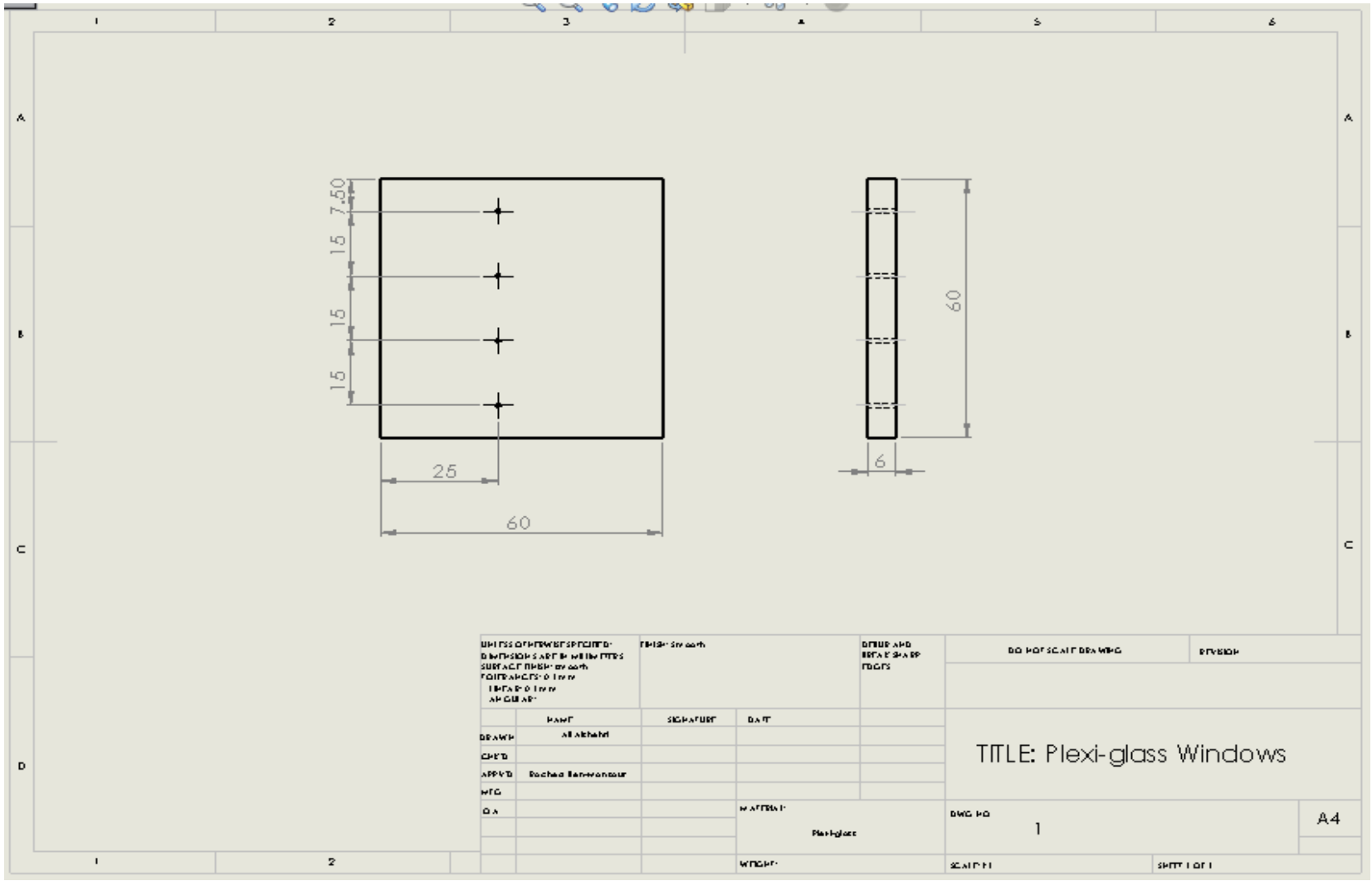
7.50
15
15
15
25
60
60
6
TITLE: Plexi-glass Windows
A4
1

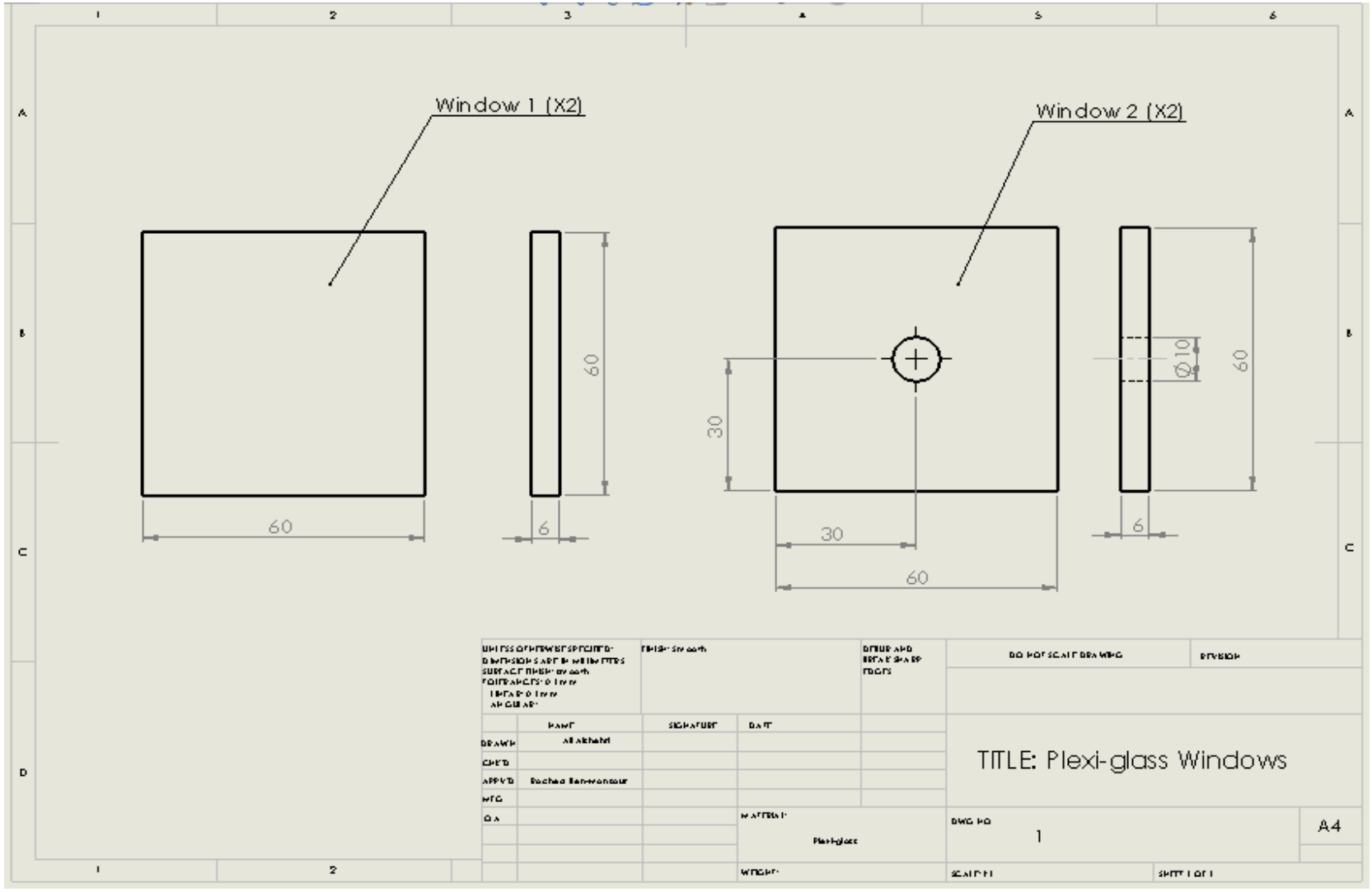
Window 1 (X2)
Window 2 (X2)
60
6
60
30
60
30
6
60
Ø10
TITLE: Plexi-glass Windows
A4
Plexi-glass
1

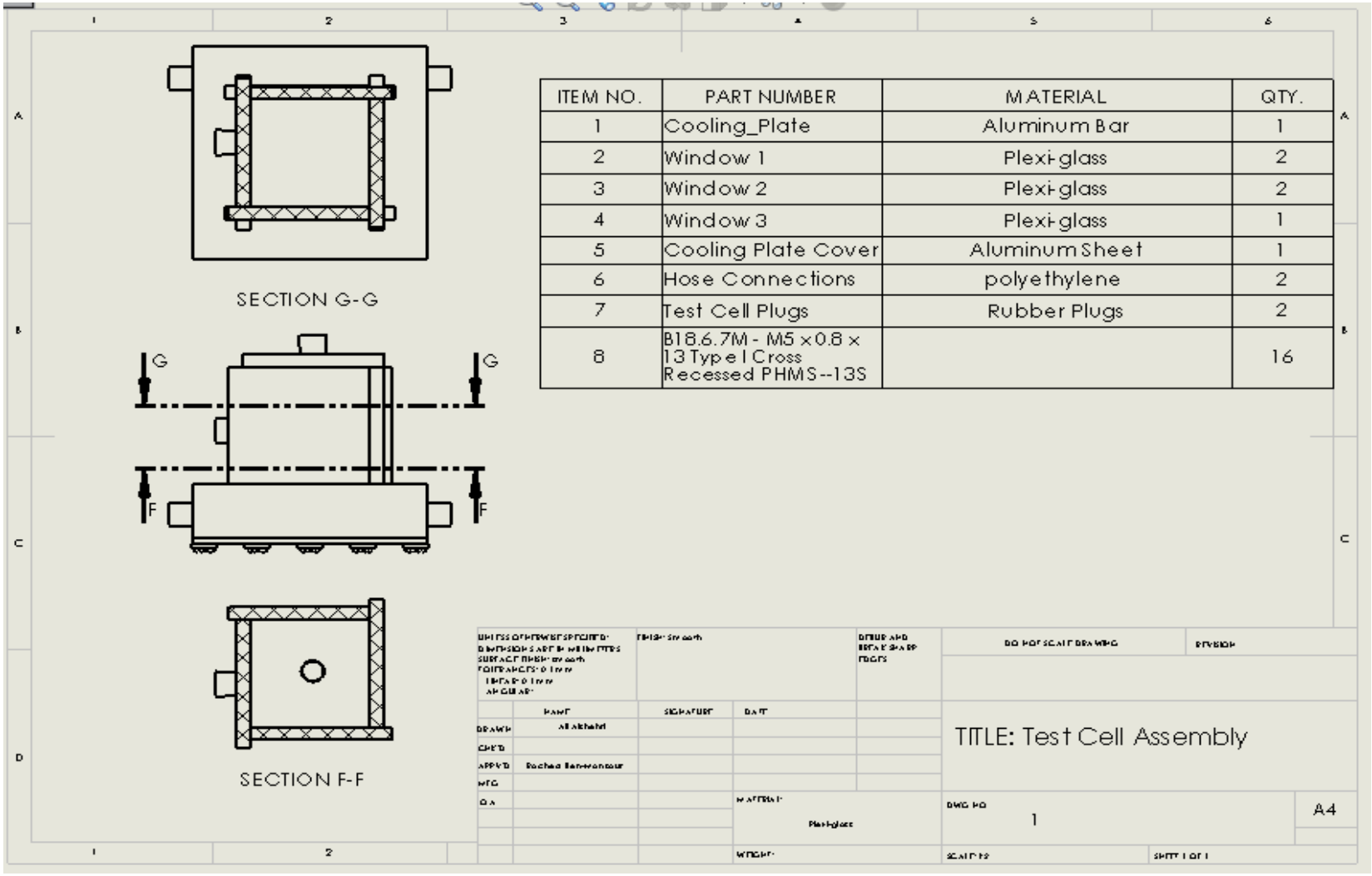

ITEM NO.	PART NUMBER	MATERIAL	QTY.
1	Cooling_Plate	Aluminum Bar	1
2	Window 1	Plexi-glass	2
3	Window 2	Plexi-glass	2
4	Window 3	Plexi-glass	1
5	Cooling Plate Cover	Aluminum Sheet	1
6	Hose Connections	polyethylene	2
7	Test Cell Plugs	Rubber Plugs	2
8	B18.6.7M - M5 x 0.8 x 13 Type I Cross Recessed PHMS--13S		16

TITLE: Test Cell Assembly

DWG NO 1

A4

Appendix B: Calibration and Accuracy Evaluation of Thermocouples

Four T-type thermocouples, i.e. Copper/Constantan wires, were fabricated for use as the temperature sensors in the freezing experiment (Chapter 3). Prior to being placed in the test cell, the thermocouples were calibrated against a liquid-in-glass thermometer as well as a trimester at several points.

Distilled water was placed in room temperature and maintained for several minutes. The thermocouples as well as the other accurate thermometers were placed in the water container. Thermocouples were connected to an eight-channel data acquisition (DAQ) unit (NI 9162, National Instruments, Austin, TX). The recordings of the thermocouples were read over a 10 minutes period at an interval of 6 seconds. Results of the temperature readings at this temperature point are presented in Figure B-1. The figure indicates that the four thermocouples are measuring room temperature to an accuracy of $0.6^{o}C$, corresponding to thermocouple number four. This temperature is going to be accepted and going to be assigned as the temperature accuracy of the experimental work.

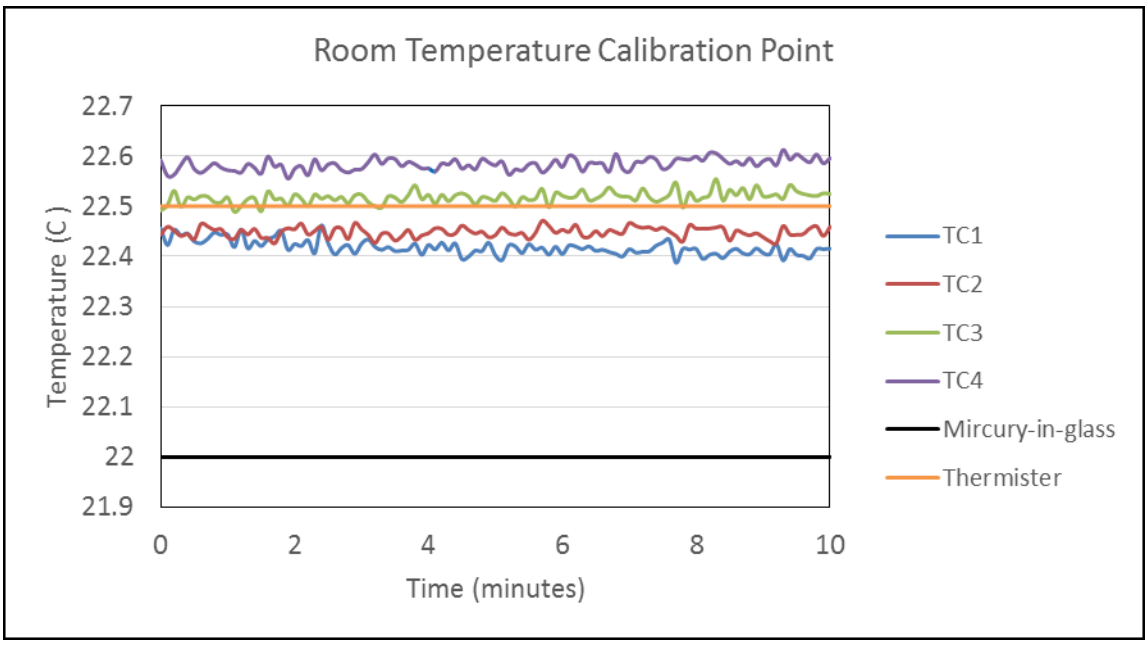

Figure B-1: Thermocouples calibration comparison at room temperature.

Distilled water was placed in a refrigerator for enough time to freeze solid. Then, the frozen distilled water was taken out and mixed very well with liquid phase of the same water. The mixture's temperature was measured using a mercury-in-glass, a thermistor and the four thermocouples. The measurements procedure is similar to the previous point hence it is not repeated. Figure depicts the temperature measurements for ten minutes. Again, the highest error is corresponding to thermocouple number four with corresponding to the same accuracy observed with the room-temperature point. Thus, the accuracy of the thermocouples are going to be set to $0.6^{o}C$.

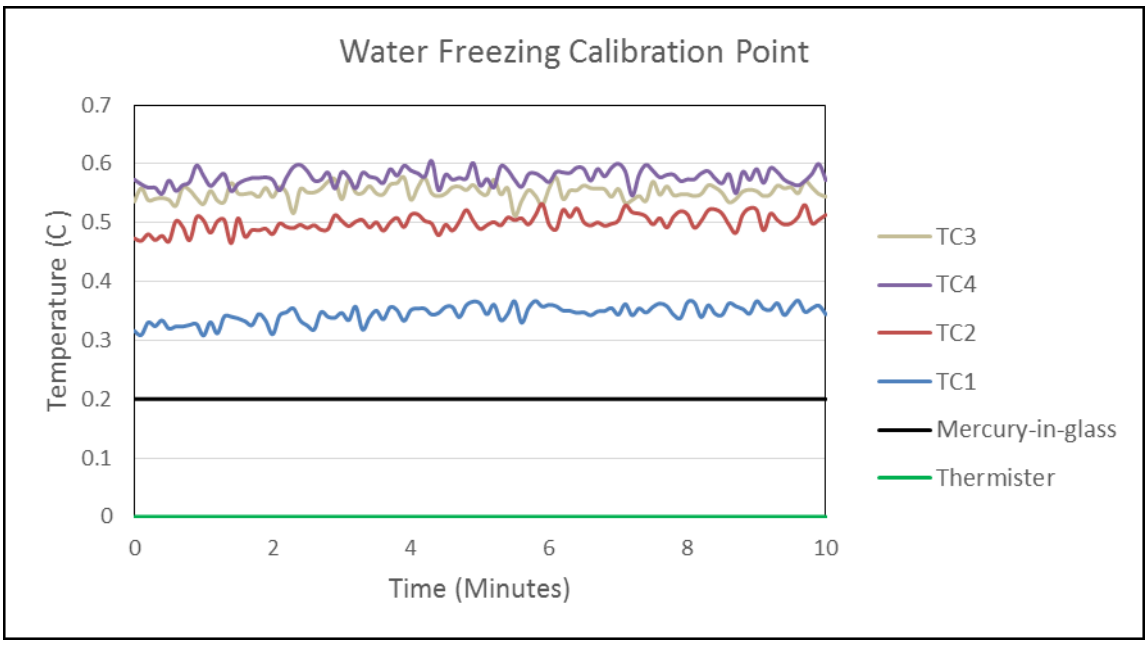

Figure B-2: Thermocouples calibration comparison at water freezing temperature.

Appendix C: LabVIEW Virtual Instrument for Data Acquisition of thermocouples

An eight-channel data acquisition (DAQ) unit (NI 9162, National Instruments, Austin, TX) was used to record thermocouple readings. The DAQ unit was connected to a personal computer and was operated by a LabVIEW virtual instrument (VI), a snap shot is shown in Figure C-1.

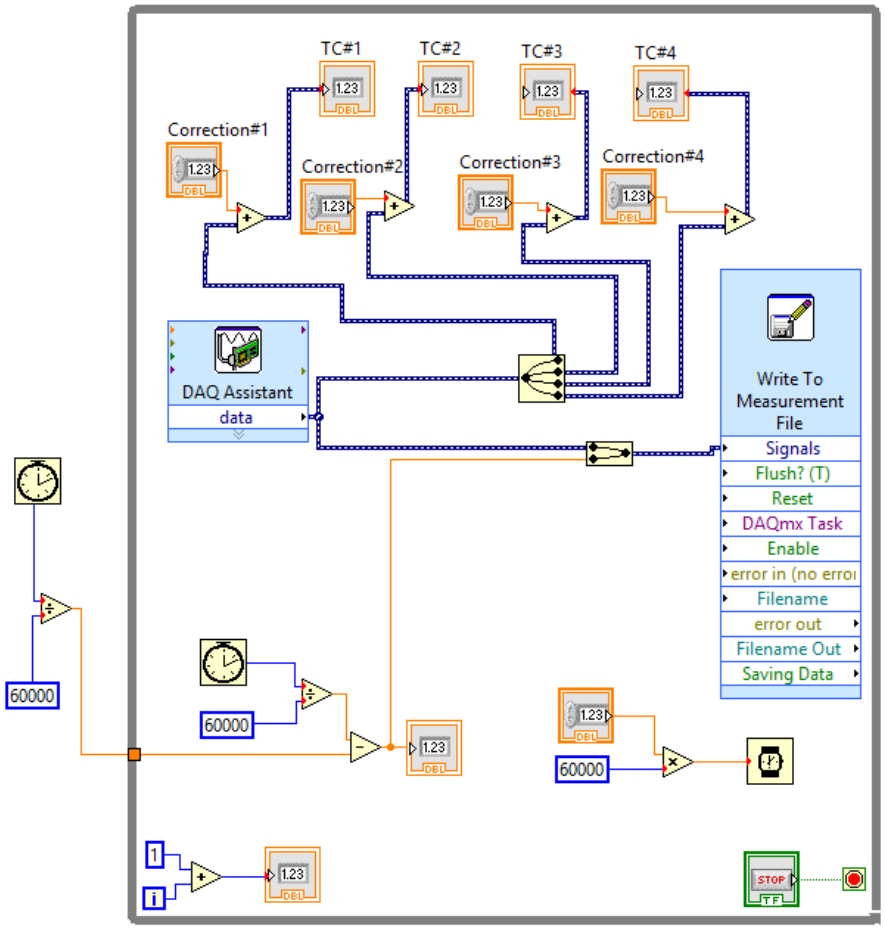

Figure C-1: Block diagram of the made LabVIEW VI for implementing real-time data acquisition of the thermocouples.

Appendix D: Uncertainty Analysis of the Experimental Results

In this appendix, the theory described by Coleman and Steele is used when presenting the experimental data.

In Chapter 2, the uncertainty of thermal conductivity measurement for a sample was represented by the standard deviation over the individual runs. Using the standard deviation accounts for all possible systematic errors, such as temperature control set up (3.5% as specified by the manufacturer).

In Chapter 3, the errors of the temperature readings were attributed to two main factors; the accuracy of the location of the thermocouple and that of the thermocouples readings. As mentioned in Appendix B, the uncertainty of temperature readings was $\pm$ 0.6 ^{o}C, whereas that of thermocouples location is about $\pm$ 0.5 mm. In addition, two sources of uncertainty exist in the freezing experimental results namely thermal insulation as well as initial liquid temperature. Each experimental run is performed three times and average values of freezing times were reported. The maximum standard deviation in the experiments was 14 minutes, which represents a relative error of about 5%.

Appendix E: Estimation of the Time Response of Thermocouples

In this appendix, a simple analysis is performed to estimate the time response of the fabricated thermocouples. This step is important since the problem at hand is transient with a high temperature change rate.

The lumped capacitance method (LCM) is going to be assumed valid when analyzing heat transfer around the soldered junction of the thermocouple. This assumption is going to be validated later on. The thermocouple junction is assumed to have a zero temperature gradient based on this method, meaning that it is at a uniform temperature at all times.

In this analysis, the junction or bead is initially at a temperature (T_i), as shown in Figure E-1. Suddenly, the ambient temperature is changed to a temperature (T_∞) for $t > 0$. As radiative heat transfer is assumed negligible, the junction is assumed to exchange heat with the surrounding medium only though natural convection. The energy conservation equation for the transient heat transfer process can be formulated as

$$\rho \forall C_p \frac{dT}{dt} = hA(T_\infty - T) \quad \text{(E-1)}$$

Where $\rho, \forall, C_p, h, and\ A$ stand for the effective density, volume, effective specific heat capacity, convective heat transfer coefficient, and surface area of the junction, respectively. Solution of the above equation gives

$$\frac{T-T_\infty}{T_i-T_\infty} = \exp(-t/\tau) \quad \text{(E-2)}$$

Where τ stand for the time constant of the junction, defined as

$$\tau = \frac{\rho \forall C_p}{hA} \quad \text{(E-3)}$$

The thermocouple junction is spherical in shape with a radius R. The time constant then can be reduced to the following

$$\tau = \frac{\rho R C_p}{3h} \tag{E-4}$$

When $t = 4.61\tau$, the junction temperature has reached to a value that is 99% of the final temperature, i.e. the ambient temperature in this case (T_∞). This corresponds to an error of about 1% in temperature readings, which can be reduced if the recording time is taken larger than the aforementioned time.

T-type thermocouple junction is made of 50% Copper and 50% Constantan soldered together. The combined effective density and specific heat capacity is difficult to obtain, however, linear averaging can be performed. In this appendix, the value of the largest properties is going to be taken as a cautious step. Density of constantan is taken as 8900 kg/m^3 and specific heat of constantan is taken as 390 J/kg-K (https://en.wikipedia.org/wiki/Constantan). The average spherical radius of the thermocouple junction is 0.4 mm. The convective heat transfer coefficient is taken as 500 W/m^2-K corresponding to a weak natural convection situation (http://www.engineeringtoolbox.com/convective-heat-transfer-d_430.html).

Substituting all thermal and geometrical properties into Equation E-4 gives a time constant of 0.9256 seconds. Therefore, it takes the thermocouple junction about 4.267 seconds to read a value that is 99% of the final temperature.

To validate the main assumption of using LCM, Biot number needs to be checked, given as

$$Bi = \frac{hR}{3k} \tag{E-5}$$

Where $R/3$ is the characteristic length of the junction, and k is the thermal conductivity of the junction, which is taken as constantan thermal conductivity since it is the lowest. It corresponds to a value of 21.1 W/m-K (https://en.wikipedia.org/wiki/Constantan). Thus, Biot number is calculated as 0.0032 which satisfies the condition for the method to be applicable [91].

The shown estimation of the time response is a simple one and does not take into account many factors, such as the soldering effect as well as electrical delays in the system. Thus, a time of 6 seconds was chosen as the sampling intervals, corresponding to a sampling rate of about 0.167 Hz.

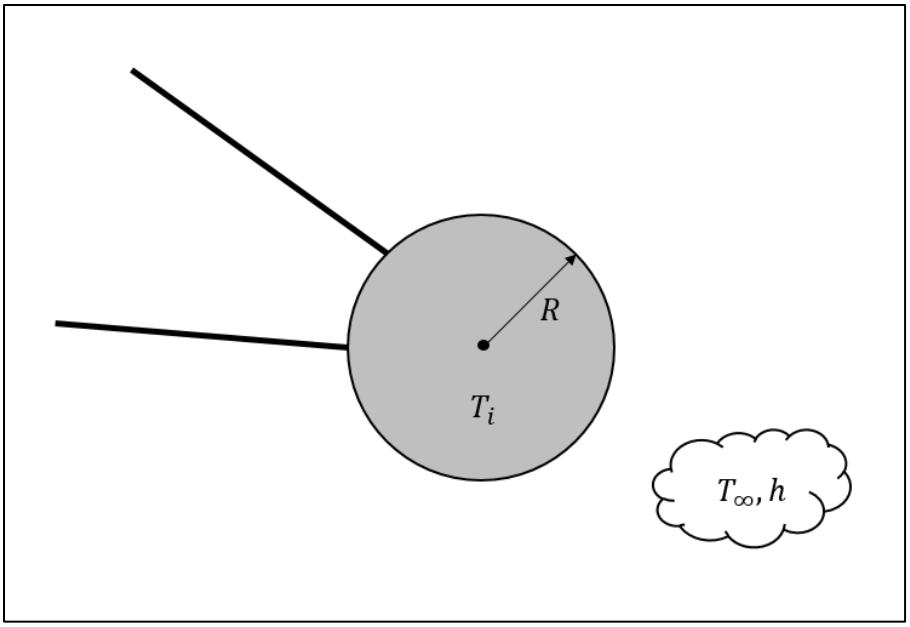

Figure E-1: Schematic diagram of the lumped Thermocouple junction initially at a temperature ($\boldsymbol{T_i}$) exposed to an ambient temperature and convective heat transfer coefficient shown.

Appendix F: MATLAB Code for Data Analysis

In this appendix, the used MATLAB code to extract experimental data is presented.

```
%% Thesis Experimental Data Analysis by Ali Alshehri - Single Reading

% Follow the steps to run the code:

% 1- before you start running this code type: clear all, close all, and clc
% 2- drag the excel file to the command window and click next
% 3- select create vectors from each column using column names
% 4- run the code to obtain the following results:
%           A- Initial temperature
%           B- Ice front arrival times at thermocouples.
%           C- Transient temperature readings.
%           D- Ice-front estimated location vs. time.
%           E- Ice-front estimated speed vs. time.
%           F- Heat Rate (in W) taken from the cell vs. time.
%% Clearing Parameters

clear FT Front Start TCW Time Time_M1 Time_M2 Time_M3 i j...
   position TC1 TC2 TC3 TC4 TC1_M2 TC2_M2 ...
    TC3_M2 TC4_M2 Speed Arrival Heat_Rate ...
    Initial_Temperature Interval Output
close all
%% Changing the time interval of readings

Interval=0.1; % time interval of readings in minutes
j=1;
for i=1:numel(Time_M0(:,1))
   if abs(rem(Time_M0(i),Interval))<=0.1
      Time(j,1)= Time_M0(i,1);
      TC1(j,1) = TC1_M0(i,1);
      TC2(j,1) = TC2_M0(i,1);
      TC3(j,1) = TC3_M0(i,1);
      TC4(j,1) = TC4_M0(i,1);
      j=j+1;
    end
   end
```

```
Time(j:i,1)=0; Time=[0;nonzeros(Time)];
TC1(j:i,1)= 0; TC1=nonzeros(TC1);
TC2(j:i,1)= 0; TC2=nonzeros(TC2);
TC3(j:i,1)= 0; TC3=nonzeros(TC3);
TC4(j:i,1)= 0; TC4=nonzeros(TC4);
%% Determining ice front arrival at thermocouple

FT = -0.5;  %Freezing Point below which phase is solid

j=0;
 for i=1:numel(Time)
   if j == 0 && TC1(i)- TC1(i+10) >= 0.5
     Initial_Temperature=mean([TC1(i);TC2(i);TC3(i);TC4(i)])
     Start = Time(i);
     j=j+1;
   elseif j == 1 && TC1(i)<=FT
      Front(j,:)=[ Time(i)-Start TC1(i) TC2(i) TC3(i) TC4(i)];
      j=j+1;
   elseif j == 2 && TC2(i)<=FT
      Front(j,:)=[ Time(i)-Start TC1(i) TC2(i) TC3(i) TC4(i)];
      j=j+1;
   end

   if j == 3 && TC3(i)<=FT
      Front(j,:)=[ Time(i)-Start TC1(i) TC2(i) TC3(i) TC4(i)];
      j=j+1;
   end

   if j == 4 && TC4(i)<=FT
      Front(j,:)=[ Time(i)-Start TC1(i) TC2(i) TC3(i) TC4(i)];
      j=j+1;
   end
end
```

```
%% Temperature Readings after cooling begins
Time_M1=Time-Start;
j=0;
for i=1:numel(Time)
   if Time_M1(i)>=0
      j=j+1;
      Time_M2(j,1)=Time_M1(i);
      TC1_M2(j,1) =TC1(i);
      TC2_M2(j,1) =TC2(i);
      TC3_M2(j,1) =TC3(i);
      TC4_M2(j,1) =TC4(i);
   end
end

Output=[Time_M2 TC1_M2 TC2_M2 TC3_M2 TC4_M2];
subplot(2,2,1);
plot(Time_M2,TC1_M2,Time_M2,TC2_M2,Time_M2,TC3_M2,Time_M2,TC4_M2);
xlabel('Time (minutes)');
ylabel(' Temperature (^{\circ}C)');
title('Transient Temperature Readings');

%%  Estimating ice front position
position = [0;5.5;20.5;35.5;50.5];%Thermocouples position from the wall in mm
Arrival  = [0 ; Front(:,1)]; % time arrival at different locations
TCW=-20; % wall temperature-corrected
subplot(2,2,2);
scatter(Arrival,position,'filled');
xlabel('Time (minutes)');
ylabel(' Location (mm)');
title('Ice-front Location');
polyfit(sqrt([0;Front(:,1)]),position,1);
```

```
%% The ice front estimated speed at different times.
j=0;
for i=2:5
   j=j+1;
   Speed(j,1)= (position(i)-position(i-1))/(Arrival(i)-Arrival(i-1));
end
subplot(2,2,3);
scatter(Arrival(2:5,1),Speed,'filled');
xlabel('Time (minutes)');
ylabel(' Speed (mm/min)');
title('Ice-front Speed');

 %% The heat rate (W) taken from the test cell at the cooling plate Vs. Time
j=0;
for i=1:numel(Time_M2)
      j=j+1;
      Heat_Rate(j,1)=-1*2.2*2.5e-3*(TC1_M2(i)-TCW)/(position(2)*1e-3);
end

subplot(2,2,4);
plot(Time_M2,Heat_Rate);
xlabel('Time (minutes)');
ylabel(' Heat Rate (W)');
title('Heat Rate at the Cooling Plate');
```

Appendix G: Modified-Boussinesq Source Term Subroutine

A C-code was written and implemented in FLUENT. It represents the source term added to the momentum equation taking care of the modified-Boussinesq approximation. In this appendix, the subroutine of the source term of pure water is presented.

```
/************************************************************************/
/*       UDF for specifying a y-momentum source term that is similar    */
/*       to Boussinesq approximation but with a temperature-dependent   */
/*       thermal expansion coefficient                                  */
/************************************************************************/
#include "udf.h"
#define rho_ref 1000.0
#define g 9.81
#define temp_ref 277.0
#define temp_solid 273.0
DEFINE_SOURCE(ymom_source_0,c,t,dS,eqn)
{
  real T = C_T(c,t);
  real source;
  real beta;
  real rho_fnc;
  real Drho_fnc;
  if ( T >= temp_solid)
    {
        /* modified Boussinesq source term */
        rho_fnc = -9965.9549313795 + 165.8045156442*T - 1.0092408807*T*T +
3.0959333e-3*T*T*T-4.7846647e-6*T*T*T*T + 2.9705375e-9*T*T*T*T*T;
        Drho_fnc = 165.8045156442 - 2.0184817614854*T + 9.2878000436e-3*T*T -
1.9138658650e-5*T*T*T + 1.4852687536e-8*T*T*T*T;
        beta = -1*Drho_fnc/rho_fnc;
        source = g*C_R(c,t)*(beta*(T-temp_ref));
        /* derivative of source term */
        dS[eqn] = 0.0;
    }
  else
        source = dS[eqn] = 0.0;

  return source;}
```

REFERENCES

[1] L. Fan and J. M. Khodadadi, "Thermal conductivity enhancement of phase change materials for thermal energy storage: a review," *Renew. Sustain. Energy Rev.*, vol. 15, no. 1, pp. 24–46, 2011.

[2] H. Mehling and L. F. Cabeza, "Phase change materials and their basic properties," in *Thermal energy storage for sustainable energy consumption*, Springer, 2007, pp. 257–277.

[3] J. M. Khodadadi and S. F. Hosseinizadeh, "Nanoparticle-enhanced phase change materials (NEPCM) with great potential for improved thermal energy storage," *Int. Commun. Heat Mass Transf.*, vol. 34, no. 5, pp. 534–543, 2007.

[4] H. Masuda, A. Ebata, and K. Teramae, "Alteration of thermal conductivity and viscosity of liquid by dispersing ultra-fine particles. Dispersion of Al2O3, SiO2 and TiO2 ultra-fine particles," 1993.

[5] S. U. S. Chol, "Enhancing thermal conductivity of fluids with nanoparticles," *ASME-Publ.-Fed*, vol. 231, pp. 99–106, 1995.

[6] "5,870 Search Results - Nanofluid and Nanofluids - ScienceDirect." [Online]. Available:http://www.sciencedirect.com/science?_ob=ArticleListURL&_method=list&_ArticleListID=-1081752090&_sort=r&_st=4&md5=310a8efdb2128aee4e84ef123e3f7145&searchtype=a. [Accessed: 04-Nov-2016].

[7] A. Grimm, "Powdered aluminum-containing heat transfer fluids," *Ger. Pat. DE*, vol. 4131516, p. A1, 1993.

[8] J. A. Eastman, S. U. S. Choi, S. Li, W. Yu, and L. J. Thompson, "Anomalously increased effective thermal conductivities of ethylene glycol-based Nanofluids containing copper nanoparticles," *Appl. Phys. Lett.*, vol. 78, no. 6, pp. 718–720, 2001.

[9] C.-H. Lo, T.-T. Tsung, L.-C. Chen, C.-H. Su, and H.-M. Lin, "Fabrication of copper oxide Nanofluid using submerged arc nanoparticle synthesis system (SANSS)," *J. Nanoparticle Res.*, vol. 7, no. 2–3, pp. 313–320, 2005.

[10] Y. Li, S. Tung, E. Schneider, S. Xi, and others, “A review on development of Nanofluid preparation and characterization,” *Powder Technol.*, vol. 196, no. 2, pp. 89–101, 2009.

[11] X. Wei and L. Wang, “Synthesis and thermal conductivity of microfluidic copper Nanofluids,” *Particuology*, vol. 8, no. 3, pp. 262–271, 2010.

[12] A. K. Singh and V. S. Raykar, “Microwave synthesis of silver Nanofluids with polyvinylpyrrolidone (PVP) and their transport properties,” *Colloid Polym. Sci.*, vol. 286, no. 14–15, pp. 1667–1673, 2008.

[13] X. Yang and Z. Liu, “A kind of Nanofluid consisting of surface-functionalized nanoparticles,” *Nanoscale Res. Lett.*, vol. 5, no. 8, pp. 1324–1328, 2010.

[14] K. A. Wepasnick, B. A. Smith, J. L. Bitter, and D. H. Fairbrother, “Chemical and structural characterization of carbon nanotube surfaces,” *Anal. Bioanal. Chem.*, vol. 396, no. 3, pp. 1003–1014, 2010.

[15] X.-Q. Wang and A. S. Mujumdar, “Heat transfer characteristics of Nanofluids: a review,” *Int. J. Therm. Sci.*, vol. 46, no. 1, pp. 1–19, 2007.

[16] S. U. S. Choi, Z. G. Zhang, W. Yu, F. E. Lockwood, and E. A. Grulke, “Anomalous thermal conductivity enhancement in nanotube suspensions,” *Appl. Phys. Lett.*, vol. 79, no. 14, pp. 2252–2254, 2001.

[17] H. Xie, J. Wang, T. Xi, Y. Liu, F. Ai, and Q. Wu, “Thermal conductivity enhancement of suspensions containing nanosized alumina particles,” *J. Appl. Phys.*, vol. 91, no. 7, pp. 4568–4572, 2002.

[18] J. A. Eastman, U. S. Choi, S. Li, L. J. Thompson, and S. Lee, “Enhanced thermal conductivity through the development of Nanofluids,” in *MRS proceedings*, 1996, vol. 457, p. 3.

[19] S. Lee, S.-S. Choi, Li S, and J. A. and Eastman, “Measuring thermal conductivity of fluids containing oxide nanoparticles,” *J. Heat Transf.*, vol. 121, no. 2, pp. 280–289, 1999.

[20] X. Wang, X. Xu, and S. U. S. Choi, “Thermal conductivity of nanoparticle-fluid mixture,” *J. Thermophys. Heat Transf.*, vol. 13, no. 4, pp. 474–480, 1999.

[21] S. K. Das, N. Putra, P. Thiesen, and W. Roetzel, “Temperature dependence of thermal conductivity enhancement for Nanofluids,” *J. Heat Transf.*, vol. 125, no. 4, pp. 567–574, 2003.

[22] C. H. Li and G. P. Peterson, “Experimental investigation of temperature and volume fraction variations on the effective thermal conductivity of nanoparticle suspensions (Nanofluids),” *J. Appl. Phys.*, vol. 99, no. 8, p. 84314, 2006.

[23] Y. Xuan and Q. Li, “Heat transfer enhancement of Nanofluids,” *Int. J. Heat Fluid Flow*, vol. 21, no. 1, pp. 58–64, 2000.

[24] T.-K. Hong, H.-S. Yang, and C. J. Choi, “Study of the enhanced thermal conductivity of Fe Nanofluids,” *J. Appl. Phys.*, vol. 97, no. 6, p. 64311, 2005.

[25] H. E. Patel, S. K. Das, T. Sundararajan, A. S. Nair, B. George, and T. Pradeep, “Thermal conductivities of naked and monolayer protected metal nanoparticle based Nanofluids: Manifestation of anomalous enhancement and chemical effects,” *Appl. Phys. Lett.*, vol. 83, no. 14, pp. 2931–2933, 2003.

[26] S. M. S. Murshed, K. C. Leong, and C. Yang, “Enhanced thermal conductivity of TiO_2-water based Nanofluids,” *Int. J. Therm. Sci.*, vol. 44, no. 4, pp. 367–373, 2005.

[27] H. Xie, J. Wang, T. Xi, and Y. Liu, “Study on the thermal conductivity of SiC Nanofluids,” *J Chin Ceram Soc*, vol. 29, no. 4, pp. 361–364, 2001.

[28] M. J. Biercuk, M. C. Llaguno, M. Radosavljevic, J. K. Hyun, A. T. Johnson, and J. E. Fischer, “Carbon nanotube composites for thermal management,” *Appl. Phys. Lett.*, vol. 80, no. 15, pp. 2767–2769, 2002.

[29] H. Xie, H. Lee, W. Youn, and M. Choi, “Nanofluids containing multiwalled carbon nanotubes and their enhanced thermal conductivities,” *J. Appl. Phys.*, vol. 94, no. 8, pp. 4967–4971, 2003.

[30] E. S. Choi *et al.*, “Enhancement of thermal and electrical properties of carbon nanotube polymer composites by magnetic field processing,” *J. Appl. Phys.*, vol. 94, no. 9, pp. 6034–6039, 2003.

[31] D. Wen and Y. Ding, “Effective thermal conductivity of aqueous suspensions of carbon nanotubes (carbon nanotube Nanofluids),” *J. Thermophys. Heat Transf.*, vol. 18, no. 4, pp. 481–485, 2004.

[32] M. J. Assael, I. N. Metaxa, J. Arvanitidis, D. Christofilos, and C. Lioutas, “Thermal conductivity enhancement in aqueous suspensions of carbon multi-walled and double-walled nanotubes in the presence of two different dispersants,” *Int. J. Thermophys.*, vol. 26, no. 3, pp. 647–664, 2005.

[33] Mj. Assael, C.-F. Chen, I. Metaxa, and W. A. Wakeham, “Thermal conductivity of suspensions of carbon nanotubes in water,” *Int. J. Thermophys.*, vol. 25, no. 4, pp. 971–985, 2004.

[34] Mj. Assael, C.-F. Chen, I. Metaxa, and W. A. Wakeham, “Thermal conductivity of suspensions of carbon nanotubes in water,” *Int. J. Thermophys.*, vol. 25, no. 4, pp. 971–985, 2004.

[35] M.-S. Liu, M. C.-C. Lin, I.-T. Huang, and C.-C. Wang, “Enhancement of thermal conductivity with carbon nanotube for Nanofluids,” *Int. Commun. Heat Mass Transf.*, vol. 32, no. 9, pp. 1202–1210, 2005.

[36] R. S. Vajjha and D. K. Das, “Specific heat measurement of three Nanofluids and development of new correlations,” *J. Heat Transf.*, vol. 131, no. 7, p. 71601, 2009.

[37] S. Zhou and R. Ni, “Measurement of the specific heat capacity of water-based Al~ 2O~ 3 Nanofluid,” *Appl. Phys. Lett.*, vol. 92, no. 9, p. 93123, 2008.

[38] P. K. Namburu, D. P. Kulkarni, A. Dandekar, and D. K. Das, “Experimental investigation of viscosity and specific heat of silicon dioxide Nanofluids,” *Micro Nano Lett. IET*, vol. 2, no. 3, pp. 67–71, 2007.

[39] M. X. Ho and C. Pan, “Optimal concentration of alumina nanoparticles in molten Hitec salt to maximize its specific heat capacity,” *Int. J. Heat Mass Transf.*, vol. 70, pp. 174–184, 2014.

[40] I. C. Nelson, D. Banerjee, and R. Ponnappan, “Flow loop experiments using polyalphaolefin Nanofluids,” *J. Thermophys. Heat Transf.*, vol. 23, no. 4, pp. 752–761, 2009.

[41] D. Shin and D. Banerjee, “Enhanced specific heat capacity of nanomaterials synthesized by dispersing silica nanoparticles in eutectic mixtures,” *J. Heat Transf.*, vol. 135, no. 3, p. 32801, 2013.

[42] B. Jo and D. Banerjee, "Enhanced Specific Heat Capacity of Molten Salt-Based Carbon Nanotubes Nanomaterials," *J. Heat Transf.*, vol. 137, no. 9, pp. 091013–091013, May 2015.

[43] S. A. Angayarkanni and J. Philip, "Review on thermal properties of Nanofluids: Recent developments," *Adv. Colloid Interface Sci.*, vol. 225, pp. 146–176, 2015.

[44] J.-H. Lee *et al.*, "Effective viscosities and thermal conductivities of aqueous Nanofluids containing low volume concentrations of Al 2 O 3 nanoparticles," *Int. J. Heat Mass Transf.*, vol. 51, no. 11, pp. 2651–2656, 2008.

[45] C. L. Snow, C. R. Lee, Q. Shi, J. Boerio-Goates, and B. F. Woodfield, "Size-dependence of the heat capacity and thermodynamic properties of hematite (α-Fe 2 O 3)," *J. Chem. Thermodyn.*, vol. 42, no. 9, pp. 1142–1151, 2010.

[46] Y. Ding, H. Alias, D. Wen, and R. A. Williams, "Heat transfer of aqueous suspensions of carbon nanotubes (CNT Nanofluids)," *Int. J. Heat Mass Transf.*, vol. 49, no. 1, pp. 240–250, 2006.

[47] S. Halelfadl, P. Estellé, B. Aladag, N. Doner, and T. Maré, "Viscosity of carbon nanotubes water-based Nanofluids: Influence of concentration and temperature," *Int. J. Therm. Sci.*, vol. 71, pp. 111–117, Sep. 2013.

[48] M. F. Demirbas, "Thermal energy storage and phase change materials: an overview," *Energy Sources Part B Econ. Plan. Policy*, vol. 1, no. 1, pp. 85–95, 2006.

[49] S. Wu, D. Zhu, X. Li, H. Li, and J. Lei, "Thermal energy storage behavior of Al 2 O 3--H 2 O Nanofluids," *Thermochim. Acta*, vol. 483, no. 1, pp. 73–77, 2009.

[50] Y.-D. Liu, Y.-G. Zhou, M.-W. Tong, and X.-S. Zhou, "Experimental study of thermal conductivity and phase change performance of Nanofluids PCMs," *Microfluid. Nanofluidics*, vol. 7, no. 4, pp. 579–584, 2009.

[51] T. P. Otanicar, P. E. Phelan, R. S. Prasher, G. Rosengarten, and R. A. Taylor, "Nanofluid-based direct absorption solar collector," *J. Renew. Sustain. Energy*, vol. 2, no. 3, p. 33102, 2010.

[52] T. P. Otanicar and J. S. Golden, "Comparative environmental and economic analysis of conventional and Nanofluid solar hot water technologies," *Environ. Sci. Technol.*, vol. 43, no. 15, pp. 6082–6087, 2009.

[53] S. P. Jang and S. U. S. Choi, “Cooling performance of a microchannel heat sink with Nanofluids,” *Appl. Therm. Eng.*, vol. 26, no. 17, pp. 2457–2463, 2006.

[54] T. S. Eriksson and C. G. Granqvist, “Radiative cooling computed for model atmospheres,” *Appl. Opt.*, vol. 21, no. 23, pp. 4381–4388, 1982.

[55] H. R. Pruppacher, J. D. Klett, and P. K. Wang, “Microphysics of clouds and precipitation,” 1998.

[56] Charlie Sorrel, “Coca Cola Plans High Tech, Super Cool Sprite,” *Wired. Condé Nast.*, 2007. [Online]. Available: http://www.wired.com/2007/09/coca-cola-plans/. [Accessed: 02-Jun-2016].

[57] G. Jacoby, K. Cohen, K. Barkan, Y. Talmon, D. Peer, and R. Beck, “Metastability in lipid based particles exhibits temporally deterministic and controllable behavior,” *Sci. Rep.*, vol. 5, 2015.

[58] J. Z. Yu, Z. L. Li, and H. Y. Hu, “Experimental Study of Nanofluids Crystallize on Low Temperature Environment,” in *Applied Mechanics and Materials*, 2013, vol. 313, pp. 262–265.

[59] T. Maré, O. Sow, S. Halelfadl, S. Lebourlout, and C. T. Nguyen, “Experimental study of the freezing point of γ-Al2O3/water Nanofluid,” *Adv. Mech. Eng.*, vol. 4, p. 162961, 2012.

[60] H. Hong, J. Wensel, S. Peterson, and W. Roy, “Efficiently lowering the freezing point in heat transfer coolants using carbon nanotubes,” *J. Thermophys. Heat Transf.*, vol. 21, no. 2, pp. 446–448, 2007.

[61] S. Mo, Y. Chen, L. Jia, and X. Luo, “Reduction of supercooling of water by TiO2 nanoparticles as observed using differential scanning calorimeter,” *J. Exp. Nanosci.*, vol. 8, no. 4, pp. 533–539, 2013.

[62] J. Stefan, “{Ü}ber die Theorie der Eisbildung, insbesondere {ü}ber die Eisbildung im Polarmeere,” *Ann. Phys.*, vol. 278, no. 2, pp. 269–286, 1891.

[63] D. V Boger and J. W. Westwater, “Effect of buoyancy on the melting and freezing process,” *J. Heat Transf.*, vol. 89, no. 1, pp. 81–89, 1967.

[64] L. A. Diaz and R. Viskanta, “Visualization of the solid-liquid interface morphology formed by natural convection during melting of a solid from below,” *Int. Commun. Heat Mass Transf.*, vol. 11, no. 1, pp. 35–43, 1984.

[65] N. W. Hale and R. Viskanta, “Solid-liquid phase-change heat transfer and interface motion in materials cooled or heated from above or below,” *Int. J. Heat Mass Transf.*, vol. 23, no. 3, pp. 283–292, 1980.

[66] W. Z. Cao and D. Poulikakos, “Experiments on the transient freezing of water in an inclined rectangular cavity,” *Int. J. Heat Fluid Flow*, vol. 12, no. 2, pp. 116–121, 1991.

[67] B. Webb, M. K. Moallemi, and R. Viskanta, “Experiments on melting of unfixed ice in a horizontal cylindrical capsule,” *J. Heat Transf.*, vol. 109, no. 2, pp. 454–459, 1987.

[68] F. E. Moore and Y. Bayazitoglu, “Melting within a spherical enclosure,” *J. Heat Transf.*, vol. 104, no. 1, pp. 19–23, 1982.

[69] S. Kashani, A. A. Ranjbar, M. Abdollahzadeh, and S. Sebti, “Solidification of nano-enhanced phase change material (NEPCM) in a wavy cavity,” *Heat Mass Transf.*, vol. 48, no. 7, pp. 1155–1166, 2012.

[70] J. A. Weaver and R. Viskanta, “Freezing of liquid-saturated porous media,” *J. Heat Transf.*, vol. 108, no. 3, pp. 654–659, 1986.

[71] F. L. Tan, S. F. Hosseinizadeh, J. M. Khodadadi, and L. Fan, “Experimental and computational study of constrained melting of phase change materials (PCM) inside a spherical capsule,” *Int. J. Heat Mass Transf.*, vol. 52, no. 15, pp. 3464–3472, 2009.

[72] L. Fan and J. M. Khodadadi, “An experimental investigation of enhanced thermal conductivity and expedited unidirectional freezing of cyclohexane-based nanoparticle suspensions utilized as nano-enhanced phase change materials (NePCM),” *Int. J. Therm. Sci.*, vol. 62, pp. 120–126, Dec. 2012.

[73] A. Kamyar, R. Saidur, and M. Hasanuzzaman, “Application of computational fluid dynamics (CFD) for Nanofluids,” *Int. J. Heat Mass Transf.*, vol. 55, no. 15, pp. 4104–4115, 2012.

[74] J. Crank, *Free and moving boundary problems*. Clarendon press Oxford, 1984.

[75] V. R. Voller and C. Prakash, “A fixed grid numerical modelling methodology for convection-diffusion mushy region phase-change problems,” *Int. J. Heat Mass Transf.*, vol. 30, no. 8, pp. 1709–1719, 1987.

[76] P. T. Zubkov, V. A. Kravchenko, and E. M. Sviridov, “Simulation of the process of water freezing in a round pipe,” *High Temp.*, vol. 39, no. 5, pp. 722–728, 2001.

[77] K. Khanafer, K. Vafai, and M. Lightstone, “Buoyancy-driven heat transfer enhancement in a two-dimensional enclosure utilizing Nanofluids,” *Int. J. Heat Mass Transf.*, vol. 46, no. 19, pp. 3639–3653, 2003.

[78] S. S. Sebti, M. Mastiani, H. Mirzaei, A. Dadvand, S. Kashani, and S. A. Hosseini, “Numerical study of the melting of nano-enhanced phase change material in a square cavity,” *J. Zhejiang Univ. Sci. A*, vol. 14, no. 5, pp. 307–316, 2013.

[79] S. Kashani, A. A. Ranjbar, M. M. Madani, M. Mastiani, and H. Jalaly, “Numerical study of solidification of a nano-enhanced phase change material (NEPCM) in a thermal storage system,” *J. Appl. Mech. Tech. Phys.*, vol. 54, no. 5, pp. 702–712, 2013.

[80] S. S. Sebti, S. H. Khalilarya, I. Mirzaee, S. F. Hosseinizadeh, S. Kashani, and M. Abdollahzadeh, “A numerical investigation of solidification in horizontal concentric annuli filled with nano-enhanced phase change material (NEPCM),” *World Appl. Sci. J.*, vol. 13, no. 1, pp. 9–15, 2011.

[81] M. Jourabian and M. Farhadi, “Melting of nanoparticles-enhanced phase change material (NEPCM) in vertical semicircle enclosure: numerical study,” *J. Mech. Sci. Technol.*, vol. 29, no. 9, pp. 3819–3830, 2015.

[82] M. Corcione, “Heat transfer features of buoyancy-driven Nanofluids inside rectangular enclosures differentially heated at the sidewalls,” *Int. J. Therm. Sci.*, vol. 49, no. 9, pp. 1536–1546, 2010.

[83] J. Ganeshkumar, D. Kathirkaman, K. Raja, V. Kumaresan, and R. Velraj, “Experimental study on density, thermal conductivity, specific heat and viscosity of water - ethylene glycol mixture dispersed with carbon nanotubes,” *Therm. Sci.*, no. 00, pp. 28–28, OnLine-First 2015.

[84] B. C. Pak and Y. I. Cho, “Hydrodynamic and heat transfer study of dispersed fluids with submicron metallic oxide particles,” *Exp. Heat Transf.*, vol. 11, no. 2, pp. 151–170, 1998.

[85] A. Zabalegui, D. Lokapur, and H. Lee, “Nanofluid PCMs for thermal energy storage: Latent heat reduction mechanisms and a numerical study of effective thermal storage performance,” *Int. J. Heat Mass Transf.*, vol. 78, pp. 1145–1154, 2014.

[86] J. Khodadadi and S. Hosseinizadeh, “Nanoparticle-enhanced phase change materials (NEPCM) with great potential for improved thermal energy storage,” *Int. Commun. Heat Mass Transf.*, vol. 34, no. 5, pp. 534–543, 2007.

[87] H. O’Hanley, J. Buongiorno, T. McKrell, and L. Hu, “Measurement and Model Validation of Nanofluid Specific Heat Capacity with Differential Scanning Calorimetry,” *Adv. Mech. Eng.*, vol. 4, p. 181079, Jan. 2012.

[88] S. Halelfadl, T. Mare, and P. Estelle, “Effciency of carbon nanotubes water based Nanofluids as coolants,” *Exp. Therm. Fluid Sci.*, no. 53, p. 2014, 110 104AD.

[89] V. B. Muratov, O. O. Vasil’ev, L. M. Kulikov, V. V. Garbuz, Y. V. Nesterenko, and T. I. Duda, “Thermodynamic properties of multiwalled carbon nanotubes,” *J. Superhard Mater.*, vol. 34, no. 3, pp. 173–178, May 2012.

[90] Q. Z. Xue, “Model for thermal conductivity of carbon nanotube-based composites,” *Phys. B Condens. Matter*, vol. 368, no. 1–4, pp. 302–307, 2005.

[91] T. A. Kowalewski and D. Gobin, *Phase Change with Convection: Modelling and Validation*. Springer, 2014.

[92] S. Patankar, *Numerical heat transfer and fluid flow*. CRC press, 1980.

[93] V. R. Voller and C. Prakash, “A fixed grid numerical modelling methodology for convection-diffusion mushy region phase-change problems,” *Int. J. Heat Mass Transf.*, vol. 30, no. 8, pp. 1709–1719, 1987.

[94] C. Gau and R. Viskanta, “Melting and solidification of a pure metal on a vertical wall,” *J. Heat Transf.*, vol. 108, no. 1, pp. 174–181, 1986.

[95] T. L. Bergman, F. P. Incropera, D. P. DeWitt, and A. S. Lavine, *Fundamentals of Heat and Mass Transfer*. John Wiley & Sons, 2011.

VITAE

Name :Alshehri, Ali M.

Nationality :Saudi

Date of Birth :12/15/1991

Email :alshehri@kfupm.edu.sa

alialshehriKFUPM@gmail.com

Address :Dhahran, Saudi Arabia

Academic Background :

- Bachelor's Degree in Mechanical Engineering, KFUPM (GPA 3.867/4)
- Master's Degree in Mechanical Engineering, KFUPM (GPA 3.964/4)

Research Interests :

Renewable Energy, Energy Storage, Thermal Energy Storage (TES), Nanofluids, and Carbon-nanotubes